Université d'Ottawa • University of Ottawa

Université d'Ottawa · University of Ottawa

FACULTÉ DES ÉTUDES SUPÉRIEURES ET POSTDOCTORALES

FACULTY OF GRADUATE AND POSTDOCTORAL STUDIES

Rafi CHAPANIAN

AUTEUR DE LA THÈSE - AUTHOR OF THESIS

M. A. Sc. (Chemical Engineering)

GRADE - DEGREE

Department of Chemical Engineering

FACULTÉ, ÉCOLE, DÉPARTEMENT - FACULTY, SCHOOL, DEPARTMENT

TITRE DE LA THÈSE - TITLE OF THE THESIS

Study of Accumulation of Gases in Vacuum Systems:
Measurement of Gas Transport Properties of Polymeric Films

B. Kruczek

DIRECTEUR DE LA THÈSE - THESIS SUPERVISOR

CO-DIRECTEUR DE LA THÈSE - THESIS CO-SUPERVISOR

EXAMINATEURS DE LA THÈSE - THESIS EXAMINERS

A. Macchi

J. Thibault

J.-M. De Koninck, Ph.D.

LE DOYEN DE LA FACULTÉ DES ÉTUDES SUPÉRIEURES ET POSTDOCTORALES

SIGNATURE

DEAN OF THE FACULTY OF GRADUATE AND POSTDOCTORAL STUDIES

STUDY OF ACCUMULATION OF GASES IN VACUUM SYSTEMS:

Measurement of Gas Transport Properties of Polymeric Films

Rafi Chapanian

Thesis submitted to the
Faculty of Graduate and Postdoctoral Studies
in partial fulfillment of the requirements for the degree of

Master of Applied Science

in

Chemical Engineering

Department of Chemical Engineering
Faculty of Engineering
University of Ottawa

Your file Votre référence
ISBN: 0-494-01433-4
Our file Notre référence
ISBN: 0-494-01433-4

ABSTRACT

A constant volume (CV) technique allows indirect measurements of very low flow rates of gases, in the order of 10^{-8} mol/s or less, for which other flow measurement techniques such as bubble-flow meters, or piston placement constant pressure systems fail, or requires sophisticated build up. The CV technique is widely utilized in characterization of polymeric films and porous materials; it allows determination of permeability, diffusion and solubility coefficients of gases in these media. It is generally assumed that there is no resistance to the transport of gas molecules when they accumulate in vacuum tubes and tanks, which are part of CV systems. In other words, it is assumed that at a given time the pressure downstream from the tested medium is uniform.

In this thesis we have proven that the resistance to accumulation of gases in vacuum tubes is not always negligible. The process of accumulation was described using the Fick's second law of diffusion. The diffusion coefficient was assumed constant and evaluated, depending on pressure, considering Knudsen diffusion, molecular diffusion, or a combination of them. Experimental system with tubes of different lengths and diameters was built and equipped with two high sensitivity pressure transducers to measure the dynamic pressure difference along the system during gas flow experiments. Two cases were considered. First, the governing partial differential equation was solved analytically assuming a constant flow of gas into the system. Experimentally, a low-flow mass flow controller provided the constant flow of gas into the system. In the second case, the governing partial differential equation was solved numerically assuming a time-dependent flow of gas given by the Barrer equation. Experimentally, this flow condition

was achieved by instantaneous pressurization of a semi permeable membrane, initially at vacuum, and then maintaining the constant pressure at the feed side of the membrane.

In both cases, experimental data was in very good agreement with the proposed mathematical models. Resistance of the system was described using the concept of time lag. A simple equation, applicable for both constant and time-dependent flows, relating the time lag of system to the position, tube length and the diffusion coefficient was proposed. The proposed equation allows to design resistance-free systems, and in case of systems with significant resistance, to optimize the location for monitoring the dynamic pressure. The results of this project have been summarized in three manuscripts, which have either been submitted, or are being submitted for review in peer-refereed journals.

RESUME

Une technique de volume constant (VC) permet d'effectuer des mesures indirectes de très faibles débits de gaz (10^{-8} mol/s ou moins), ce que ne peuvent faire d'autres méthodes tels que les débitmètres à bulles ou les systèmes de pistons destinés à maintenir une pression constante. La technique de VC est utilisée principalement pour la caractérisation de films polymériques et de matériaux poreux. Elle permet la détermination de la perméabilité ainsi que les coefficients de diffusion et de solubilité de gaz dans ces milieux. Il est généralement supposé qu'il n'y a pas de résistance au transport de molécules de gaz lorsqu'elles s'accumulent dans les tubes à vide et les réservoirs qui font partie des systèmes à VC. Autrement dit, il est supposé qu'à un temps donné la pression en aval du milieu testé est uniforme.

Nous avons prouvé que la résistance à l'accumulation de gaz dans les tubes à vide n'est pas toujours négligeable. La seconde loi de diffusion de Fick a permis de décrire le processus d'accumulation de gaz. Le coefficient de diffusion a été supposé constant et a été évalué en tenant compte de la pression et en considérant la diffusion Knudsen, la diffusion moléculaire, ou une combinaison des deux. Un système expérimental, doté de tubes de longueurs et de diamètres différents, a été construit et équipé de deux capteurs de pression à forte sensibilité pour mesurer la différence de pression dynamique à travers le système durant les expériences d'écoulement de gaz. Deux cas ont été considérés: d'une part, l'équation différentielle partielle directrice a été résolue de façon analytique en supposant un écoulement constant de gaz dans le système. Au point de vue expérimental, un contrôleur de débit massique a fourni un écoulement constant dans le système. D'autre part, l'équation différentielle partielle directrice a été résolue de façon

numérique en supposant un écoulement dépendant du temps donné par l'équation de Barrer. Au point de vue expérimental, cette condition d'écoulement a été atteinte par la pressurisation instantanée d'une membrane semi-perméable, d'abord à vide, et ensuite en maintenant la pression constante du côté d'alimentation à la membrane.

Dans les deux cas, les données expérimentales s'accordaient très bien avec les modèles mathématiques. Le concept de décalage de temps a permis de décrire la résistance du système. Une équation simple, applicable pour un écoulement constant et pour un écoulement dépendant du temps, reliant le décalage de temps du système à la position, la longueur du tube et le coefficient de diffusion a été proposée. Cette équation permet de concevoir des systèmes sans résistance et, dans le cas de systèmes à forte résistance, permet d'optimiser le positionnement de la mesure de la pression dynamique. Les résultats de ce projet ont été résumés dans trois manuscrits, qui ont été soumis ou sont sur le point d'être soumis pour évaluation à des revues avec comité de lecture.

STATEMENT OF CONTRIBUTIONS AND COLLABORATORS

I hereby declare that I am the sole author of this thesis. I have performed the mathematical modeling, designed the experimental setup, ordered most of the components of the experimental system, and conducted the experiments.

Assembling of the system was performed by Mr. Franco Ziroldo and connecting the system to Labview data acquisition program was done by Mr. Gerard Nina. My supervisor Dr. Boguslaw Kruczek provided an excellent scientific guidance, important editorial input, comments, corrections, and enrichment to my written work.

Signature:

Date: 19/12/2003

ACKNOWLEDGMENTS

I would like to express my gratitude to many people, without whom it would be impossible to be at this final stage of my M.A.Sc. program.

First of all, my deep respect to Dr. Boguslaw Kruczek, who accepted me as a student and supported me financially. He was patient and friendly, together we solved many difficulties and crossed to the other side of the river.

I am very grateful to our talented technicians in the department: Franco Ziroldo for setting the experimental set-up, Gerard Nina for installing Lab-view data acquisition program, and Louis Tremblay for his kind directions.

I would like also to thank all the professors who have taught me in the department and all my colleagues and friends, specially Jamal Kurdi, Salvador Rego, and George Psofoianakis, from whom I learned many things.

Finally, my endless love goes to my family members for their continuous support and encouragement.

TABLE of CONTENTS

LIST OF TABLES

LIST OF FIGURES

CHAPTER II

CHAPTER I

Introduction

The first step in assessing the potential of polymer for gas separation is the determination of its permeability for various gases. This is done by the measurement of gas permeation rates through homogeneous films (membranes) of known thickness prepared from a given polymer. In general, three techniques are used for the measurement of gas permeation rates. These are a constant pressure technique, a constant pressure technique with a sweep gas, and a constant volume technique.

The first of these, the constant pressure technique is the simplest one that utilizes a direct measurement of permeation rate using a bubble flow or any other kind of flow meter. The permeate-side of film is open to atmosphere, and consequently it is at atmospheric pressure. In the constant pressure technique with a sweep gas, the permeate-side of film is swept with a gas at a known flow rate. The mixture of permeate and sweep gas is sent into a gas chromatograph for the analysis of gas composition, which allows the determination of the actual permeation rate through the membrane.

In the constant volume technique, which is the most common one used for the determination of permeability coefficients of gases in polymeric membranes, the gas permeates into a closed volume, and as a result the pressure at the permeate-side increases. The permeation rate is determined from the rate of pressure rise in a known permeate-side volume using the following equation, which is derived from the ideal gas law [Arkilic et. al., 1998; Mohammadi et. al., 1995]:

$$\frac{dn}{dt} = \frac{V}{RT}\frac{dp}{dt} \qquad (1)$$

where n is the number of moles, t is the time, V is the volume at the permeate side of membrane, R is the universal gas constant, and p is the pressure. The constant volume technique allows measurements of flow rates in the order of 10^{-8} mol/s or less, where other measurement techniques fail or require sophisticated built up. Another advantage of the constant volume technique is that along with the permeability coefficient it also allows determination of the diffusion and solubility coefficients from a single gas permeation experiment [Rutherford and Do, 1997].

Flow measurements using the constant volume technique are indirect ones, which rely on the assumption that there is no resistance to accumulation of gases in the permeate side volume of the CV system. Reporting gas transport properties of high molecular weight sulfonated polyphenylene oxide, which were evaluated in a constant volume system, Kruczek and Matsuura, (2000a) observed that a 0.2% decrease in the pressure driving force was consistently associated with up to 10% decrease in gas permeation rates through the tested membranes. While the observed phenomenon was most likely due to changes in the solubility, diffusion and permeability coefficients of gases in tested membranes; it could also be partly due non-negligible resistance effects [Kruczek and Matsuura, 2000b]. Moreover, in order to accurately assess possible changes in the gas transport coefficients in membranes, the process of accumulation of gases at the permeate side of membrane must be well understood. Therefore, the major objective of this thesis is to investigate the mechanism of gas accumulation in vacuum systems and to evaluate the constant volume technique in characterization of gas transport properties in semi permeable membranes.

There are many variations of constant volume systems described in the literature [Mohammadi et. al., 1995; Heilman et. al., 1956; Stern et. al., 1963].

Generally a CV system consists of one or multiple membrane cells connected to large tank by tubing. The length and the diameter of tubes are normally not specified, as well as, the information on the initial pressure is rarely provided. Although not explicitly stated, the lack of these information arises from the assumption of negligible resistance to gas molecules accumulating at the permeate side of membrane. An implication of this assumption is a uniform pressure, at a given time, in the closed volume at the permeate side of membrane.

To simplify mathematical analysis, the permeate side of membrane was modeled as a straight cylindrical tube, closed at one end, which is initially in equilibrium. The equilibrium state is disturbed by a flow of gas at the open end of the tube. Two types of flow were taken into consideration: constant flow and time-dependent flow given by the analytical solution of the Barrer equation. The latter equation describes a response to a step change in the driving force for the flow [Rutherford and Do, 1997]. The accumulation process was described by a one-dimensional form of the Fick's second law of diffusion. The Fick's first law of diffusion was used as a boundary condition at the open end of tube. The other boundary condition was obtained by realizing that at the closed end of the tube there is no pressure gradient, regardless of the flow conditions at the open end of the tube. The diffusion coefficient was assumed to be constant and evaluated, depending on the initial pressure and the internal diameter of tube, using one of the following models: Knudsen flow, slip flow, combination of Knudsen and slip and Poiseuille flow [Loeb, 1961; Maxwell, 1879]. The analytical solution of the governing partial differential equation was obtained for the case of constant flow, using the method of separation of variables,

and a numerical solution was obtained for the case of variable flow using a finite difference method.

To verify the mathematical models a system composed of tubes of different lengths and diameters was built and equipped with two pressure transducers to measure the dynamic pressures at different locations. The pressure transducers had a linear range of 1333 Pa (10 mmHg) with a reading ability of 2.67×10^{-2} Pa (0.0002 mmHg) and the accuracy corresponding to 99.88% of the reading. Constant flow into the experimental CV system was provided using a mass flow controller with a range of 0.2 cm^3(STP)/min. Time-dependent flow given by the solution of Barrer equation was effected by a step increase in feed side pressure of membrane, which was initially at vacuum.

The first paper, which is presented in Chapter II, deals with the case of constant flow. It includes both the theoretical model and the experimental data. The first paper emphasizes the effect of resistance on the error in measurement of flow rate of gas in constant volume systems. The second and third papers, which are presented in Chapters III and IV, respectively, represent a series focusing on the case of time-dependent flow. The theoretical considerations are given in Chapter III, whereas, the experimental considerations are given in Chapter IV. This series of papers emphasizes influence of non-negligible resistance on the measurement of time lag of membranes in constant volume systems. Chapter V presents general conclusions and recommendations from the entire thesis. Appendices contain more detailed information on the major models for prediction of the diffusion coefficient in tubes, the analytical solution by separation of variables of the governing partial differential equation for the case of constant flow into the system, information on the experimental repeatability, additional graphs related to the first paper, the numerical solution by the finite difference method of the governing partial

differential equation for the case of time dependent flow into the system, a C++ program to compute the numerical solution, and the configuration of the membrane cell.

References:

1. E. B. Arkilic, M. A. Schmidt, and K.S. Breuer, "Sub-nanomol per second flow measurement near atmospheric pressure", Experiments in Fluids 25, 37-41 (1998).
2. A. Tabe Mohammadi, T. Matsuura, S. Sourirajan, Design and conctruction of gas permeation system for the measurement of low permeatoin rated and permeate compositions, J. Membrane. Sci., 98 281-286 (1995).
3. S.W. Rutherford and D.D. Do, Review of Time Lag Permeation Technique as a Method for Characterization of Porous Media and Membranes, Adsorption, 3, 283-312 (1997).
4. B. Kruczek, T. Matsuura, "Limitations of a constant pressure-type testing system in determination of gas transport properties of hydrophilic films", J. Membrnae Sci., 177, 2000, 129-142.
5. B. Kruczek, T. Matsuura, "Influence of the Permeation Measurement Technique on Gas transport Properties of High Molecular Weight Sulfonated Polyphenylene Oxide", presented at the 50th Annual Conference of Canadian Society of Chemical Engineering, Montreal QC, October 16 – 18, 2000.
6. B. Kruczek, in "Polyphenylene Oxide and Modified Polyphenylene Oxide Membranes Gas, Vapor and Liquid Separation", edited by G. Chowdhury, B. Kruczek, and T. Matsuura, Kluwer Academic Publishers, Boston, 2001.
7. W. Heilman, V. Tammela, J.A. Meyer, V. Stannett, and M. Szwarc, Permeability of polymer films to hydrogen sulfide gas, Ind. Eng. Chem. 48, 821-824 (1956).

8. S. A. Stern, P. J. Garies, T. F. Sinclair, and P. H. Mohr, Performance of a variable-volume permeability cell. comparision of gas permeability measurements by the variable-volume and variable-pressure methods, J. App. Polymer Sci., 7, 2035-2051 (1963).
9. L. B. Loeb, The Kinetic Theory of Gases, 3rd ed., Dover publications, Inc., New York, 1961.
10. J. C. Maxwell, in "The Scientific Papers of James Clerk Maxwell", edited by W. D. Niven, M.A., F.R.S. ,Dover publications, Inc., New York, 1965.

CHAPTER II

Resistance to Accumulation of Gases in High Vacuum Systems

R. Chapanian, B. Kruczek*

Department of Chemical Engineering
University of Ottawa
161 Louis Pasteur Street
Ottawa, ON K1N 6N5
Canada

* To whom correspondence should be addressed.
(Submitted to: Journal of Vacuum Science & Technology A, September 8, 2003)

Abstract

Accumulative flow of gases into vacuum tubes has been studied, and a mathematical model, based on the Fick's 2nd law of diffusion, has been developed to describe the pressure response in vacuum tubes to a constant flow of gases. Depending on the pressure and the size of tubing, the diffusion coefficient was evaluated using one of the following four models, Knudsen flow; slip flow; combination of Knudsen and slip flows; and Poiseuille flow. The developed model indicates the existence of a non-linear pressure response period immediately after initiation of the constant flow of the gas into the system.

To verify the mathematical model a system consisting of tubes of two different inside diameters, 3.86×10^{-3} m and 10.2×10^{-3} m, respectively, and different lengths was built. A low flow mass flow controller, with a 0.2 cm^3(STP)/min range, provided constant flow rates of nitrogen into the system. The tubes were equipped with two sensitive pressure transducers allocated at different distances from the mass flow controller.

The existence of a non-linear pressure response has been confirmed experimentally. For the lowest experimental pressure of 4.13 Pa, the nonlinear pressure response in the smaller tube lasts approximately 15 s. At the end of this period, there is a pressure gradient within the tube, which because of an increasing pressure, decreases as the experiment progresses. As a result, after disappearance of the nonlinear pressure response predicted by the model, the pressure response remains to be a function of time and position, until the pressure within the system becomes uniform. The resistance imposed by vacuum tubes is normally not taken into consideration. This, in turn may lead to an error in experimentally determined permeability and diffusivity coefficients of gases in media such as gas separation membranes. To facilitate the

discussion on the resistance imposed by vacuum tubes the concepts of time lag and time delay are utilized.

Key words: Pressure Rise Technique, Diffusion Coefficient of Gases, Time Lag, Time Delay.

1. Introduction:

Constant-volume mass accumulation systems (CVS), in which gases accumulate in a vacuum chamber of known volume, are encountered in applications such as food packaging, construction of materials, nuclear and chemical waste vessels, calibration of mass flow meters and mass flow controllers, and characterization of gas separation membranes [1]. The primary purpose of using CVS is the measurement of very low flow rates of gases, in the order of 10^{-8} mol/s and less [2], for which other flow measurement techniques such as bubble-flow meters, or piston placement constant pressure systems fail, or require sophisticated technical building procedures. The second purpose of using CVS is the measurement of the diffusivity coefficient of gases in different media, such as gas permeation membranes and films, and beds of solid particles. This technique, often referred to as a time lag method, utilizes the transient pressure response at the downstream side of the medium to the step pressure change at the upstream side of the medium. The major advantage of using CVS in characterization of membranes and films is that both the diffusivity and permeability coefficients can be measured in a single permeation experiment [3], and the fact that the effect of moisture on the membrane properties is reduced or eliminated [1,4].

It is generally assumed that gases are not subject to any resistance, or momentum loss while accumulating in tubes that are part of CVS. Therefore, the following equation, which is derived from the ideal gas law, is utilized to describe the accumulation process in CVS [3,5-7]:

$$Q_{STP} = \frac{V v_{STP} \frac{dp}{dt}}{RT} \qquad (1)$$

where, Q_{STP} is the flow rate at standard temperature and pressure [cm^3(STP)/s], V is the volume of CVS [m^3], v_{STP} is the volume of one mole of gas at standard temperature and pressure [cm^3(STP)/mol], dp/dt is the rate of pressure increase in CVS [Pa/s], R is the universal gas constant [J/mol K], and T is the absolute temperature [K].

The purpose of this paper is to investigate the effects, if any, of the resistance imposed by vacuum tubes on the pressure response and the flow rate determined from the pressure response during accumulation of gases in CVS. Starting from the Fick's 2nd law of diffusion, a mathematical model describing the theoretical pressure response to a constant flow of gases into CVS was developed. The required diffusivity coefficient was evaluated depending on the initial pressure in CVS considering Knudsen flow, slip flow, combination of Knudsen and slip flows, or Poiseuille flow. The developed model was verified experimentally in a system consisting of tubes with different internal diameters and lengths, which was equipped with two sensitive pressure transducers. A low-flow mass flow controller (MFC) provided different constant flow rates of nitrogen into the experimental CVS. The experiments were performed at different initial pressures. To facilitate the discussion of the results the concepts of time lag and time delay of CVS are utilized.

2. Experimental Set-up and Procedure:

The experimental CVS utilized in this project is shown in Fig. 1. It is composed of two parts, the feed part and the vacuum part, which are separated by a low-flow MFC (C). The feed part of the system is equipped with a pressure gauge (A) and an ultra high purity (UHP) ceramic filter (B). The pressure gauge monitors the absolute pressure at the

feed side, which corresponds to the differential pressure across the MFC; it has a 0 to 207 kPa range and a 0.685 kPa reading accuracy. The UHP ceramic filter (Swagelock model SS-SCF3-VR4-P-30) is capable of removing 99.9999999% of particles as small as 0.003 μm at 30×10^3 cm^3(STP/min), thus protecting the MFC from any mechanical impurities. The maximum flow rate through the MFC (MKS model M-200S) is 0.2 cm^3(STP)/min, while its control ability is 1 - 100% with a 1% accuracy of the full scale. Consequently, the MFC allows controlling very low flow rates that are similar to permeation rates often encountered in characterization of gas separation membranes.

The vacuum part of the system consists of stainless steel tubing (F), or (I) and a large tank (E). The vacuum part is equipped with two pressure transducers (D), several two-way valves, and a vacuum pump (H). All valves in the vacuum side are manually operated diaphragms (Swagelock model SS-DSVCR4) equipped with VCR fittings. The volume of the experimental CVS depends on the inside diameter, the length of the utilized tubing, and the dead volumes associated with the valves and the pressure transducers. For tubing (F) (Swagelock SS-T4-S-049-20) having the inside diameter of 0.00386 m the tube length between the MFC and V5, with V1 closed and V2 opened, is 2.42 m. The tubes downstream from V5 have the same inside diameter as tubing (F) so with V5 opened and V1, V3, V4, V6 closed, the effective length of tubing (F) is increased to 3.83 m. For tubing (I) (Swagelock SS-T8-S-049-20) having the inside diameter of 0.0102 m, the tube length between the MFC and V5 is 7.67 m. The positions of valves V2 and V5 are fixed; therefore, to fit a longer tube between these valves tubing (I) is bended as shown in Fig. 1. Total volumes of the experimental CVS, as determined using a gas expansion technique, are 55.4×10^{-6} m^3 for tubing (F) with V5 closed, 80.4 x

10^{-6} m^3 for tubing (F) with V5 open, and 641 x 10^{-6} m^3 for tubing (I). Tubing (F) and (I) have two slots each, for the installation of pressure transducers. The slots in the idle tubing are capped. In tubing (F) the slots are located 0.513 m and 2.30 m from the MFC, while in tubing (I) they are 0.595 m and 7.36 m from the MFC. The pressure transducers (MKS model 627B11TBC1B) have a linear range from 0 to 1,333 Pa with a 2.67 x 10^{-2} Pa reading accuracy. The tank (E), which has a volume of 8.69 x 10^{-3} m^3, is used to absorb the flow from the MFC immediately after its activation, when the flow rate is trying to reach the set value. The vacuum pump (H) (Edwards model RV3) is used to evacuate the CVS before the actual experiments. The highest vacuum (the lowest absolute pressure), achieved in the experimental CVS was 4.13 Pa. The experimental CVS was tested for leaks at the highest vacuum that could be reached in the system. For tubing (F) with the tube lengths of 2.42 m and 3.83 m, the leak rates were 2.82 x 10^{-7} cm^3(STP)/min and 5.14 x 10^{-7} cm^3(STP)/min, respectively. For tubing (I) the leak rate was 5.97 x 10^{-7} cm^3(STP)/min. The experiments were performed using different initial pressures ranging from 4.13 Pa to 666.61 Pa. The initial pressure was adjusted by means of the vacuum pump and the MFC, letting the system to stabilize after reaching the desired initial pressure. All experiments were performed with an ultra-pure N_2 and the feed side pressure of 108 kPa to prevent air leaks into the system.

Experiments were started by setting a nonzero flow rate through the MFC with V1 opened, and V2, V3, V4 closed. This allowed sending the initially irregular flow rate into the tank (E). After stabilization of the flow rate, which required from 2 s for the maximum flow rate to 15 s for the minimum flow rate, V1 was closed while V2 was subsequently opened, and the gas started to accumulate inside the experimental tube. The

effect of gas existing inside the tubes enclosed between the valves V2, V1 and the MFC at time zero on the accumulation process was neglected. The lowest controllable, constant flow rate of N_2 obtained through the MFC was 0.017 cm^3(STP)/min. The MFC and both pressure transducers were connected to a personal computer equipped with a Lab-View program for recording the values of the flow rate and the dynamic pressures every second.

The experiments in Tubing (F) were performed at 293.16 K, while the experiments in Tubing (I) were performed at 295.16 K.

3. Mathematical Model

Considering that the resistance to accumulation of gases in vacuum tubing of CVS is not negligible, the process is described by the Fick's 2nd law of diffusion:

$$\frac{\partial c}{\partial t} = \nabla(D\nabla c) \tag{2}$$

where, c is the concentration of the gas [mol/m^3] and D is the diffusion coefficient of the gas in tubing [m^2/s]. The experimental CVS consisted of cylindrical tubes of the internal radius r and the length L. Assuming that c does not change in the radial direction, the accumulation process becomes a one-dimensional problem. Furthermore, if D is assumed to be independent of c, Eq. (2) can be written as:

$$\frac{\partial c}{\partial t} = D\frac{\partial^2 c}{\partial x^2} \tag{3}$$

where, x is the distance from the MFC. Assuming applicability of the ideal gas law Eq. (3) can also be written in terms of pressure rather than concentration:

$$\frac{\partial p}{\partial t} = D\frac{\partial^2 p}{\partial x^2} \tag{4}$$

where $p = cRT$, R is the universal gas constant, and T is the absolute temperature.

To solve Eq. (4) it is necessary to specify the initial and two boundary conditions. Initially there is no flow of the gas into the tubing and the pressure is uniform:

$$p(x, t = 0) = p_o = const. \tag{5}$$

At time $t > 0$, the gas starts to flow into the system at $x = 0$ at a constant flow rate Q_{STP} [cm^3(STP)/min]. The condition of constant flow at the entrance can be expressed using the Fick's 1st law of diffusion:

$$\frac{\partial p(x = 0, t)}{\partial x} = -\frac{qRT}{D} \tag{6}$$

where, q is the molar flux of the gas [mol/m^2s] at $x = 0$. On the other hand, at the closed end of the tube ($x = L$) the pressure gradient is always zero:

$$\frac{\partial p(x = L, t)}{\partial x} = 0 \tag{7}$$

The governing partial differential equation – Eq. (4) can now be solved subject to the initial condition specified by Eq. (5) and the two boundary conditions specified by Eqs. (6) and (7). The solution procedure using the principle of superposition and the method of separation of variables is shown in the Appendix; it leads to the following equation:

$$p(x,t) = p_o + \frac{qRT}{DL}\left(Dt + \frac{(L-x)^2}{2} - \frac{L^2}{6}\right) - \frac{2qRT}{DL}\sum_{n=1}^{\infty}\frac{(-1)^n}{\lambda_n^2}e^{-\lambda_n^2 Dt}\cos[\lambda_n(L-x)] \tag{8}$$

where, $\lambda_n = \frac{n\pi}{L}$. The MFC provides the flow rate rather than the molar flux. Replacing q by Q_{STP} and making the other necessary rearrangements, Eq. (8) becomes:

$$p(x,t) = p_o + \frac{Q_{STP}RT}{FDV}\left(Dt + \frac{(L-x)^2}{2} - \frac{L^2}{6}\right) - \frac{2Q_{STP}RT}{FVD}\sum_{n=1}^{\infty}\frac{(-1)^n}{\lambda_n^2}e^{-\lambda_n^2 Dt}\cos[\lambda_n(L-x)] \tag{9}$$

where, V is the volume of the experimental CVS [m^3] and $F = 60 \times 22\,414 = 1.3448 \times 10^6$ is a factor incorporating the conversion of minutes into seconds and moles into cm^3 at standard temperature (273.16 K) and pressure (101 315 Pa) conditions.

The differentiation of Eq. (9) with respect to time gives the following equation:

$$\frac{dp}{dt} = \frac{Q_{STP} RT}{FV}\left[1 + 2\sum_{n=1}^{\infty}(-1)^n e^{-\lambda_n^2 Dt}\cos[\lambda_n(L-x)]\right] \qquad (10)$$

When the product of diffusion coefficient and time is large, the second term of Eq. (10) disappears and it becomes identical to Eq. (1). However, when the product of D and t is small the dp/dt is not a linear function of t and thus the flow rate calculated using Eq. (1) would be associated with an error.

During the course of experiments, as the gas flows into the CVS, the pressure and thus the diffusivity coefficient change. However, utilization of the low-flow MFC allowed performing the experiments using very low gas flow rates resulting in small pressure changes during the course of short experiments.

4. Evaluation of Diffusion Coefficient

The most important parameter in equations (9) and (10), which determines whether there is a resistance to accumulation of gases in CVS, is the diffusivity coefficient. If D were infinitely large, the pressure response to a constant gas flow would be linear, and there would not be any error associated with the use of Eq. (1) for the estimation of flow rate. In other words, the resistance to accumulation of gases would be negligible.

The diffusion coefficient depends on the pressure and the inside diameter of tubing utilized in the CVS. When the mean free path of gas molecules is much smaller

than the diameter of tubing, a gas molecule collides much more frequently with other gas molecules than with the walls of tubing, and the Poiseuille flow occurs. Such conditions exist at relatively high pressures and/or in tubing having large internal diameter. The diffusion coefficient in the Poiseuille flow regime is estimated from the following equation [8]:

$$D = \frac{pr^2}{8\eta} \tag{11}$$

where, p is the pressure [Pa], r is the inside radius of tubing [m], and η is the dynamic viscosity of the gas [kg/m s]. Equation (11) assumes no slipping at the wall of tube. To include possible effects of slipping, Eq. (11) is modified by incorporating the coefficient of slip [8]:

$$D = \frac{pr^2}{8\eta}\left(1 + \frac{4\zeta}{r}\right) \tag{12}$$

where, ξ is the coefficient of slip [m], which is evaluated using the Maxwell's deduction from the kinetic theory of gases [9]:

$$\xi = \frac{\eta}{p}\sqrt{\frac{\pi RT}{2M}}\left(\frac{2-f}{f}\right) \tag{13}$$

where, M is the molecular weight of the gas [kg/kmol], and f, known as the Maxwell's f, is a fraction of gas molecules, which lose their momentum as a result of adsorption and desorption at the walls of tubing. The parameter f depends on the nature of the gas and the tube surface. Using the deflection method for the determination of ξ, Stacy [10] and Van Dyke [11] reported that for air and oxygen in machined brass surfaces f is very close to unity. For pure N_2 and stainless-steel tubing used in this work f was also assumed to be unity.

It is evident from Eq. (13) that the coefficient of slip decreases as the pressure in tube increases. In turn, at relatively high pressures and/or in tubing of large internal diameter, that is, in the Poiseuille flow regime, the term involving the coefficient of slip approaches to unity, and Eq. (12) becomes Eq. (11). Consequently, Eq. (12) is applicable for estimation of D in both, the Poiseuille flow and the slip flow regimes.

When a gas molecule collides much more frequently with the walls of tube rather than with other gas molecules, that is in the Knudsen flow regime, the diffusion coefficient is evaluated using the following equation [8,12]:

$$D = \frac{2}{3} r \sqrt{\frac{8RT}{\pi M}} \tag{14}$$

The Knudsen flow regime occurs in high vacuum and/or in tubes with very small internal diameters. The diffusion coefficient determined from Eq. (14), often referred to as the Knudsen diffusion coefficient, is independent of pressure.

Interestingly, at low p and r, however, before the transition to pure Knudsen region, D calculated from Eq. (12) is less than D calculated from Eq. (14), which indicates that there is another flow regime between the slip flow and the Knudsen flow regimes. The existence of this distinct flow regime, which is referred to as a combination of the slip and Knudsen flows, was confirmed experimentally by steady state flow rates of gases in capillary tubes at different pressure gradients and different mean pressures in the capillaries [13]. In this regime D is determined from the following equation, which is derived from the empirical model of Knudsen [8,13,14]:

$$D = ap + b\frac{1 + c_1 p}{1 + c_2 p} \tag{15}$$

Constant b in Eq. (15) is the Knudsen coefficient of diffusion given by Eq. (14), while constant a is calculated from:

$$a = \frac{r^2}{8\eta} \tag{16}$$

The product ap in Eq. (15) represents the diffusion coefficient in the Poiseuille flow regime. Constants c_1 and c_2 are determined by solving the following set of equations:

$$\frac{c_1}{c_2} = \frac{3\zeta\sqrt{\frac{\pi M}{RT}}p}{8\sqrt{2}\eta} \tag{17}$$

$$c_2 - c_1 = 0.6117\frac{\sqrt{\frac{M}{RT}}}{\eta}r \tag{18}$$

The empirical model of Knudsen allows estimating the pressure at which the minimum diffusion coefficient occurs, and provides a bridge between the Knudsen flow and the slip flow regimes.

Tables 1a and 1b summarize the diffusion coefficients at different pressures, determined using the equations for different flow regimes in tubing (F) and (I), respectively. Underlined pressures show the initial pressures at which the actual experiments were performed. The bold pressures in Table 1a and 1b, represent the conditions at which, according to the empirical Knudsen model, the minimum diffusion coefficient occurs in tubing (F) and (I), respectively. At pressures greater than the pressure at which the minimum diffusion coefficient occurs, the diffusion coefficient determined from the empirical Knudsen model is compared with the diffusion coefficient from the slip flow model. At pressures lower than the pressure at which the minimum

diffusion coefficient occurs, the diffusion coefficient determined from the empirical Knudsen model is compared with the diffusion coefficient for the pure Knudsen flow.

5. Results and discussion:

In this section, the theoretical model for the accumulation of gases in high vacuum tubing, described by Eqs. 9 and 10 is compared with the experimental data. The effects of the distance of pressure transducer from the MFC, the length and diameter of tubing, and the initial pressure are presented. The concepts of time lag and time delay are introduced and discussed.

5.1 The effect of location of pressure transducer

Figures 2a and 2b present the theoretically predicted and experimentally observed pressure responses at different distances from the MFC. The experimental data in both figures is identical; it comes from the experiment performed in Tubing (F) with the valve V5 open, in which N_2 was let into the system through the MFC at a constant flow rate of 0.019 cm^3(STP)/min. Before activation of the MFC, the tubing was in equilibrium at 4.13 Pa. The only difference between figures 2a and 2b is the value of D used for the prediction of the theoretical pressure response. Fig. 2a utilizes D = 0.4666 m^2/s determined from the slip flow model, while Fig. 2b utilizes D = 0.5420 m^2/s determined from the empirical model of Knudsen.

The differences in the diffusion coefficients evaluated from different models are not subject of this paper. However, it appears that a better match between the experimental and theoretical data exist in Fig. 2a, which utilizes the D from the slip flow

model. This model was therefore used for the evaluation of the diffusion coefficient at other initial pressures investigated in this project. As shown in Tables 1a and 1b, as the pressure increases the diffusion coefficients evaluated from the Knudsen empirical model and the slip flow model become identical.

Regardless of the model for D the experimental data follows closely the theoretically predicted shapes of the pressure response curves. The shape of curves in Fig. 2 depends on the distance from the MFC. The curve at 0.513 m from the MFC is concave while the curve at 2.30 m is convex with respect to the time axis. Consequently, there is a pressure difference between the two locations. This pressure difference is a result of a resistance imposed by tubing that prevents a uniform distribution of gas molecules entering the system through the MFC.

According to the theoretical model given by Eq. (9), the pressure response can be divided into two regions, nonlinear and linear. In reality however, the pressure response can be divided into three regions, nonlinear, apparently linear, and linear. The nonlinear region in Fig. 2 disappears at $t > 15$ s, that is, when the product Dp becomes relatively large. Theoretically, at this point the pressure difference between two locations should be constant and equal to 4 Pa. However, as shown in Fig.2a the experimental pressure difference slightly decreases towards the end of the experiment at 30 s.

The validity of the theoretical model strongly depends on the relative pressure increase during the experiment. As the pressure increases, the diffusion coefficient increases and the resistance imposed by the tubing decreases. The decrease in tubing resistance allows for a more uniform distribution of gas molecules in the system, and thus a decrease in the pressure difference between any two points of the system. Therefore,

although the pressure response following the nonlinear region appears to be linear, in reality it is not, and this is why it will be referred to as an "apparent linear response". The slope of the lower pressure response curve increases, while the slope of the upper response curve decreases with time. The apparent linear response lasts until the two slopes become identical, which occurs only when there is no pressure gradient within the tube. Consequently, the apparent linear response might last for a relatively long time, much longer that the nonlinear response region predicted by the model.

Figure 3 presents the plots of the pressure difference at two different locations for two different flows as a function of time. The experiments depicted in Fig. 3 were performed in Tubing (I) that was initially in equilibrium at 13.3 Pa. The pressure responses to two constant flow rates of N_2 of 0.018 and 0.032 cm^3(STP)/min, respectively, were simultaneously monitored 0.595 m and 7.36 m from the MFC. It can be noticed that before the time axis breaks at 30 s there is a relatively good match between the experimental and theoretical data, which indicates that the pressure difference between the two locations, as predicted by Eq. (9), is proportional to Q_{STP}. After five minutes, however, the experimentally determined pressure difference decreases considerably, although it is still not equal to zero. This small pressure difference is inherent to the system and it is due to non-ideality of the system. It should be noted that for the higher flow rate the decreasing tendency begins even before the break in the time axis.

5.1.1 Concept of time lag and resistance of the vacuum system.

For the purpose of the following discussion, it is assumed that the slope of pressure response in the second region - the apparent linear response region, is independent of the position. This assumption is valid for relatively short experiments, during which the coefficient of the diffusion evaluated at the initial pressure is practically constant.

Considering the analogy with the gas transport in porous media and membranes [12], the process of accumulation of gases in vacuum tubing can be characterized by two parameters: the time lag and the resistance of the system. The time lag is obtained by extrapolating the linear portion of the pressure versus time curve to the time axis after the linear pressure response has been attained. The mathematical expression for the time lag (θ_v) of a vacuum tube of uniform diameter and length L can be obtained as follows. When the product Dt becomes large, Eq. (9) simplifies to:

$$p = p_0 + \frac{Q_{STP} RT}{FVD}\left[Dt + \frac{(L-x)^2}{2} - \frac{L^2}{6} \right] \tag{19}$$

Setting p equal to p_o in the above equation and solving for t gives the desired expression for θ_v:

$$t = \theta_v = \frac{L^2}{6D} - \frac{(L-x)^2}{2D} \tag{20}$$

According to Eq. (20), θ_v depends on the distance from the MFC, the length of tubing, and the diffusion coefficient. Depending on x, θ_v can be positive or negative. For $x = 0$, Eq. (20) becomes:

$$\theta_v = -\frac{L^2}{3D} \tag{21}$$

For $x = L$, Eq. (20) becomes:

$$\theta_v = \frac{L^2}{6D} \tag{22}$$

The existence of positive and negative time lags is evident in Fig. 2. For the upper curve obtained at the position near to the MFC, the experimental θ_v is negative. On the other hand, for the lower curve obtained at the position near to the closed end of the tube, the experimental θ_v is positive. Theoretically, it is possible to determine the position for which the time lag is zero. Setting $\theta_v = 0$ in Eq. (20) and solving for x leads to:

$$x = \frac{3-\sqrt{3}}{3} L \cong 0.423L \tag{23}$$

According to Eq. (23) the position for which $\theta_v = 0$ is independent of D and thus independent of the initial pressure and the diameter of tubing.

Equations (21) and (22) are identical with the expressions for the entrance and exit time lag, respectively, in one-dimensional media such as flat sheet membranes [12]. Using this analogy, the resistance (R_S) to gas accumulation in a tube of length L can be expressed by the following equation:

$$R_S = \alpha \frac{L^2}{D} \tag{24}$$

where, α is a constant. The length in Eq. (24) is analogous with the membrane thickness. The diffusion coefficients in membranes are orders of magnitude lower than those listed in Tables 1a and 1b. However, the resistance to gas transport in vacuum systems might be comparable to that in membranes, because the length of vacuum tubing is normally much greater than the membrane thickness. Consequently, the resistance of vacuum tubes

should be taken into consideration when determining the diffusion coefficient of gases in membranes using the time lag method.

5.1.2 Error in gas flow rate determined from the pressure rise and the concept of time delay

The resistance to gas transport in vacuum tubing results in time lag of the system and the difference in pressures measured at different locations of the system. Another consequence of the resistance to gas transport in vacuum tubing is a possible error associated with the measurement of gas flow rate by the pressure rise technique.

As already mentioned in the introduction, it is generally assumed that the resistance to gas accumulation in vacuum tubes is negligible, and consequently the flow rate of gas into CVS is considered to be proportional to the rate of pressure increase (dp/dt). On the other hand, the rate of pressure increase resulting from initiation of the constant flow rate of gas into a vacuum tube is governed by Eq. (10), and when the product Dt is small, the rate of pressure increase is not proportional to the flow rate of the gas. In other words, Eq. (1) will accurately describe the flow only after the pressure response to the constant flow rate becomes a linear function of time.

Figure 4 presents the plots of the flow rate as a function of time at two different distances from the MFC. The apparent flow rates were calculated from Eq. (1) using dp/dt evaluated from the pressure transducers readings and dp/dt calculated from Eq. (10). In addition, Fig. 4 also includes the flow rate of N_2 measured by the MFC. The experiment depicted in Fig. 4 was performed in Tubing (F) with the valve V5 opened.

The system was initially in equilibrium at 4.13 Pa; the actual value of the flow rate of N_2 was 0.019 cm^3(STP)/min.

It is evident in Fig. 4 that immediately after initiation of the gas flow, the flow rates determined from the pressure rise are significantly different from the actual flow rate. Except for the first second at the position near to the MFC the flow rates determined using the experimentally measured and theoretically calculated dp/dt are consistent with each other. The discrepancy between the experimental and theoretical dp/dt near the MFC is probably due to the manual control of the valves.

The error in the flow rate determined from the pressure rise depends on time and the distance from the MFC. This error can be predicted theoretically by considering the nonlinear term in Eq. (10). The effects of time and position on the theoretical error that would occur in Tubing (F), initially at 4.13 Pa, with V5 opened are presented in Figure 5. Apart from the positions near the MFC (x/L = 0.0765) and near the closed end of the tube (x/L = 0.924), Fig. 5 also includes x/L = 0.423, which corresponds to the zero time lag, and x/L = 0.5.

The negative error of 100% at a given time and position indicates the zero flow rate, which means that gas molecules entering the system through the MFC have not yet reached that location. Regardless of the position, for some time after initiation of the flow, a negative error exists. Although not shown in Fig. 5, even at x/L = 0.0765 for t < 0.01 s there is a negative error. Generally, for any x/L < 0.5 after the initial negative values the error becomes positive and then approaches to zero. This is best illustrated in case of x/L = 0.423. While the value of the negative error is limited to 100%, there is no

such limit for the positive error. For example, at x/L = 0.0765 the error after 1 second is estimated as 162%.

It is interesting to note that the time for the error to disappear at the position corresponding to the zero time lag (x/L = 0.423) is greater than at x/L = 0.5. This indicates that the position for the zero time lag might not be the optimum location of the pressure transducer for the pressure rise method. The time for the error to disappear, or more conveniently the time for the error to fall within a certain percentage of actual flow rate, might be a convenient measure of the resistance to gas transport in high vacuum tubing. This time, which will be referred as a time delay, can be determined by solving the following equation:

$$\left| 2\sum_{n=1}^{\infty} (-1)^n e^{-\lambda_n^2 Dt} \cos[\lambda_n (L-x)] \right| \times 100\% = A \tag{25}$$

where, A is an arbitrary percentage related to the actual flow rate of the gas. The absolute value from the term on the left hand side reflects the fact that the error can be positive or negative. It is important to note that according to Eq. (25) the error in the apparent flow rate does not depend on the actual flow rate of the gas into the system.

Figure 6 presents the effect of time on the error in the apparent flow rate for different actual flow rates of the gas. The results shown in Fig. 6 were obtained in the experiments in Tubing (I) at the initial pressure of 4.13 Pa, based on the pressure readings taken 7.36 m from the MFC, that is, near to the closed end of the tube. For comparison, a solid line, which represents the error determined from the theoretically predicted dp/dt, is also included in Fig. 6. It can be noticed that while there are some deviations between different actual flow rates, all experimental points follow a trend similar to the theoretical line, thus confirming that the error is independent of the actual flow rate.

The most noticeable deviation between the theoretically predicted and experimentally observed errors in Fig. 6 is the fact that the latter becomes positive after approximately 8 seconds while the former remains negative. This deviation is due to the existence of the apparent linear response region, which is not predicted by the mathematical model. The resistance imposed by the tubes at high vacuum leads to a non-uniform distribution of gas molecules entering the system. There is an excess of gas molecules near to the MFC and their deficiency near to the closed end of the tube. Since the resistance is inversely proportional to the diffusion coefficient, which in turn increases with pressure, the resistance decreases during the course of the experiment. The decreasing resistance leads to a decrease in excess and deficiency of gas molecules at the two opposite ends of the tube with time. As a result, in the apparent linear response region, the flow rate evaluated from the pressure rise near the MFC underestimates the actual flow rate, while the flow rate evaluated near to the closed end of the tube overestimates the actual flow rate of the gas entering through the MFC.

Figure 7 presents the plot of the theoretical time delay as a function of dimensionless position (x/L). The calculations were performed for Tubing (F) with V5 opened, for the initial pressure of 4.13 Pa, assuming A = 1%. The plot shown in Fig. 7 appears to be symmetrical with respect to x/L = 0.5. However, the minimum theoretical time delay occurs at x/L = 0.49 rather than at x/L = 0.50. This is because after changing the sign from negative to positive, the error at x/L = 0.49 does not go above the set 1%. If A were greater than 1%, the position for the minimum time delay would be at $x/L < 0.49$. On the other hand, if A were less than 1%, the position for the minimum time delay would be at $x/L > 0.49$; however, it would never exceed x/L = 0.50.

It is important to emphasize that because of the existence of the apparent linear response region, the actual time delays might be orders of magnitude greater than those shown in Fig. 7, especially at the positions near the MFC and near the closed end of the tube.

5.2 Effect of other parameters

Apart from the distance from the MFC, the pressure response and the apparent flow rate also depend, according to Eqs. (9) and (10), on the length of tube, and through the diffusion coefficient, on the initial pressure and the tube diameter.

5.2.1 Effect of the initial pressure and the diameter of tubing

According to the empirical model of Knudsen and the slip flow model; the diffusion coefficient depends on the pressure and diameter of tubing. For the initial pressures considered in this work, the diffusion coefficient of N_2 increases with the pressure and the internal diameter of the tube.

Figures 8 and 9 present the theoretical and experimental pressure responses at two different locations for two different initial pressures in Tubing (F) and Tubing (I), respectively. The two initial pressures considered in both tubes were of 4.13 Pa and 13.3 Pa. In case of the experiments in Tubing (F), the actual flow rates of N_2 were 0.019 cm^3(STP)/min for the lower initial pressure and 0.018 cm^3(STP)/min for the higher initial pressure. (See Appendix D for figures similar to Fig. 9 with higher flow rates and different tubing.) In case of the experiments in Tubing (I), the actual flow rates of N_2

were 0.017 cm^3(STP)/min for the lower initial pressure and 0.018 cm^3(STP)/min for the higher initial pressure.

It is evident that the theoretical pressure response at both locations and for both initial pressures follows closely the experimental data in Figs. 8 and 9. Focusing on the apparent linear response region, it can be noticed that the difference between the pressures at two locations depends on both the initial pressure and the diameter of tubing. For the experiments performed at in Tubing (F), the pressure difference at the beginning of the apparent linear response region is 3.9 Pa when the initial pressure is 4.13 Pa and 2.5 Pa when the initial pressure is 13.3 Pa. The decrease in the pressure difference is entirely due to increase in the diffusion coefficient. As the initial pressure in Tubing (F) increases from 4.13 Pa to 13.3 Pa, the diffusion coefficient increases from 0.467 m^2/s to 0.711 m^2/s. As shown in Fig. 9, a similar effect of the initial pressure on the pressure difference exists in Tubing (I).

The comparison of the pressure difference in two experiments performed at the same initial pressure but in different tubes, indicates that the pressure difference in Tubing (F) is greater than the pressure difference in Tubing (I). For example, in the experiments performed at the initial pressure of 4.13 Pa, these differences are 3.9 and 0.8 Pa, respectively. The difference in pressures recorded at two different locations is proportional to the actual flow rate of the gas. The flow rate of N_2 in Tubing (F) was 10% greater than the flow rate of N_2 in Tubing (I), and this partly contributes to the greater pressure difference observed in the former tube. On the other hand, the distance between the pressure transducers in Tubing (F) of 1.79 m is much smaller than that of 6.76 m in Tubing (I). It seems logical that placing pressure transducers further apart should increase

the difference between the pressures they record. In this case however, the dominant factor is the diffusion coefficient. For the initial pressure of 4.13 Pa, the diffusion coefficients in Tubing (F) and Tubing (I) are 0.467 m^2/s and 1.71 m^2/s, respectively. This more than three–fold difference in D is entirely due to the difference in the internal diameters of the utilized tubes. The internal diameters of Tubing (F) and Tubing (I) are 3.86×10^{-3} m and 10.2×10^{-3} m, respectively. Figures 8 and 9 prove that in relatively short experiments the combined effect of the initial pressure and the internal diameter on the pressure response is well predicted by the theoretical model. They also confirm the validity of the estimated diffusion coefficients.

The difference between the pressures recorded at two different locations results from the resistance to gas accumulation in high vacuum tubes. However, since this difference also depends on the actual flow rate of the gas, it is not suitable for the characterization of the system resistance. The theoretical time delay, on the other hand, is independent of the actual flow rate of the gas, and therefore is more suitable for characterization of the system resistance than the pressure difference.

Table 2 presents the summary of calculations of the theoretical time delay at the position x/L = 0.5 for different combinations of the initial pressures, ranging from 1 to 100 Pa, and the sizes of standard stainless steel tubing ranging from 1/8" to 1". The time delay was calculated using Eq. (25) with A = 1% assuming the tube length of 1 m. Since for some internal diameters the considered initial pressures were lower that the pressures for which the minimum diffusion coefficient occurs, the diffusion coefficients were evaluated from the empirical model of Knudsen rather than the slip flow model.

Generally, for a given pressure the theoretical time delay increases with decrease in tube diameter. On the other hand, the relationship between the theoretical time delay and the pressure depends on the internal diameter of tubing. For the two larger tubes the time delay decreases with increase in pressure. For the two smaller tubes, because of the minimum diffusion coefficient, the maximum time delay occurs at pressures greater than 1 Pa. Regardless of the combination of the internal diameter and the initial pressure all theoretical time delays listed in Table 2 are less than one second, and could be considered as negligible. On the other hand, as shown in Fig. 7, the theoretical time delay near x/L = 0.5 is a very strong function of the dimensionless position. Any shift from x/L = 0.5 might increase the time delay several times. Moreover, because of the existence of the apparent linear response region, not predicted by the theoretical model, the actual time delays might be considerably greater than the values listed in Table 2.

5.2.2 Effect of tube length

In the previous section it was pointed out despite significantly greater distance between the pressure transducers in Tubing (I), the difference between the recorded pressures was significantly smaller than that in Tubing (F), in which the pressure transducers were much closer to each other. Based on this observation one could conclude that the influence of the tube length on the resistance to gas accumulation is not as significant as that of the internal diameter. To evaluate the actual effect of tube length the experiments were performed in Tubing (F) with V5 either opened, or closed. Opening V5 allowed increasing the tube length from 2.42 m to 3.83 m, while the internal diameter remained the same.

Figure 10 presents the comparison of the experimental and theoretical pressure responses in two tests in Tubing (F) performed at the same initial pressures (4.13 Pa) with the same actual gas flow rates (0.019 cm^3(STP)/min), however using different tube lengths. It can be noticed that once the apparent linear response region is reached, the difference between pressure readings in the shorter tube is approximately 2.4 Pa compared to 4.0 Pa in the longer tube. The experimental data follows very closely the theoretical pressure response curves. The slight difference between the theoretical and experimental values in the shorter tube is probably due to the neglected effect of the gas existing in the small portion of tubing between the MFC and the valves V1 and V2.

The effect of the length of tubing on the resistance to gas accumulation is assessed in Figure 11 by considering the effect of tube length on the theoretical time delay at x/L = 0.5 for different internal diameters. The calculations of time delay were performed for the pressure of 4.13 Pa, that is, the lowest pressure obtained in the experimental system. It is evident that regardless of the tube diameter, the time delay increases with the increase of the tube length. Moreover, the relationships between the time delay and the tube length appears to be parabolic. This is consistent with Eq. (24) according to which, the resistance to gas accumulation in a tube of uniform diameter is proportional to the square of the tube length.

6. Conclusions:

The proposed mathematical model originating from the Fick's second law of diffusion was found to successfully describe the accumulation behavior of gases in vacuum tubing immediately after initiation of the gas flow into the system. In particular,

the existence of a nonlinear pressure response region, in which a local dynamic pressure is not proportional to the flow rate of the gas entering the system, has been confirmed experimentally. The presence of a nonlinear pressure response region indicates a non-negligible resistance encountered by gas molecules accumulating at typical conditions existing in constant-volume mass accumulation systems. As a result, such systems could be characterized by their time lag. The model predicts the transition from the nonlinear region into the linear region, in which the local dynamic pressure is proportional to the flow rate of the gas entering the system, within 15 seconds. The time required for the nonlinear region to disappear, that is, the time delay, was considered to be another convenient measure of the system resistance to gas accumulation. Even when the non-linear region disappears, the distribution of gas molecules in the system is not uniform, that is, there is a nonzero pressure gradient in the direction of gas flow.

The proposed model assumes that the diffusion coefficient is constant. While this assumption is valid in short experiments, it fails in long experiments because of the dependence of the diffusion coefficient on pressure. In particular, for the conditions studied in this project the diffusion coefficient increases with pressure. Consequently, the resistance and hence the pressure gradient existing in the system after the disappearance of the nonlinear response region, decrease with time. The decrease in the pressure gradient with time, not predicted by the proposed model, is responsible for a nonlinear pressure response even after the theoretically calculated time delay. This second region, referred to as the apparent linear response region, exist until there is no resistance to gas accumulation, that is, until there is a uniform pressure anywhere within the system. The flow rate measured from the pressure rise in the apparent linear response region is

therefore associated with an error. In particular, at the positions near to the closed end of the tube, the flow rate evaluated from the pressure rise overestimates the actual flow rate. At the positions near to the open end of the tube the situation is opposite. While the magnitude of the error associated with measurement of the flow rate in the apparent linear response region is generally much lower than in the nonlinear response region, it is far from being negligible.

To minimize the error associated with the measurement of gas flow rates by the pressure rise technique in a constant-volume mass accumulation system consisting of a tube of uniform diameter, the pressure should be monitored in the middle between the open and the closed end of the tube. In addition, the length of the tube should be minimized while its diameter maximized; if possible, very high vacuum should be avoided.

7. List of Symbols

D: Diffusion coefficient (m^2/s)

f: Fraction of gas molecules absorbed by tube walls (-)

L: Length of tube (m)

M: Molecular weight (kg/kmol)

p: Pressure (Pa)

p_o: Initial pressure (Pa)

t: Time (s)

q: Molar flux ($mol/m^2 s$)

Q_{STP}: Flow at standard temperature and pressure (cm^3(STP)/min)

R: Universal gas constant (J/mol K)

r: Inside radius of tubing (m)

T: Absolute temperature (K)

V: Volume of vacuum tube or system (m^3)

v_{STP}: Molecular volume at standard pressure and temperature (cm^3/mol)

x: Location (m)

c : Concentration of gas [mol/m^3]

F: Conversion factor (-)

R_S: Resistance in vacuum system (s)

a, b, c_1, c_2: Knudsen empirical model's constants

Greek Symbols

θ_v: Time lag of the vacuum system (s)

η: Dynamic viscosity of gases (kg/m s)

ξ: Coefficient of slip (m)

8. References:

1. S. A. Stern, P.J. Gareis, T.F. Sinclair, and P.H Mohr, J. Appl. Polymer Sci. 7, 2035 (1963).
2. E. B. Arkilic, M.A. Schmidt, and K.S. Breuer, Experiments in Fluids **25**, 37 (1998).
3. R. M. Barrer, Trans. Faraday Soc. **35**, 628 (1939).
4. B. Kruczek, in Polyphenylene Oxide and Modified Polyphenylene Oxide Membranes Gas, Vapor and Liquid Separation, edited by G. Chowdhury, B.

Kruczek, and T. Matsuura (Kluwer Academic Publishers, Boston, 2001), pp 83-87.

5. W. Heilman, V. Tammela, J.A. Mayer, V. Stannett, and M. Szwarc, Ind. Eng. Chem. **48**, 821(1956).
6. R. M. Barrer and G. Skirrow, J. Polymer Sci. **3**, 549 (1948).
7. G. J. Van Amerongen, J. Applied Phys. **17**, 972 (1946).
8. L. B. Loeb, The Kinetic Theory of Gases, 3rd ed. (Dover publications, Inc., New York, 1961), pp 278-300.
9. J. C. Maxwell, in The Scientific Papers of James Clerk Maxwell, edited by W. D. Niven, M.A., F.R.S. (Dover publications, Inc., New York, 1965), pp 703-712.
10. L. J. Stacy, Phys. Rev. **21**, 239 (1923).
11. K. S. V. Dyke, Phys. Rev. **21**, 250 (1923).
12. S. W. Rutherford and D.D. Do, Adsorption **3**, 283 (1997).
13. Knudsen, Ann. der Physik **28**, 117 (1909).
14. R. A. Millikan, Phys. Rev. **21**, 217 (1923).
15. R. Haberman, Elementary Applied Partial Differential Equations with Fourier Series and Boundary Value Problems (Prentice-Hall, Inc., New Jersey, 1983), pp 28-123.

Table Ia. Evaluation of the diffusion coefficient of N_2 in tubing (F) of the internal diameter of 0.00386 m at $T = 293.16$ K using different models.

Pressure [Pa]	Diffusion Coefficient - D [m^2/s] Knudsen empirical model - Eq. (17)	Knudsen flow Eq. (16)	Slip flow Eq. (14)
1.333×10^{-3}	0.6056	0.5997	-
1.333×10^{-2}	0.6043	0.5997	-
0.7999	0.5504	0.5997	-
1.333	0.535	0.5997	-
2.306	**0.5272**	**0.5997**	**0.4181**
4.133	0.542	-	0.4666
6.666	0.587	-	0.5339
9.999	0.66	-	0.6225
13.33	0.741	-	0.7111
33.33	1.255	-	1.242
66.66	2.135	-	2.128
99.99	3.018	-	3.014
133.3	3.903	-	3.899

Table Ib. Evaluation of the diffusion coefficient of N_2 in tubing (I) of the internal diameter of 0.0102 m at $T = 295.16$ K using different models.

Pressure [Pa]	Diffusion Coefficient - D [m^2/s] Knudsen empirical model - Eq. (17)	Knudsen flow Eq. (16)	Slip flow Eq. (14)
1.333×10^{-3}	1.606	1.591	-
1.333×10^{-2}	1.597	1.591	-
0.1333	1.525	1.591	-
0.4	1.438	1.591	-
0.8799	**1.399**	**1.591**	**1.11**
4.133	1.805	-	1.711
6.666	2.241	-	2.179
9.999	2.837	-	2.795
13.33	3.443	-	3.411
33.33	7.12	-	7.107
66.66	13.27	-	13.27
99.99	19.43	-	19.43
133.3	25.59	-	25.59

Table II. Effect of the initial pressure and the internal diameter (ID) of tube on the theoretical time delay (s) at $x/L = 0.5$. The theoretical time delay calculated from Eq. (25) assuming $A = 1\%$ for stainless steel tubes of length $L = 1$ m.

Time delays at x/L = 0.5 in standard 1 m long stainless steel tubes				
Tubig ID* p_0 [Pa]	0.175×10^{-2} m	0.386×10^{-2} m	1.02×10^{-2} m	2.12×10^{-2} m
1	0.53	0.25	0.1	0.05
2	0.55	0.26	0.1	0.04
4	0.56	0.25	0.08	0.03
10	0.54	0.21	0.05	0.02
20	0.47	0.15	0.03	<0.01
40	0.35	0.1	0.02	<0.01
100	0.19	0.05	<0.01	<0.01

* The above internal diameters correspod to the outside dimeters (OD) of standard stainless steel tubes of 1/8", 1/4", 1/2", 1", respectively.

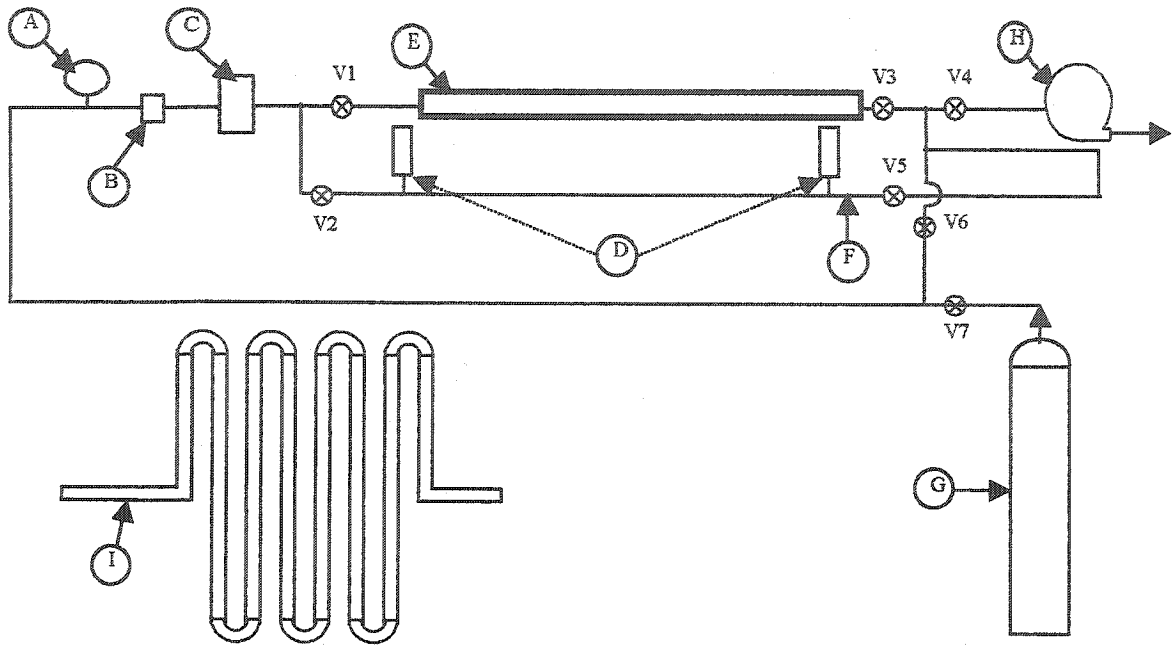

Figure 1. Schematic diagram of the experimental set-up: (A) pressure gage; (B) ceramic filter; (C) MFC; (D) pressure transducers; (E) auxiliary tank; (F) & (I) tubing; (G) feed tank; (H) vacuum pump.

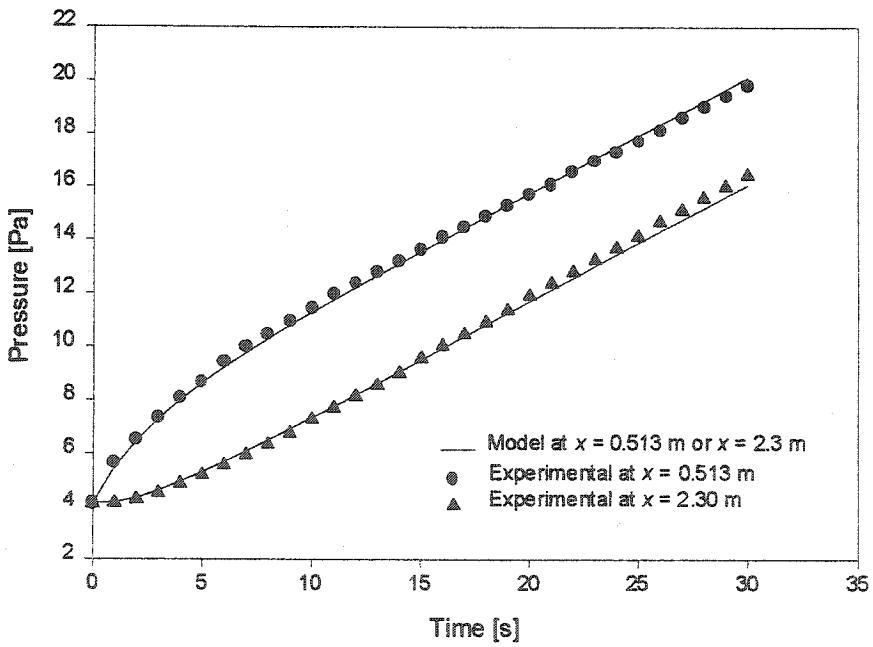

Figure 2-a. Comparison of the experimental pressure response to the constant flow rate of N_2 of 0.019 cm^3(STP)/min at the positions x = 0.513 m and x = 2.30 m in a 3.83 m long, 0.00386 m internal diameter tube, initially in equilibrium at 4.13 Pa, with the theoretical pressure response determined using the diffusion coefficients estimated from the slip flow model.

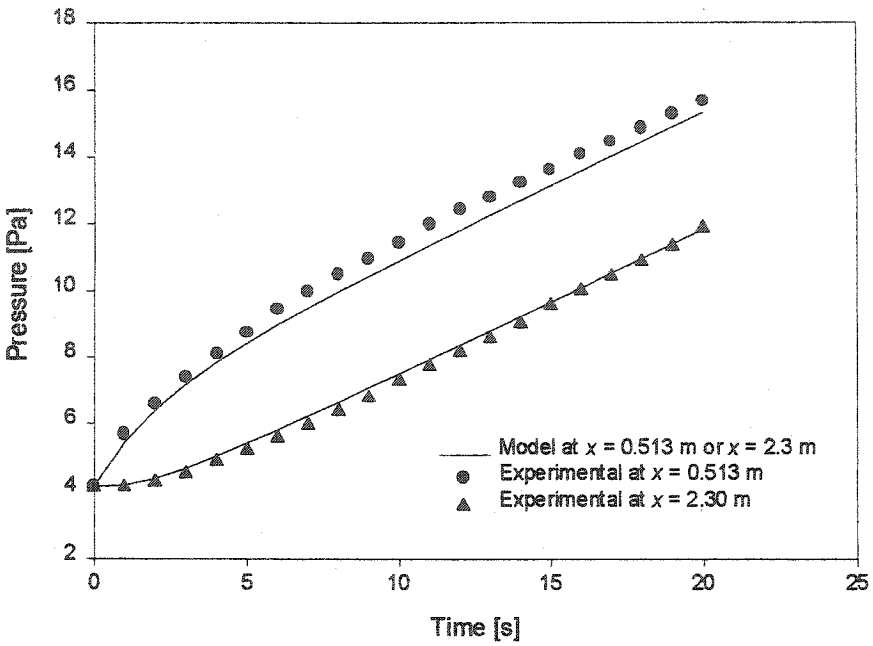

Figure 2-b. Comparison of the experimental pressure response to the constant flow rate of N_2 of 0.019 cm^3(STP)/min at the positions x = 0.513 m and x = 2.30 m in a 3.83 m long, 0.00386 m internal diameter tube, initially in equilibrium at 4.13 Pa, with the theoretical pressure response determined using the diffusion coefficients estimated from the empirical model of Knudsen.

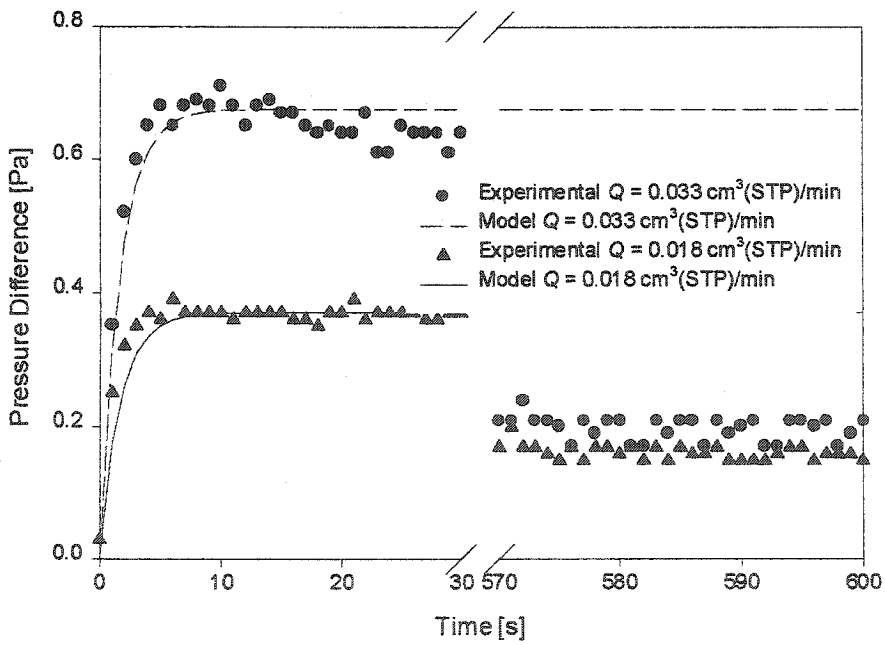

Figure 3. Effect of the actual flow rate on the pressure difference between the positions x = 0.595 m and x = 7.36 m in a 7.67 m long, 0.0102 m internal diameter tube, initially in equilibrium at 13.3 Pa.

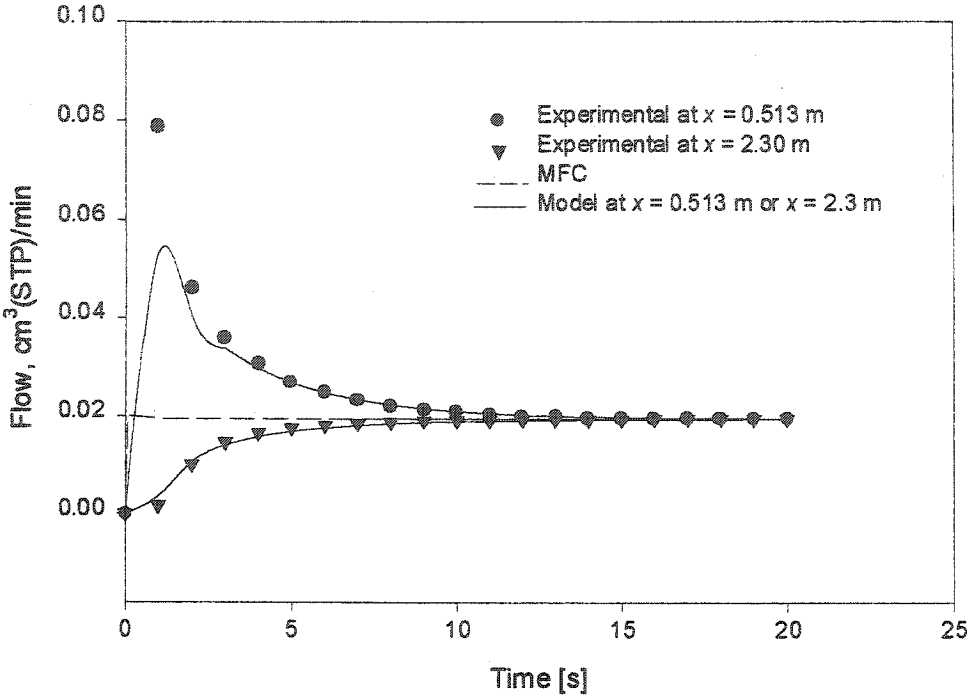

Figure 4. Comparison of the apparent flow rates of N_2 determined from the experimentally observed and theoretically predicted pressure responses to the constant flow rate of 0.019 cm^3(STP)/min at x = 0.513 m and x = 2.30 m in a 3.83 m long, 0.00386 m internal diameter tube, initially in equilibrium at 4.13 Pa.

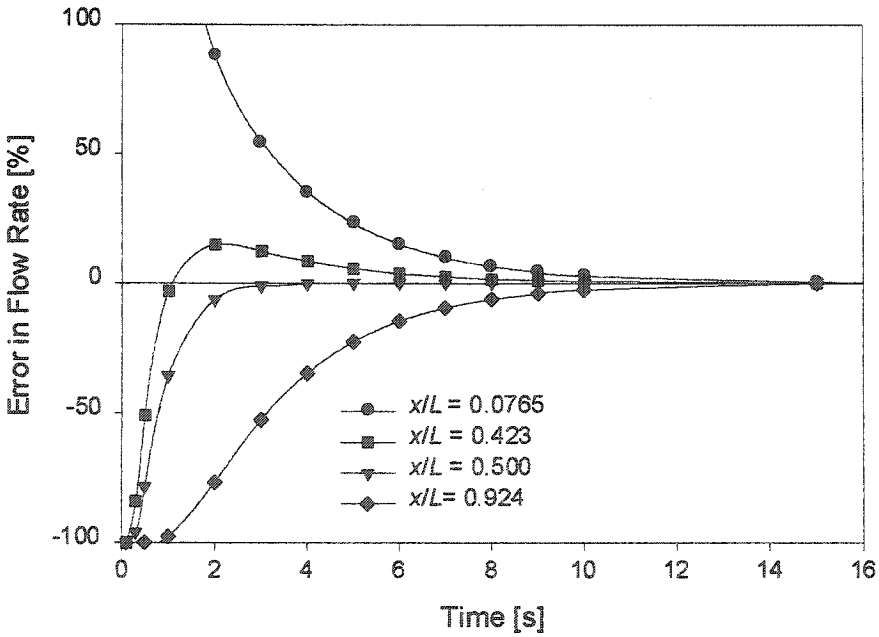

Figure 5. Effect of time and the dimensionless distance from the MFC on the theoretically predicted error in the apparent flow rate of N_2 in a 3.83 long, 0.00386 m internal diameter tube, initially in equilibrium 4.13 Pa.

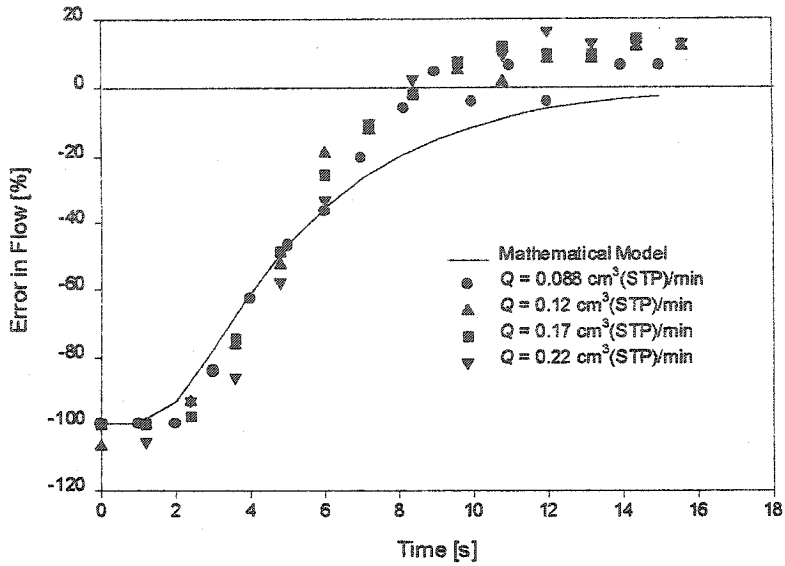

Figure 6. Effect of time and the actual flow rate on the experimentally observed error in the apparent flow rate of N_2 at x = 7.36 m in a 7.67 m long and 0.0102 m internal diameter tube, initially in equilibrium at 4.13 Pa.

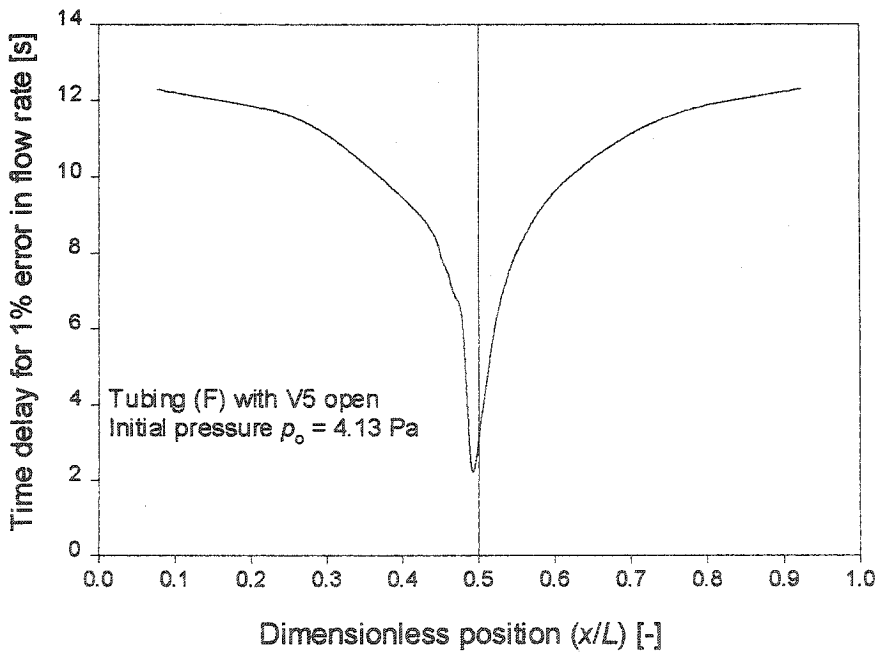

Figure 7. Effect of the dimensionless distance from the MFC on the theoretical time delay in a 3.83 m long, 0.00386 m internal diameter tube, initially in equilibrium at 4.13 Pa. The theoretical time delay calculated from Eq. (25) assuming A = 1%.

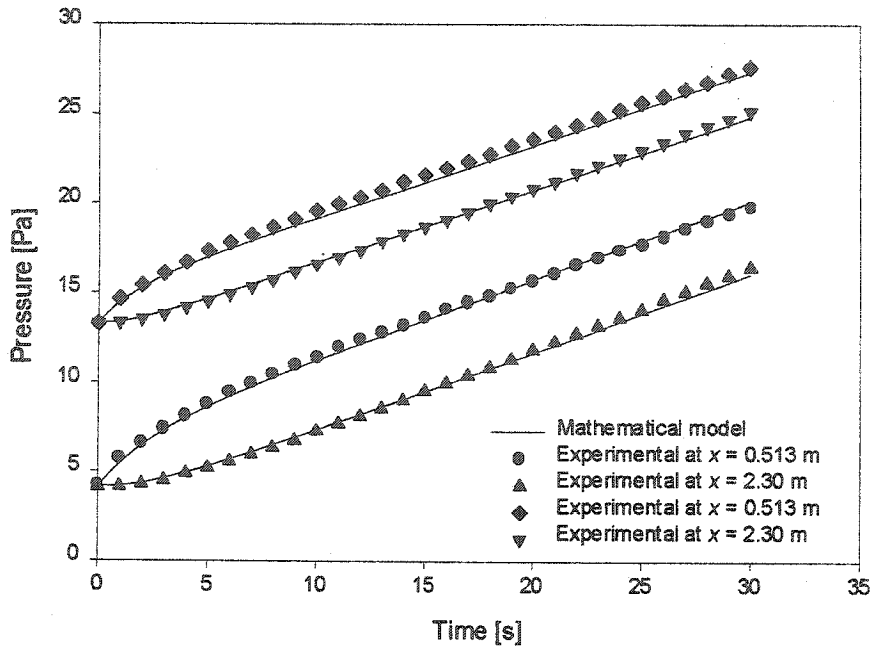

Figure 8. Effect of the initial pressure on the theoretical and experimental pressure responses to the constant flow rate of N_2 at the positions x = 0.513 m and x = 2.30 m in a 3.83 m long, 0.00386 m internal diameter tube. For the initial pressure 4.13 Pa, Q_{STP} = 0.019 cm^3(STP)/min; for the initial pressure of 13.3 Pa, Q_{STP} = 0.018 cm^3(STP)/min.

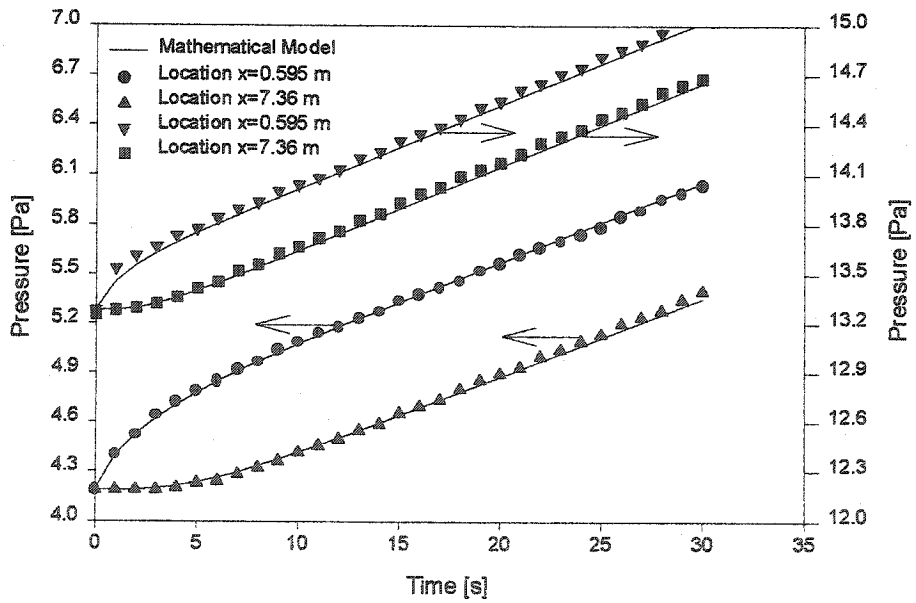

Figure 9. Effect of the initial pressure on the theoretical and experimental pressure responses to the constant flow rate of N_2 at the positions x = 0.595 m and x = 7.36 m in a 7.67 m long, 0.0102 m internal diameter tube. For the initial pressure 4.13 Pa, Q_{STP} = 0.017 cm^3(STP)/min; for the initial pressure of 13.3 Pa, Q_{STP} = 0.018 cm^3(STP)/min.

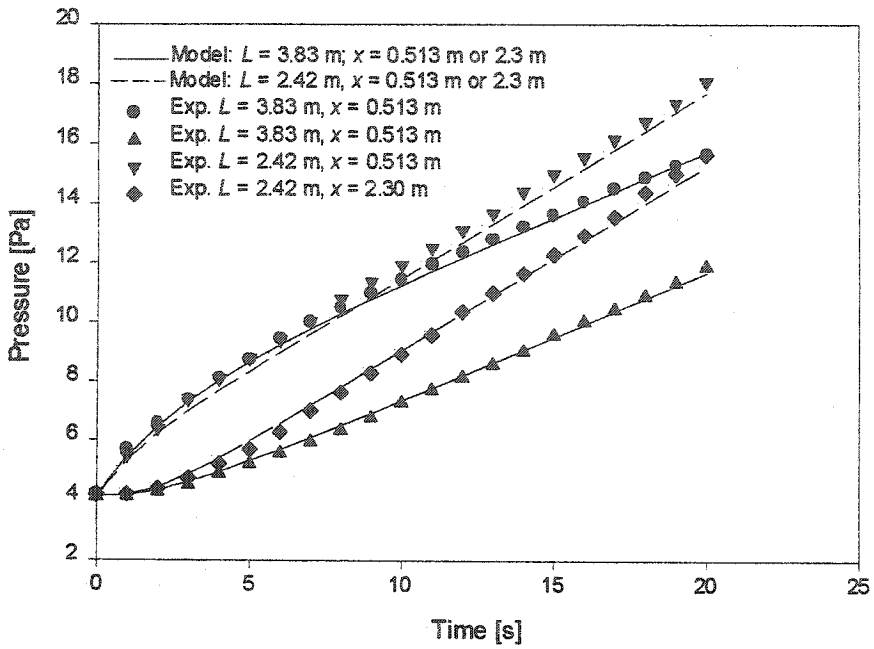

Figure 10. Effect of tube length on the theoretical and experimental pressure responses to the constant flow rate of N_2 of 0.019 cm^3STP/min at the positions x = 0.513 m and x = 2.30 m in a 0.00386 m internal diameter tube, initially in equilibrium at 4.13 Pa. The tube lengths considered: 2.42 m and 3.83 m, respectively.

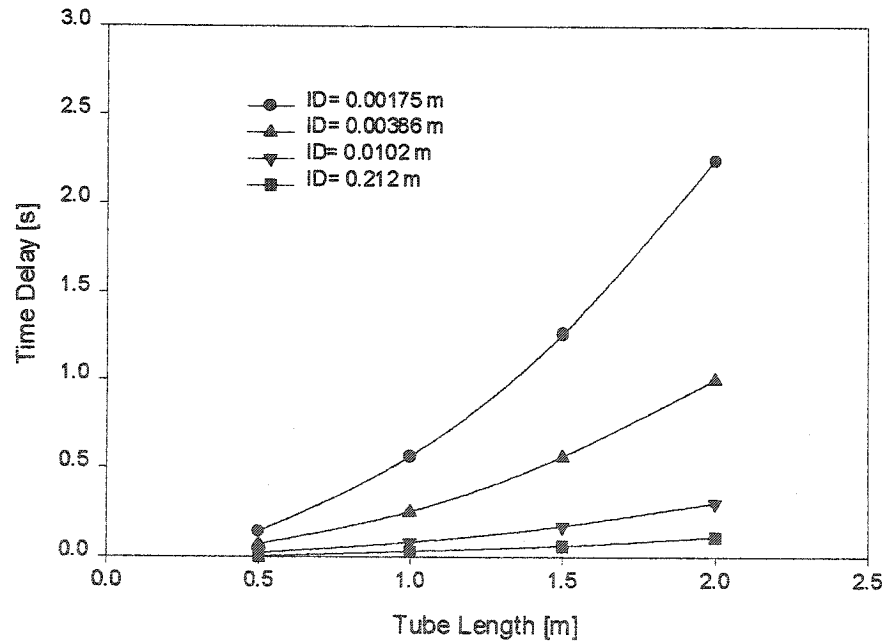

Figure 11. Effect of length and internal diameter of tube, initially in equilibrium at 4.13 Pa, on the theoretical time delay at the dimensionless position x/L = 0.5. The theoretical time delay calculated from Eq. (25) assuming A = 1%.

CHAPTER III

Effect of Resistance of Vacuum Tubes on Time Lag of Membrane in Constant Volume Systems. Part I: Theoretical Considerations

R. Chapanian, B. Kruczek*

Department of Chemical Engineering
University of Ottawa
161 Louis Pasteur Street
Ottawa, ON K1N 6N5
Canada

* To whom correspondence should be addressed.
(Submitted to: Journal of Membrane Science, December 2, 2003)

Abstract

The concept of time lag, which was first introduced in 1920 by Daynes, has been widely used for the determination of diffusion coefficient of gases in porous and non-porous media. In case of solution-diffusion membranes this concept is even more appealing because in addition to the diffusion coefficient, the permeability and solubility coefficients can be determined from a single gas permeation experiment. Specifically, the gas permeation experiment is performed in a constant volume (CV) testing system, in which tested membrane, initially at vacuum, is instantaneously pressurized at the feed side and the resulting pressure rise is monitored at the permeate side of membrane. Although not explicitly stated, the concept of time lag assumes that the entire resistance to gas transport during the gas permeation experiment comes from the tested medium. In other words, the pressure downstream from the tested medium is uniform at a given time.

To verify this assumption, the volume downstream from the tested membrane was assumed to be a straight cylindrical tube, which is closed at the end opposite to the tested membrane. The pressure response in tube to the time dependent flow through the tested membrane was predicted by solving the governing partial differential equation given by the Fick's 2^{nd} law of diffusion. For simplicity, the diffusion coefficient in tube was assumed constant. The numerical value of the diffusion coefficient was evaluated based on the initial pressure and the internal diameter of tube using the empirical model of Knudsen.

The results of simulations for different initial pressures, internal diameters and lengths of tube allow identifying the conditions at which the resistance to accumulation in tube is not negligible. If the resistance is not negligible, it may lead, depending on the

position within the tube, to over or underestimation of the time lag of tested medium. Regardless of the resistance, for the simple tubular geometry of the permeate side volume, the pressure response measured at the position corresponding to 0.423 of the length of tube would give the exact value of the time lag of membrane.

Key words: Time Lag, Diffusion Coefficient, Resistance to Gas Accumulation, Fick's 2nd Law of Diffusion

1. Introduction

Constant volume (CV) systems are commonly used for the determination of diffusion and permeability coefficients of gases in homogeneous membranes. Both coefficients are determined in a single permeation experiment, in which a step change in the feed pressure is monitored at the permeate side of membrane. The diffusion coefficient is determined from the transient part of the pressure response curve, while the permeability coefficient is determined from the steady state part of the pressure response curve.

A typical CV system is composed of one or multiple membrane cell units connected to a large tank by a system of tubes. The specifications of tubes, that is, their length and the internal diameter are normally not provided. Similarly, the information on the initial pressure before a step change in the feed side pressure occurs, is rarely included. Amerongen started his experiments at 0.1 mmHg [1], Heilman *et al.* at 10^{-5}mmHg [2], while Barrer *et al.* after thoroughly degassing the system [3]. Most likely the initial pressure, at which different research groups perform the experiments, depends on the capacity of the utilized vacuum pump and other technical considerations. The lack of information on the utilized tubes and the initial pressure arise from the assumption that tubes do not impose any resistance to the gas that accumulates in the CV system, that is, the CV system does not have any effect on the membrane properties determined experimentally.

The purpose of this series of papers is to identify the conditions at which the resistance to accumulation of gases in vacuum tubes is not negligible and to discuss how

this non-negligible resistance affects the measurement of time lag of membrane in CV systems. In the first paper of this series, a theoretical model describing accumulation of gases permeating through membrane in a straight tube of uniform diameter is developed. Mathematically, the Fick's 2nd law of diffusion and a time dependent flow of gas through the membrane, as one of two boundary conditions, describe the process of accumulation. The time dependent flow, which results from a step increase in pressure at the feed side of membrane, is described by the solution of the Barrer equation. The effects of initial pressure, tube length and diameter, as well the distance from the membrane at which the pressure is monitored are discussed. In the second paper of this series, the existence of a non-negligible resistance to accumulation process is demonstrated experimentally. The effect of this resistance on the experimentally measured effective diffusivity of N_2 in high molecular weight polyphenylene oxide (PPO) membrane is discussed.

2. Concept of Time Lag and its Utilization in Membrane Characterization:

The mechanism of gas transport through practical polymeric gas separation membranes is exclusively described by the solution-diffusion mechanism. In this model the permeability coefficient (P_m) is a fundamental property of materials, which is expressed as a product of a thermodynamic factor (S_m) called the solubility coefficient, and a kinetic parameter (D_m) called diffusion coefficient [4]:

$$P_m = S_m D_m \tag{1}$$

Experimentally, the permeability coefficient is determined from the steady state permeation rate of a gas at standard temperature and pressure condition (Q_{STP}) through a homogeneous membrane:

$$P_m = \frac{Q_{STP} l}{A_m \Delta p} \tag{2}$$

where l and A_m are the membrane thickness and area, respectively, and Δp is the pressure difference across the membrane.

The diffusion coefficient of a gas in a homogeneous membrane is determined experimentally using the concept of time lag. This concept was first introduced by Daynes [5] and was later refined by Barrer [3]. Considering the applicability of the solution-diffusion mechanism, it represents a convenient way to separate the thermodynamic contributions from the kinetic contributions in the overall transport process of gas molecules through plastic films and membranes.

A common experimental technique involves the procedure in which the feed and permeate sides of tested membrane are evacuated to absolute vacuum, or to the lowest possible pressure. The feed side is then instantaneously pressurized and a constant feed pressure is maintained during the course of the experiment [6,7]. As a result, gas molecules start to diffuse through the membrane and then accumulate in a tank of known volume. The pressure rise in the tank is recorded. In relatively short experiments, the pressure rise resulting from accumulation of permeating gas is negligible compared to the feed side pressure, and the driving force for the diffusion of gas molecules through the membrane remains practically constant. Consequently, once the steady state transport rate across the membrane is established, the gas permeation rate required for the determination of permeability coefficient, can be evaluated from the following expression:

$$Q_{STP} = \frac{V v_{STP}}{RT} Z \tag{3}$$

where, V is the permeate side volume, R is the universal gas constant, T is the absolute temperature, Z is the slope of the pressure response curve, and v_{STP} is the volume of one mole of gas at standard temperature (273.16 K) and pressure (101 325 Pa).

Generally, the gas transport in homogeneous membranes after a step increase in the feed pressure, described above, is governed by the Fick's 2nd law of diffusion:

$$\frac{\partial C(x,t)}{\partial t} = -D_m \frac{\partial^2 C(x,t)}{\partial x^2} \tag{4}$$

where, C is the concentration of gas in membrane, D_m is the diffusion coefficient of gas in membrane, x is the distance along the membrane thickness from the feed side of the membrane, and t is the time elapsed from the step change in the feed side pressure. It is important to note that D_m in Eq. (4) is assumed to be independent of C. In addition, if the membrane is initially free of the diffusing gas, the initial and boundary conditions can be expressed by:

$$\begin{aligned} &t = 0, && C(x,0) = 0 \\ &t > 0, \quad x = 0, && C(0,t) = C_f \\ &t > 0, \quad x = l, && C(l,t) \approx 0 \end{aligned} \tag{5}$$

where, C_f is the gas concentration at the upstream face of membrane. In the solution-diffusion model C_f can be related to the feed pressure (p_f) by the following expression:

$$C_f = p_f S_m = p_f \frac{P_m}{D_m} \tag{6}$$

If S_m is independent of pressure, Eq. (6) represents the Henry's law of sorption.

Analytical solution of Eq. (4), subject to the specified initial and boundary conditions, can be obtained either by Laplace transform, or by separation of variables, and is given by the following expression:

$$C(x,t) = C_f\left(1 - \frac{x}{l}\right) - 2\frac{C_f}{\pi} \times \sum_{n=1}^{\infty} \frac{1}{n} \sin\left(\frac{n\pi x}{l}\right) \exp\left(-\frac{D_m n^2 \pi^2 t}{l^2}\right) \quad (7)$$

The diffusive flux of the gas within the membrane (J) is given by the Fick's 1st law of diffusion:

$$J(x,t) = -D_m \frac{\partial C(x,t)}{\partial x} \quad (8)$$

Substituting the first derivative of Eq. (7) with respect to x into Eq. (8) and evaluating the obtained expression at $x = l$ yields the equation for the time dependent flux of gas entering the permeate side of membrane:

$$J(l,t) = \frac{D_m C_f}{l} + \frac{2D_m C_f}{l} \times \sum_{n=1}^{\infty} (-1)^n \exp\left(\frac{-n^2 \pi D_m t}{l^2}\right) \quad (9)$$

Substituting Eq. (6) into Eq. (9) eliminates C_f and provides a more convenient expression for the time dependent flux:

$$J(l,t) = \frac{p_f P_m}{l} + \frac{2p_f P_m}{l} \times \sum_{n=1}^{\infty} (-1)^n \exp\left(\frac{-n^2 \pi D_m t}{l^2}\right) \quad (10)$$

Multiplying Eq. (10) by the membrane area and integrating it with respect to t yields the expression for the amount of gas (F) that has accumulated at the permeate side of the membrane at a given time:

$$F(t) = -A_m \int_0^t J(l,t)dt = \frac{A_m p_f P_m}{l}\left[t - \frac{l^2}{6D_m} + \frac{2l^2}{\pi^2 D_m} \times \sum_{n=1}^{\infty} \frac{(-1)^{n+1}}{n^2} \exp\left(-\frac{D_m n^2 \pi^2 t}{l^2}\right)\right] \quad (11)$$

Assuming applicability of the ideal gas law, the time dependent change in the pressure at the permeate side of membrane is given by the following equation:

$$p(t) = \frac{F(t)RT}{V} = \frac{A_m p_f P_m RT}{Vl}\left[t - \frac{l^2}{6D_m} + \frac{2l^2}{\pi^2 D_m} \times \sum_{n=1}^{\infty} \frac{(-1)^{n+1}}{n^2} \exp\left(-\frac{D_m n^2 \pi^2 t}{l^2}\right)\right] \quad (12)$$

A general shape of the pressure response curve given by Eq. (12) is presented in Fig. 1. It can be noticed that after the initial nonlinear pressure increase, the pressure response becomes a linear function of time. This is because the last term on the right-hand side of Eq. (12) contains an exponential function with a negative argument, which is proportional to t. Consequently as t increases, the last term on the right-hand side of Eq. (12) disappears and it becomes:

$$p(t) = \frac{A_m p_f P_m RT}{Vl}\left[t - \frac{l^2}{6D_m}\right] \tag{13}$$

The term in front of the bracket in the above equation corresponds to the slope Z in Eq. (3). The extrapolation of the linear part of the pressure response curve into the time axis represents time lag (θ_m) of tested membrane. Mathematically, the expression θ_m is obtained by setting $p = p_o$, in Eq. (13) and solving for t. According to the initial condition, $C(x,0) = 0$, and therefore, $p_o = 0$. Consequently,

$$t = \theta_m = \frac{l^2}{6D_m} \tag{14}$$

Equation (14), which was first deduced by Daynes in 1920 [9], is a fundamental equation in characterization of gas transport properties of membranes, because it allows estimating the diffusion coefficient of a gas in membrane from the experimentally measured time lag. Moreover, knowing D_m and P_m allows estimating S_m form Eq. (1).

3. Influence of the Vacuum System

The time lag of membrane results from the resistance (R_m) to gas transport in membrane. This resistance can simply be expressed by the following equation:

$$R_m = B\frac{l^2}{D_m} \tag{15}$$

where B is a proportionality constant.

Although not explicitly stated, the derivation of the expression for time lag of membrane relies on the assumption that there is no resistance to accumulation of gases at the permeate side of the membrane. Usually, the gases permeating through the membrane are collected in a large tank connected to a membrane cell or cells through a system of tubes. While the diffusion coefficient of gases in membranes is orders of magnitude greater than the diffusion coefficient of gases accumulating in tubes at the permeate side of membrane, the length of these tubes (L) is orders of magnitude greater than the membrane thickness. In case of CV system described by Tabe Mohammadi *et al.*, a tubing of approximately 2.5 m length and outside diameter of 1/4" connects 3 membrane cells to two large tanks, where the pressure transducer is allocated just before the large tanks [8]. Consequently, the resistance to accumulation of gases permeating through the membrane during the time lag experiment might not necessarily be negligible.

Similarly to gas transport in membrane, the accumulation of gases at the permeate side of membrane can be described by the Fick's second law of diffusion,

$$\frac{\partial c}{\partial t} = \nabla(D\nabla c) \tag{16}$$

where, c is the concentration while D is the diffusion coefficient of a gas accumulating at the permeate side of membrane. Assuming that the permeate side has a tubular configuration of the internal diameter (d) and the length (L) such that $L >> d$, the accumulation of gases can be considered as a one-dimensional process. Furthermore, assuming that D is constant and independent of c, Eq. (16) becomes similar to Eq. (1),

$$\frac{\partial c(x,t)}{\partial t} = D\frac{\partial^2 c(x,t)}{\partial x^2} \tag{17}$$

where, x is the distance from the downstream side of the membrane. Assuming applicability of the ideal gas law Eq. (17) can also be written in terms of pressure,

$$\frac{\partial p(x,t)}{\partial t} = D\frac{\partial^2 p(x,t)}{\partial x^2} \tag{18}$$

One initial and two boundary conditions are required to solve Eq. (18). Initially, there is no flow of the gas, and the pressure at the permeate side of the membrane is uniform:

$$p(x, t=0) = p_o = const. \tag{19}$$

At the closed end of the tube ($x = L$) the pressure gradient regardless of the flow is always zero:

$$\frac{\partial p(x=L,t)}{\partial x} = 0 \tag{20}$$

The second boundary condition is obtained by considering a time-dependent flux at the tube entrance ($x = 0$), which is given by Eq. (5). Using the Fick's 1st law of diffusion, this boundary condition is expressed by:

$$\frac{\partial p(x=0,t)}{dx} = -\frac{J(l)RT}{D} = -\frac{RT}{D}\left\{\frac{p_f P_m}{l} + \frac{2p_f P_m}{l} \times \sum_{n=1}^{\infty}(-1)^n \exp\left(\frac{-n^2\pi D_m t}{l^2}\right)\right\} \tag{21}$$

The governing PDE subject to the initial and boundary conditions given by Eqs. (19), (20) and (21), respectively, can only be solved numerically, and quantification of the solution requires the numerical value of D.

4. Evaluation of Diffusion Coefficient in Vacuum Tubes

The diffusion coefficient of gas at the permeate side of membrane depends on the pressure and the internal diameter of tube. When the mean free path of gas molecules is much smaller than the diameter of tube, gas molecules collide much more frequently with each other rather than with the walls of tube, and the Poiseuille flow occurs. Such conditions exist at relatively high pressures and/or in tubing having large internal diameter. The diffusion coefficient in the Poiseuille flow regime is predicted from the following equation [9]:

$$D = \frac{pr^2}{8\eta} \tag{22}$$

where, p is the pressure, r is the inside radius of tubing, and η is the dynamic viscosity of the gas. Equation (22) assumes no slipping at the wall of tube. To include the effects of slipping, Eq. (22) is modified by incorporating the coefficient of slip (ζ) [9]:

$$D = \frac{pr^2}{8\eta}\left(1 + \frac{4\zeta}{r}\right) \tag{23}$$

The coefficient of slip is evaluated using Maxwell's deduction from the kinetic theory of gases [10]:

$$\xi = \frac{\eta}{p}\sqrt{\frac{\pi RT}{2M}}\left(\frac{2-f}{f}\right) \tag{24}$$

where, M is the molecular weight of gas, and f, known as the Maxwell's f, is a fraction of gas molecules, which lose the momentum as a result of adsorption and desorption at the walls of tube. The f depends on the nature of gas and tube surface. Using the deflection method for the determination of ξ, Stacy [11] and Van Dyke [12] reported that for air and oxygen in machined brass surfaces f is very close to unity.

The coefficient of slip decreases as the pressure increases. In turn, at relatively high pressures and/or in tubing of large internal diameter, the term involving the coefficient of slip approaches to unity, and Eq. (23) becomes Eq. (22). Consequently, Eq. (23) is applicable for estimation of D in both, the Poiseuille flow and the slip flow regimes.

When gas molecules collides much more frequently with the walls of tube rather than with themselves, that is, in the Knudsen flow regime, the diffusion coefficient is evaluated using the following equation [9]:

$$D = \frac{2}{3} r \sqrt{\frac{8RT}{\pi M}} \tag{25}$$

The Knudsen flow regime occurs at high vacuum and/or in tubes with a very small internal diameter. The diffusion coefficient determined from Eq. (25), often referred to as the Knudsen diffusion coefficient, is independent of pressure.

There is no direct transition from the slip flow to the Knudsen flow regime. As the pressure decreases and D calculated from Eq. (23) becomes comparable with D calculated from Eq. (25), it is recommended to evaluate the diffusion coefficient from the empirical model of Knudsen [9]:

$$D = ap + b\frac{1 + c_1 p}{1 + c_2 p} \tag{26}$$

Constant b in Eq. (26) is the Knudsen coefficient of diffusion given by Eq. (25), while constant a is calculated from:

$$a = \frac{r^2}{8\eta} \tag{27}$$

The product ap in Eq. (27) represents the diffusion coefficient in the Poiseuille flow regime. Constants c_1 and c_2 are determined by solving the following set of equations:

$$\frac{c_1}{c_2} = \frac{3\zeta\sqrt{\frac{\pi M}{RT}}p}{8\sqrt{2}\eta} \tag{28}$$

$$c_2 - c_1 = 0.6117\frac{\sqrt{\frac{M}{RT}}}{\eta}r \tag{29}$$

The empirical model of Knudsen predicts the existence of a minimum diffusion coefficient before the transition to pure Knudsen flow. At very low pressures, D from Eq. (26) becomes similar to D from Eq. (25). On the other hand, at relatively high pressures D from Eq. (26) becomes similar to D from Eq. (23). Therefore, the empirical model of Knudsen can be used for prediction of D for the entire spectrum of pressures. The validity of this model for prediction of the diffusion coefficient in dynamic flow experiments was confirmed in our previous publication [13].

Figure 2 plots the diffusion coefficient of N_2 at 35°C determined from Eq. (26) as a function of pressure for tubes of different internal diameters. The tubes considered in Fig. 2 include standard 1/8", 1/4", and 1/2" stainless steel tubes having the corresponding internal diameters of 0.175×10^{-2} m, 0.386×10^{-2} m, 1.021×10^{-2} m, respectively. The coefficient of slip required by Eq. (26) was calculated assuming f to be equal to unity.

It can be noticed that at relatively low pressures D is rather insensitive to pressure changes. On the other hand, at relatively high pressures, D is a strong function of pressure. The transition at which D begins to be affected by p depends on the diameter of tube. In the 1/8" tube the transition occurs at approximately 13.3 Pa (0.1 mmHg), while in the 1/4" and 1/2" tubes the transition occurs at approximately 6.67 Pa (0.05 mmHg) and

1.33 Pa (0.01 mmHg), respectively. The fact that for a given diameter of tube there is a pressure range where D is practically not affected by p indicates that the assumption of constant D, on which the numerical solution of Eq. (18) relies, is not unreasonable.

5. Results and Discussion

If the resistance to accumulation of gases at the permeate side of membrane is negligible the numerical solution of Eq. (18) at any position would be similar to the pressure response predicted by Eq. (12). If two pressure responses were similar, the time lags determined from the two pressure responses would also be similar. Prediction of time lag requires the properties of membrane and the conditions of the experiment.

5.1 Properties of membrane and experimental conditions

In the following simulations the membrane will have gas transport properties of polyphenylene oxide (PPO) reported by Aguilar-Vega and Paul [14], which for N_2 are: $P_m = 2.63 \times 10^{-17}$ m^3(STP) m/(s m^2 Pa) (3.5 Barrer), $D_m = 6.68 \times 10^{-12}$ m^2/s. Furthermore, the experimental conditions required for the simulation will correspond to those at which the above properties were obtained. These are, p_f = 1.5 atm and T = 35°C. The other parameters pertinent to the membrane, which are required in simulations, that is, A_m and l are set arbitrary to be 10×10^{-4} m^2 and 20×10^{-6} m, respectively. According to Eq. (14), the membrane having above properties should yield the time lag equal to 9.98 s.

The other parameters, which must be specified and whose effect will later be investigated, include p_o, d, and L, as well as, the position (x) at which the pressure response is monitored. Specification of p_o and d allows estimation of D. To demonstrate

the numerical solution of Eq. (18) at different x it will be assumed that p_o = 1.33 Pa (0.01 mmHg) , $d = 0.386 \times 10^{-2}$ m (and thus $D = 0.55$ m^2/s), and L = 2 m.

5.2 Numerical solution – effect of location of pressure transducer

Figure 3 presents the plot of flux as a function of time, determined from Eq. (10) for the conditions specified in Section 5.1. Therefore, Fig. 3 is a graphical representation of the boundary condition for Eq. (18) at the entrance of the system. The dotted vertical line in Fig. 3 represents the actual time lag of membrane of 9.98 s. It is important to emphasize that the time after which the steady state flux is attained is approximately 10 times the time lag. Therefore, to avoid an error in experimentally determined permeation rate and time lag, sufficient time must be allowed to ensure that the pressure response becomes a truly linear function of time.

Figure 4 presents the numerical solution of Eq. (18) at the positions x = 0.2 m and x = 1.8 m, respectively, for the parameters specified in Section 5.1. For comparison, the pressure response given by Eq. (12) is also included.

It is evident that the pressure response at x = 0.2 m precedes the pressure response, which would exist at this location, if there were no resistance to accumulation of gases in this tube. On the other hand, at the position x = 1.8 m the situation is opposite, that is, the actual pressure response follows the pressure response, which would exist at this location in tube with no resistance.

The shift of the pressure response to the left, or to the right, depending on x, relative to the pressure response predicted by Eq. (12) results in an error in time lag of membrane. For the specified D_m and l, θ_m according to Eq. (14), is 9.98 s. If one applies

Eq. (14) to the vacuum tube utilized in this simulation, its time lag would be 1.2 s. On the other hand, θ_m determined at x = 0.2 m is 8.15 s, while θ_m at x = 1.8 m is 11.16 s. Interestingly, the difference between θ_m at x = 1.8 m and θ_m of membrane is roughly 1.2 s, which corresponds to the time lag of the vacuum tube. On the other hand, the difference between θ_m of membrane and θ_m at x = 0.2 m is 1.83 s, that is, considerably greater than 1.2 s. Moreover, θ_m at x = 0.2 m underestimates, while θ_m at x = 1.8 m overestimates the actual time lag of membrane.

The fact that θ_m at x = 0.2 m underestimates, while θ_m at x = 1.8 m overestimates the actual time lag of membrane indicates that there is a position within the tube, at which the time lag of membrane would be measured accurately, despite the resistance to accumulation of gases.

Figure 5 presents the plot of the time lag of membrane, specified in Section 5.1, as a function of x. It can be noticed that indeed, there is a position (x = 0.846 m) at which the time lag of membrane could be determined accurately. The values of time lag in Fig. 5 can be described by the following expression:

$$\theta_m = 9.98 + \frac{L^2}{6D} - \frac{(L-x)^2}{2D} \tag{30}$$

where 9.98 represents the actual time lag of membrane, which from now on will be denoted as θ_m^0. It is important to emphasize that Eq. (30) is similar to the expression for time lag of vacuum tube derived analytically in our earlier publication for the case in which at $t > 0$, gas starts to flow into a closed vacuum tube at a constant rate [13]. Equation (30) implies that the optimum location for the measurement of time lag of

membrane is independent of D. Moreover, according to Eq. (30), regardless of L, the optimum location occurs at the same dimensionless location of $x/L = 0.423$.

If pressure transducer is located at a position different than $x/L = 0.423$, the actual time lag of membrane can be evaluated from the measured time lag using the following expression, which is obtained by rearranging Eq. (30):

$$\theta_m^0 = \theta_m - \frac{L^2}{6D} + \frac{(L-x)^2}{2D} \tag{31}$$

In other words, Eq. (31) allows correcting the experimentally measured time lag of membrane for the effects of system resistance provided that the parameters, such as L, d, p_o, and x are known.

5.3 Effect of Diameter of Tube and Initial Pressure

The initial pressure and the diameter of tube determine the diffusion coefficient of a gas in tube. According to Eq. (30), the magnitude of the error in time lag at a given position, except for $x/L = 0.423$, strongly depends on D, and therefore on p_o and d.

The effect of diameter of tube on the error in time lag of membrane is presented in Fig. 6, in which θ_m is plotted versus x for three 2 m-long tubes of the internal diameters corresponding to those of standard 1/8", 1/4" and 1/2" stainless steel tubes. Each tube is initially at the same pressure of 13.3 Pa (0.10 mmHg) and 35°C. The effect of the initial pressure on the error in the measured time lag of membrane is presented in Fig. 7, in which θ_m is plotted versus x for a standard 1/4" stainless steel tube at three different initial pressures of 1.33, 13.3, 133 Pa (0.01, 0.10, and 1.00 mmHg). The error in the measured time lag decreases with increase in both the diameter of tube and the initial pressure. For the conditions depicted in Figs. 6 and 7, the influence of tube diameter is

stronger than the influence of the initial pressure. This is despite the fact that the pressures in Fig. 6 differ by a factor of 10, while the tube diameters in Fig. 6 differ roughly by a factor of 2.

Figures 6 and 7 indicate that apart from the location of pressure transducer the magnitude of error in the measured time lag can also be controlled by the initial pressure and the size of tube used at the permeate side of membrane. While D depends on both p_o and d, one of the assumptions for using the time lag method is that the membrane is initially free from the permeating species. This means that in the actual CV systems D should be maximized by means of increasing the diameter of utilized tubing at the permeate side of membrane rather than by increasing the initial pressure in the system. According to Fig. 7, for a 2 m-long tube the error in measured time lag becomes very small, when a standard 1/2" stainless steel tube is utilized. This error would decrease even more if the total length of tubing were less than 2 m.

5.4 Effect of Length of Tube

Another parameter, which according to Eq. (30) strongly affects the magnitude of error in the measured time lag of membrane, is the length of tube. In real CV systems accumulation of gases that permeate through membrane occurs in vacuum chambers rather than in tubes. On the other hand, tubes are necessary to connect permeation cell or cells to the vacuum chamber. As already mentioned, the total length of a 1/4" tubing in the CV system described by Tabe Mohammadi *et al.*, [8] is approximately to 2.5 m. Generally, the length of tubing increases with the number of permeation cells utilized in the CV system.

Figure 8 presents the plot of the absolute and relative errors in the measured time lag of membrane at $x = 0$ as a function of tube length for standard 1/8" and 1/4" and 1/2" stainless steel tubes that are initially at 1.33 Pa (0.01 mmHg) and 35°C. It is important to emphasize that, as shown in Figs. 5-7, the absolute error at $x = 0$ is greater than at any other location. Therefore, the lines shown in Fig. 7 represent the limiting error for the specified conditions. It can be noticed that for the maximum error in θ_m to be less than 1 s, the length of standard 1/2" tubing should not exceed 2 m. To fulfill the condition of the maximum error in θ_m to be less than 1 s in standard 1/4" and 1/8" tubes, their respective lengths should not exceed 1.28 m and 0.88 m.

The requirement for the maximum error in θ_m to be less than 1 s is completely arbitrary. For the membrane specified in Section 5.1, 1 s corresponds to 10% error in the measured time lag. If the thickness of membrane were decreased from 20 to 10 μm, its time lag would decrease from 9.98 s to 2.5 s, and the absolute error of 1 s would represent 40% rather than 10% of the actual time lag of membrane. Consequently, for the maximum relative error in θ_m not to exceed 10% the length of standard 1/2", 1/4", and 1/8" tubes should not exceed 1.04 m, 0.64 m, and 0.44 m, respectively.

6. Conclusions

The process of accumulation of gases at the permeate side of membrane in a hypothetical CV system has been modeled using the Fick's 2nd law of diffusion. To simplify the analysis, the hypothetical CV system has been considered to be a straight cylindrical tube of the length much greater than its internal diameter. One of two required boundary conditions has been obtained by realizing that the pressure gradient at the

closed end of tube is always zero, regardless of the flow at the open end of tube. The solution of the Barrer equation, which is widely used for the determination of the diffusion coefficient of gas in homogeneous membranes, has been taken as the other boundary condition. The diffusion coefficient of gas in tube, which is assumed constant, has been evaluated from the empirical model of Knudsen.

According to the developed model, the experimentally measured time lag (θ_{exp}) in the hypothetical CV system is given by:

$$\theta_{exp} = \theta_m + \frac{L^2}{6D} - \frac{(L-x)^2}{2D} \tag{32}$$

where θ_m is the time lag due to resistance to gas transport in tested membrane, L is the length of tube, D is the diffusion coefficient of gas in tube, and x is the distance from the permeate side of membrane at which the pressure response is monitored. The above equation suggests that regardless of L and D, at x such that $x/L = 0.423$, $\theta_{exp} = \theta_m$. In other words, $x/L = 0.423$ represents the optimum location for monitoring of the pressure rise during the actual gas permeation experiment. If $x/L < 0.423$, the resistance to accumulation of gas results in underestimation of θ_m and thus overestimation of the diffusion coefficient in tested membrane. If $x/L > 0.423$, the resistance to accumulation of gas results in overestimation of θ_m and thus underestimation of the diffusion coefficient in tested membrane. The effects of resistance to gas accumulation can be practically eliminated if tubes of the diameter 1/2" or larger are utilized and if the total length of tubes at the permeate side of membrane is not excessively long.

7. List of Symbols

A_m: Membrane area (m^2)

C: concentration of gas in membrane (mol/m^3)

c: concentration of gas in tube

C_f: Concentration of gas at the upstream face of the membrane (mol/m^3)

D: Diffusion coefficient in tube (m^2/s)

D_m : Effective diffusion coefficient in membrane (m^2/s)

f : Fraction of gas molecules absorbed by tube walls (-)

$F(t)$: Accumulated amount of gas in vacuum system (m^3)

J: Flux (mol/m^2 s)

l: Membrane thickness (m)

L: Length of tube (m)

M: molecular weight (kg/kmol)

p: Pressure (Pa)

p_o : Initial pressure (Pa)

P_m : Effective permeability coefficient (mol/m Pa s)

Q_{STP}: Flow at standard temperature and pressure (cm^3(STP)/min)

R: Universal gas constant (J/mol K)

R_m: Resistance in membrane (s)

r: Inside radius of tube (m)

S_m: Effective solubility coefficient (mol/m^3 Pa)

t: Time (s)

T: Absolute temperature (K)

V: Permeate side volume (m^3)

v_{STP}: Molecular volume at standard temperature and pressure (m^3/mol)

x: Location (m)

Z: Slope (Pa/s)

Greek Symbols :

θ_m : Apparent time lag of membrane

θ_m^o : Actual time lag of membrane (s)

η : Dynamic viscosity of gases (kg/m s)

ξ : Coefficient of slip (m)

8. References

1. G. J. Van Amerongen, The permeability of different rubbers to gases and its relation to diffusivity and solubility, J. Applied Phys., 17 (1946) 972.
2. W. Heilman, V. Tammela, J.A. Meyer, V. Stannett, M. Szwarc, Permeability of polymer films to hydrogen sulfide gas, Ind. Eng. Chem. 48 (1956) 821.
3. R. M. Barrer, G. Skirrow, Transport and equilibrium phenomena in gas-elastomer systems. I Kinetic phenomena, J. Polym. Sci., 3 (1948) 549.
4. W. J. Koros, G. K. Fleming, Membrane-based gas separation, J. Membr. Sci., 83, 1 (1993).
5. H. A. Daynes, The process of diffusion through a rubber membrane, Roy. Soc. Proc., 97 (1920) 286.
6. W. R. Vieth, J. M. Howell, J. H. Hsieh, Dual sorption theory, J. Membr. Sci., 1 (1976) 177.

7. R. M. Barrer, Permeation, diffusion and solution of gases in organic polymers, Trans. Farad. Soc., 35 (1939) 628.
8. A. Tabe Mohammadi, T. Matsuura, S. Sourirajan, Design and conctruction of gas permeation system for the measurement of low permeatoin rated and permeate compositions, J. Membr. Sci., 98 (1995) 281.
9. L. B. Loeb, The Kinetic Theory of Gases, Dover Publications, Inc. New York, 1961.
10. J. C. Maxwell, in The Scientific papers of James Clerk Maxwell, edited by W. D. Niven, M. A., F. R. S., Dover publications, New York, 1965.
11. L. J. Stacy, A determination by the constant deflection method of the value of the coefficient of slip for rough and for smooth surfaces in air, Phys. Rev., 21 (1923) 239.
12. K. S. V. Dyke, The coefficients of viscosity and slip of air and of carbon dioxide by the rotating cylinder method, Phys. Rev., 21 (1923) 250
13. R. Chapanian, B. Kruczek, Resistance to accumulation of gases in high vacuum systems, J. Vac. Sci. Technol. A, (submitted 8 Sept., 2003).
14. M. Aguilar-Vega, D.R. Paul, Gas transport properties of polyphenylene ethers, J. Polym. Sci., 31 (1993) 1577.

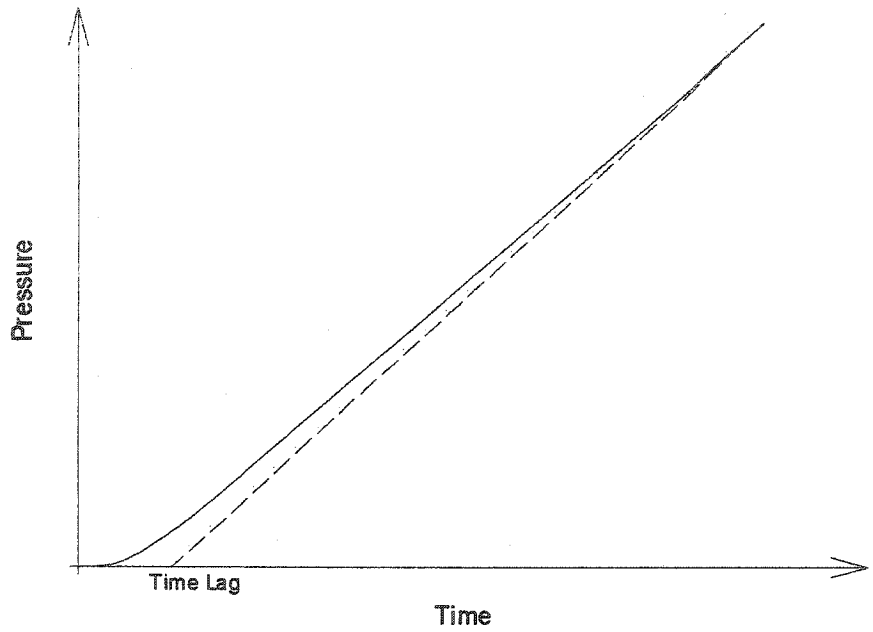

Figure 1. Graphical representation of pressure response to a step change in feed side pressure predicted by the Barrer equation and the concept of time lag.

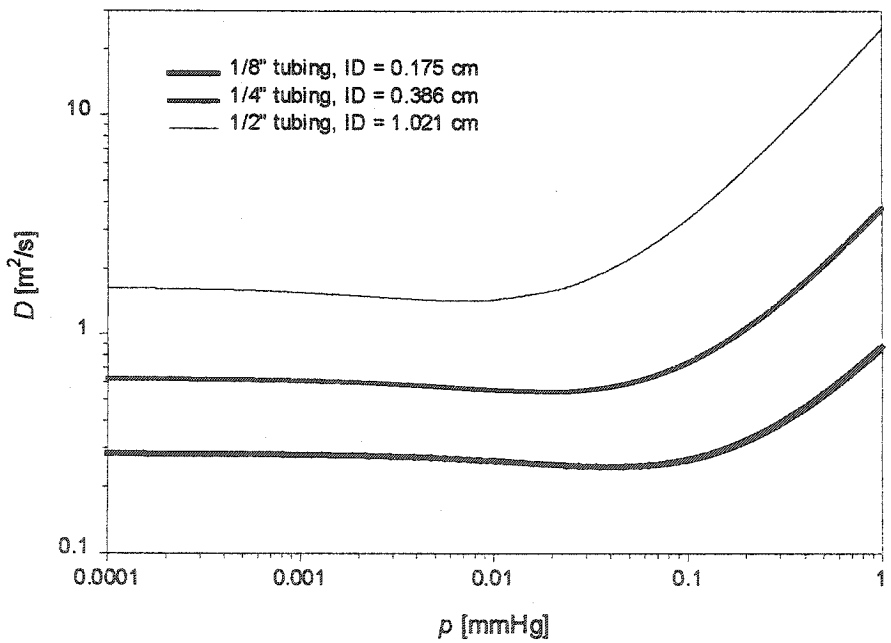

Figure 2. Effect of pressure on the diffusion coefficient of N_2 in different stainless steel tubes (1/8", 1/4", 1/4") predicted by the empirical model of Knudsen.

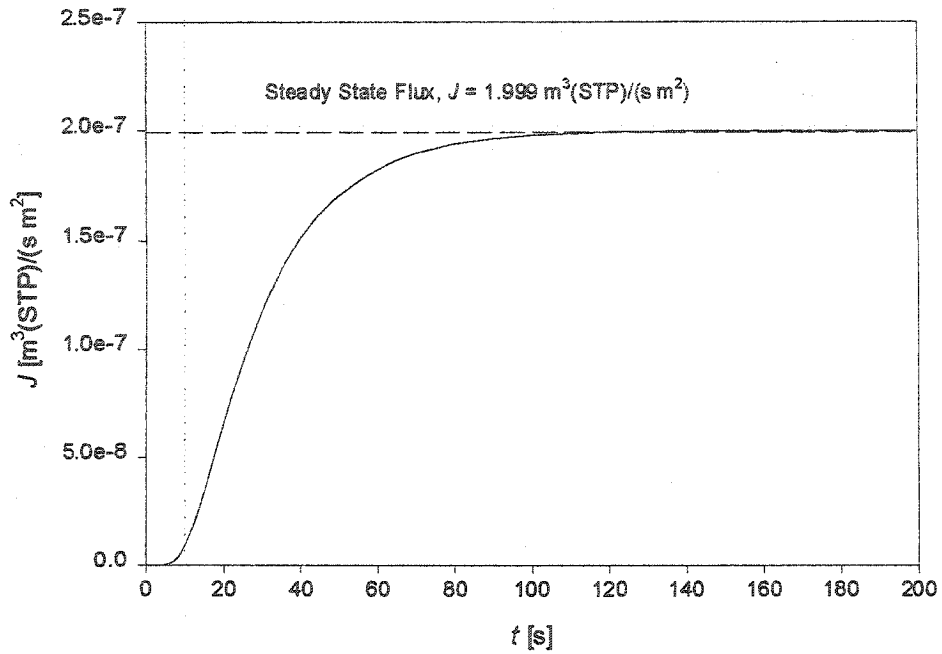

Figure 3. Time dependent flux at $T = 35°C$ from a membrane resulting from step change in feed pressure from 1.33 Pa to 152×10^3 Pa. Properties of membrane: $P_m = 2.63 \times 10^{-17}$ m³(STP) m/(s m² Pa), $D_m = 6.68 \times 10^{-12}$ m²/s, $l = 20 \times 10^{-6}$ m.

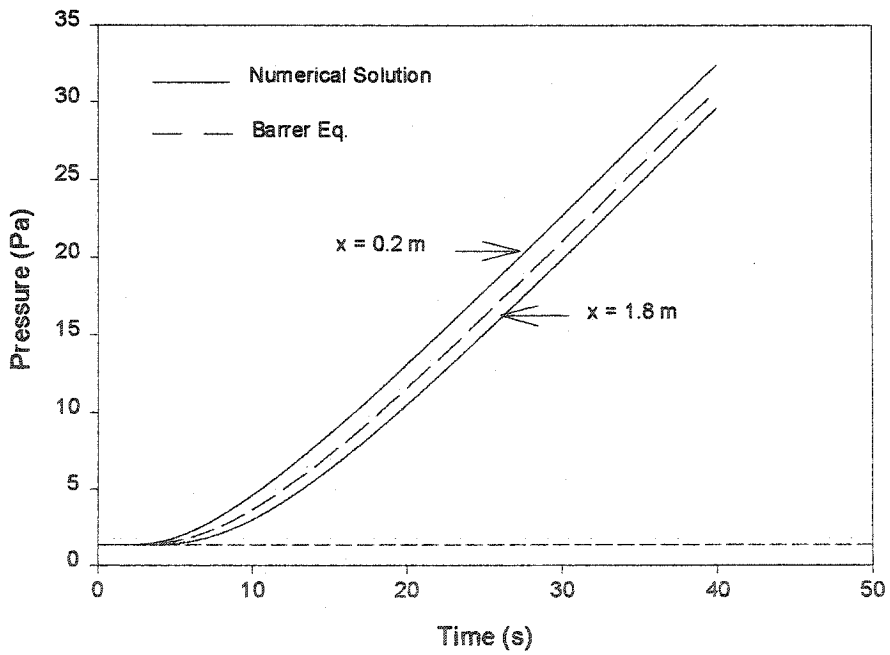

Figure 4. Pressure response at $T = 35°C$ to step change in feed pressure from 1.33 Pa to 151988 Pa in a 2 m-long 1/4" stainless steel tube at $x = 0.2$ m and $x = 1.8$, initially at $p_o = 1.33$ Pa. Properties of membrane: $P_m = 2.63 \times 10^{-17}$ m³(STP) m/(s m² Pa), $D_m = 6.68 \times 10^{-12}$ m²/s, $l = 20 \times 10^{-6}$ m, $A_m = 10 \times 10^{-4}$ m². The diffusion coefficient of gas in tube, $D = 0.55$ m²/s, assumed to be constant.

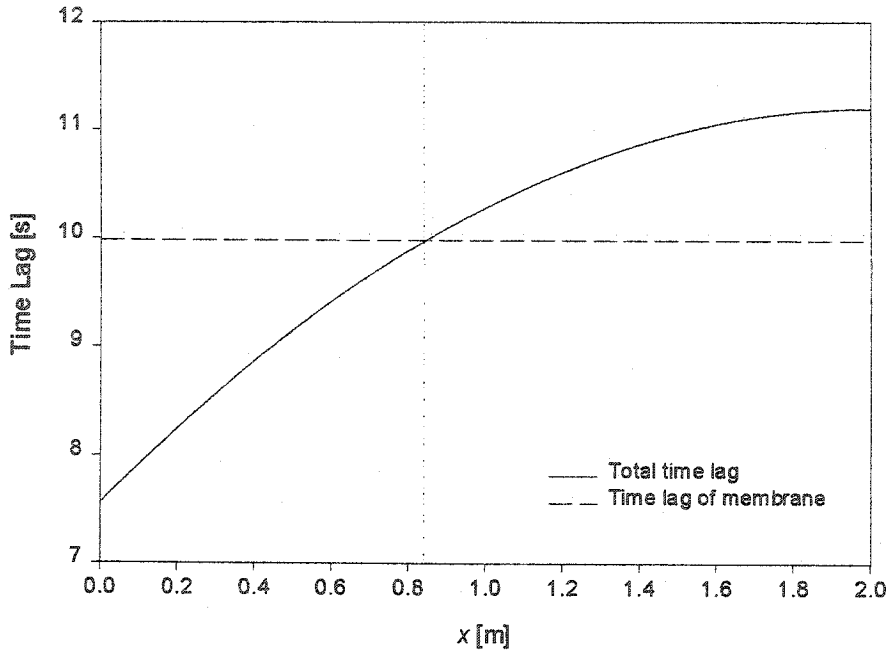

Figure 5. Effect of position within a 2 m-long 1/4" stainless steel tube on the measured time lag of membrane having the following properties: P_m = 2.63 x 10^{-17} m^3(STP) m/(s m^2 Pa), D_m = 6.68 x 10^{-12} m^2/s, l = 20 x 10^{-6} m, A_m = 10 x 10^{-4} m^2. Other parameters: T = 35°C, p_o = 1.33 Pa, p_f = 152 × 10^3 Pa. The diffusion coefficient of gas in tube, D = 0.55 m^2/s, assumed to be constant.

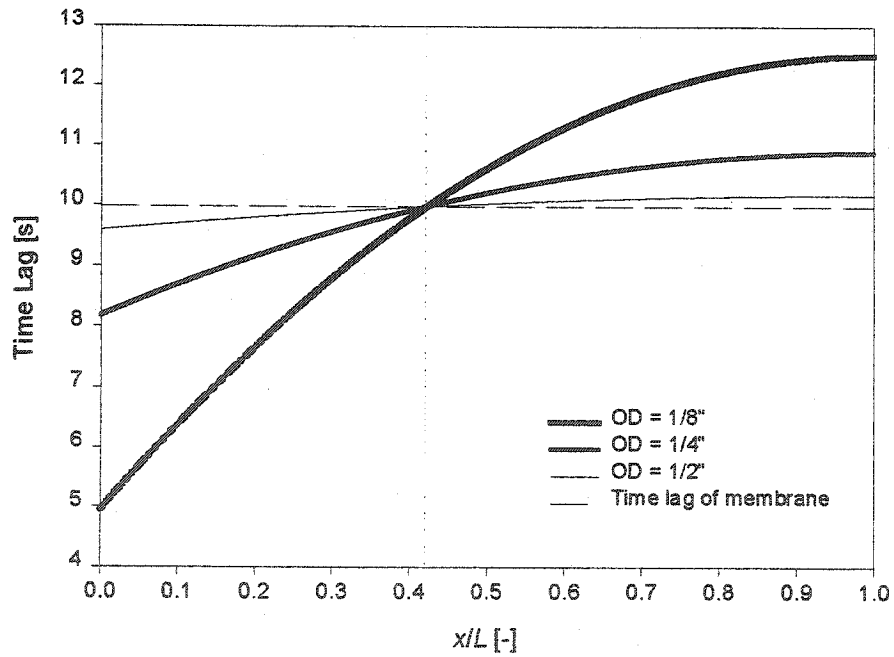

Figure 6. Effect of internal diameter of a 2 m-long stainless steel tube on the measured time lag of membrane having the following properties: P_m = 2.63 x 10^{-17} m^3(STP) m/(s m^2 Pa), D_m = 6.68 x 10^{-12} m^2/s, l = 20 x 10^{-6} m, A_m = 10 x 10^{-4} m^2. Other parameters: T = 35°C, p_o = 13.3 Pa, p_f = 152 × 10^3 Pa. The diffusion coefficient of gas for a given tube diameter assumed to be constant.

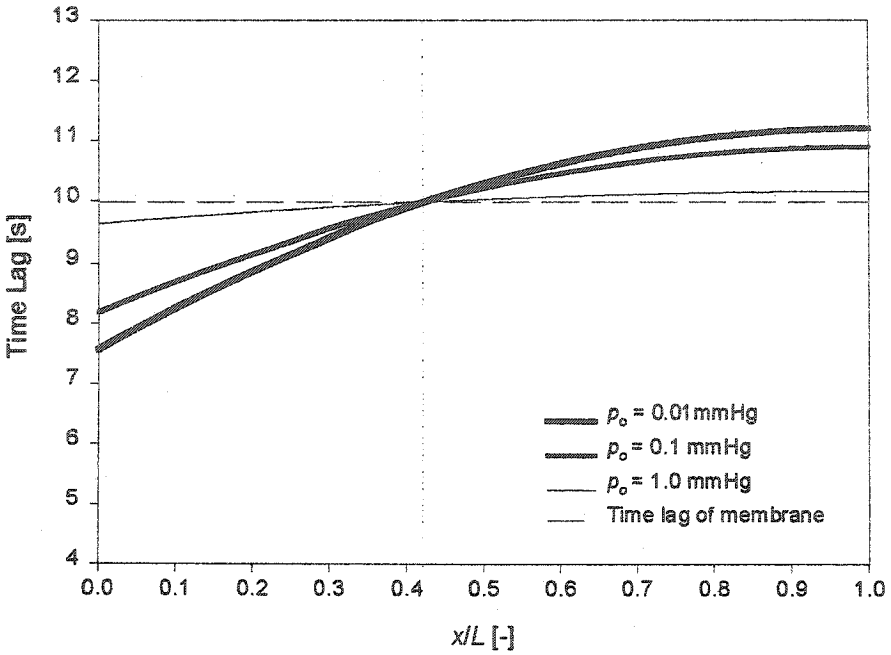

Figure 7. Effect of initial pressure in a 2 m-long 1/4" stainless steel tube on the measured time lag of membrane having the following properties: P_m = 2.63 x 10^{-17} m^3(STP) m/(s m^2 Pa), D_m = 6.68 x 10^{-12} m^2/s, l = 20 x 10^{-6} m, A_m = 10 x 10^{-4} m^2. Other parameters: T = 35°C, p_f = 152 × 10^3 Pa. The diffusion coefficient of gas for a given initial pressure assumed to be constant.

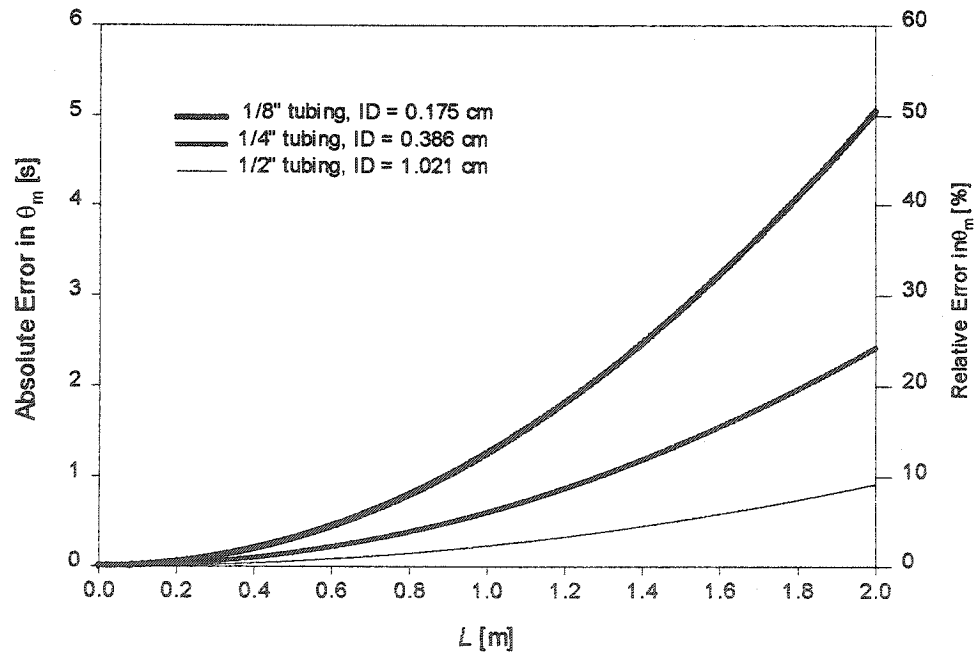

Figure 8. Effect of length of stainless steel tube, initially at p_o = 0.01 mmHg, on the measured time lag of membrane having the following properties: P_m = 2.63 x 10^{-17} m^3(STP) m/(s m^2 Pa), D_m = 6.68 x 10^{-12} m^2/s, l = 20 x 10^{-6} m, A_m = 10 x 10^{-4} m^2. Other parameters: T = 35°C, p_f = 152 × 10^3 Pa. The diffusion coefficient of gas for a given tube diameter assumed to be constant.

CHAPTER IV

Effect of Resistance of Vacuum Tubes on Time Lag of Membrane in Constant Volume Systems. Part II: Experimental Demonstration

R. Chapanian, B. Kruczek*

Department of Chemical Engineering
University of Ottawa
161 Louis Pasteur Street
Ottawa, ON K1N 6N5
Canada

* To whom correspondence should be addressed.
(Submitted to Journal of Membrane Science, December 2, 2003)

Abstract

In part I of this series of papers, the conditions at which the resistance to accumulation of gases downstream from a medium such as membrane are not negligible, were identified. To verify these theoretical findings, a constant volume system consisting of either 1/4" or 1/2" tubing at the permeate side of membrane was build and equipped with two sensitive pressure transducers installed at different distances from the membrane cell. A membrane for gas permeation tests was prepared from high molecular weight polyphenylene oxide (PPO). Since PPO is a glassy polymer, all permeation experiments were performed at the same feed pressure, to avoid possible variation in gas transport properties with pressure. The properties of PPO required for simulation of the actual pressure response in gas permeation tests were determined experimentally at the configuration imposing the minimum resistance to gas accumulation. The effects of the location of pressure transducer, the length and internal diameter of tube, and the initial pressure were investigated.

The theoretically predicted pressure response at a given position follows closely the actual pressure response during the first 20 – 30 s of experiments. In case of some experiments the experimental pressure response is shifted to the left compared to the theoretically predicted response. Despite this shift the difference between experimentally observed pressure responses at different locations is comparable to the theoretically predicted ones. As time progresses beyond the first 20 –30 s, the theoretically predicted pressure difference starts to overestimate the experimentally observed value. This is because the model assumes constant diffusion coefficient of gas in tube, while in reality,

the diffusion coefficient increases with time as the pressure at the permeate side of membrane increases during the course of experiments.

Key words: Resistance to Gas Accumulation, Time Lag, Diffusion Coefficient, Polyphenylene Oxide

1. Introduction

The theoretical model developed in Part I of this series of papers allows identifying the combinations of parameters such as pressure, tube length, and tube diameter, at which the resistance to accumulation of gases is not negligible. In turn, if the resistance to accumulation of gases is not negligible, the experimentally determined diffusion coefficient of gas, which is one of the fundamental properties of materials [1], might be in error.

One of the assumptions in the original analysis of Daynes for the determination of diffusion coefficient is constant, zero concentration of gas at the low-pressure side of tested medium [2]. Because of this assumption the early constant volume (CV) systems, also referred to as the diffusion cells, had relatively large volume of about 50-70 cm^3 [3,4]. It is important to keep in mind that until 1970s the pressure rise was exclusively measured by a manometer-type devices, which constituted a part of the permeate side volume. A displacement of mercury in such devices by the permeating gas resulted in an increase in volume of the system. In practice however, the pressure would increase by only a few microns of mercury allowing to assume the volume of the permeate side to be practically constant. On the other hand, the accurate monitoring of such small pressure increases was very challenging.

In 1959 Dow Chemical Company Shuman developed a self-contained diffusion cell that was later commercialized by Custom Scientific Instruments Inc. Unlike the early cells, the permeate side volume in the self-contained cell was small and the pressure increase during accumulation of permeating gases could be as large as 65 mmHg, thus making monitoring of the pressure increase much easier [4]. To account for the fact that

the pressure as well as the volume at the permeate side were no longer constant Paul and DiBenedetto refined the original model of Daynes thus making it suitable for the determination of the diffusion, solubility and permeability coefficients of gases in tested media [4].

Considering the self-contained cell presented by Paul and DiBenedetto [4], it is very unlikely that the results obtained in that system were influenced by the resistance effects discussed in the first part of this series [5]. With the advances in pressure devices, mercury-based pressure sensors were replaced by more sensitive electronic pressure transducers, and the issue of increasing the permeate side volume ceased to exist. Larger volumes at the permeate side were employed again. For example, depending on the actual permeability of membrane, Koros *et al.* could set the permeate side volume at 43 x 10^{-6} m^3 or 109 x 10^{-6} m^3 [6] by means of opening or closing appropriate valves in a system consisting of series of interconnected vessels [7].

Unlike 1960s when the Dow self-contained cell was commercially available, there is no standard CV system today. Different research groups use different configurations of the vacuum part of the system [8-14]. While most groups provide information on the initial pressure at which gas permeation tests are performed, the parameters such as the length and the diameter of tubes at the permeate side of membrane are usually not specified. In case of the system used by Favre *et al.* [14] these details are irrelevant because according to the provided diagram, the vacuum volume consists of a cylinder of the diameter equal to the diameter of the membrane. On the other hand, judging from the available diagrams the configuration of the permeate side volume may sometimes be quite complicated [8,12,13]. In case of the CV system described by Tabe Mohammadi *et*

al. [8], to which we had an access, the total length of a 1/4" is approximately 2.5 m. Therefore, if the analysis presented in Part I of this series were valid; the permeation data from some of currently utilized CV systems might be influenced by the effects of system resistance [5].

Gas diffusion data reported by Sanchez *et al.* was corrected for the apparatus "delay times", which varied from 0.30 to 0.67 s [13]. It is not clear however how these delay times were established. The possibility of system resistance was also considered by Shishatskii *et al.* [10]. The resistance imposed by the system, which was referred to as a "time resolution", was examined by a sudden exposure of the permeate side volume, initially at vacuum, to a pressure of 1,000 Pa and measuring the time for a pressure transducer to detect the increase in pressure. The authors concluded that the apparatus error in time lag determination was significantly lower than 1 s [10]. It is important to emphasize that unless the internal diameter of tube is very small, at 1,000 Pa the diffusion coefficient of gases is relatively large, thus making the effects of system resistance negligible [5]. Therefore, the method employed by Shishatskii *et al.* [10] might not be relevant for the examination of system resistance. Moreover, gas flow rates resulting from a 1,000 Pa pressure gradient in a vacuum tube would be orders of magnitude greater than those associated with permeation of gases through membranes.

The purpose of Part II of this series of papers is to experimentally verify the existence of non-negligible resistance to accumulation of gases in the actual gas permeation experiments involving polymeric membranes. The method of evaluation of system resistance employed in this work is different from that used by Shishatskii *et al.* [10]. It simulates the model developed in Part I of this series [5], that is, transient flows

resulting from a step change in feed pressure are monitored at different distances from the membrane by two pressure transducers simultaneously. The membrane used in this study was prepared from high molecular weight polyphenylene oxide (PPO). The properties of membrane required for the verification of the theoretical model from Part I were determined in a system configuration imposing a minimum resistance to accumulation of gases at the permeate side of membrane.

2. Experimental Setup and Procedure

According to the model developed in Part I, if permeate side of membrane consists of a 1/2" (or larger) tube; the effects of resistance are practically negligible, unless the tube is very long. On the other hand, if the permeate side of membrane consists of a 1/4" (or smaller) tube the effects of resistance should be evident [2]. Consequently, the permeate side of the experimental CV system was designed to consists of either 1/4" or 1/2" tubes. The latter tube was designated for characterization of the actual gas transport properties of membrane, while the former tube for the demonstration of the validity of the developed model.

2.1 Description of constant volume system

The CV system utilized in this project is shown in Fig. 1. A membrane is sandwiched between the two cylindrical parts of a stainless steel cell (A). The effective area for gas permeation in the membrane cell A_m = 9.08 x 10^{-4} m^2. The feed side of the cell consists of a standard 1/4" stainless steel tube and a tank (B) of volume 26.50×10^{-3} m^3, which can be pressurized up to 931 kPa (135 psia) using a compressed gas cylinder

(C). The tank is equipped with a pressure gauge (D) having a 0 - 1,207 kPa (175 psia) range and a 6.9 kPa (1 psia) reading accuracy. The permeate side of the cell consists of a straight tube (E) or (F), several connecting tubes, and an auxiliary tank (G), which is not utilized in this project. The permeate side is equipped with two pressure transducers (H) and a rotary vacuum pump (I) (Edwards model RV3). In addition, there are several two-way valves at both sides of the membrane cell. All valves are manually operated diaphragms (Swagelock model SS-DSVCR4) equipped with VCR fittings. The pressure transducers (MKS model 627B11TBC1B) have a linear range from 0 to 1,333 Pa (10 mmHg) with a 2.67 $\times 10^{-2}$ Pa (2 $\times 10^{-4}$ mmHg) reading accuracy and the maximum error corresponding to 0.12 % of the read pressure. They are connected to a personal computer equipped with a LabView program to record the dynamic pressure every second.

The length of tubes E and F is 2.04 m each. This length represents the distance between valves V4 and V7. In addition, the length of connecting tubes between the cell and the valves V3 and V4 is 0.46 m, and the length between the valves V7, V8, V5 and V6 is 1.40 m. Tubes E and F have two slots each, for the installation of pressure transducers. When installed, the pressure transducers are 0.59 m and 2.38 m from the cell, regardless of the utilized tube. Tubes E and F are the same except of their diameter size. Tube E is a standard 1/4" stainless steel tube (Swagelock SS-T4-S-049-20), while tube F is a standard 1/2" stainless steel tube (Swagelock SS-T8-S-049-20). The corresponding inside diameters of tubes E and F are 0.00386 m and 0.0102 m, respectively. All connecting tubes at the permeate side are of the same type as tube E. Consequently, when tube E is installed, the total length of a 1/4" tubing between the cell and the valve V7 in 2.50 m. This length increases to 3.90 m when the valve V7 is opened,

while the valves V5, V6, and V8 remain closed. The corresponding total volumes of the permeate side of membrane are 57.47 $\times 10^{-6}$ m^3 and 82.43 $\times 10^{-6}$ m^3. When tube F is installed, 2.04 m of 1/2" tubing is preceded by 46 cm of 1/4" tubing. The corresponding total volume of the permeate side is 196.22 $\times 10^{-6}$ m^3 and the volume of the feed side up to the valve V3 is 10 x 10^{-6} m^3. The volumes provided above were determined by a gas expansion technique. They include dead volumes associated with valves, fittings, pressure transducers, and the membrane cell.

2.2 Membrane preparation

A symmetric, high molecular polyphenylene oxide (PPO) membrane was utilized as a medium to provide time lag in pressure response. The membrane was prepared by a solvent evaporation technique, that is, 2 cm^3 of a dilute PPO solution (3 wt%) in TCE was poured onto a levelled glass plate within a 5 cm diameter metal ring and the solvent was let to evaporate for 2 days. To slow down the evaporation process, a filter paper was placed on the metal ring. The membrane was then removed from the glass plate by immersing it into a distilled water bath for 5 minutes, after which it was dried for several days at ambient conditions. The dried membrane had the average thickness, as determined by a micrometer, l = 18.4 x 10^{-6} m. To minimize possible variation in membrane properties due to the presence of residual solvent, moisture, etc., as well as, due to physical aging, the system with the membrane installed in it was degassed for 25 days. The lowest absolute pressure achievable in the system with membrane was 5.5 Pa.

2.3 Experimental conditions

All gas permeation tests were performed using nitrogen from a gas cylinder. Since polyphenylene oxide is a glassy polymer the permeability (P_m), diffusivity (D_m) and solubility (S_m) coefficients of N_2 depend on pressure [1]. To avoid possible variation in gas transport coefficients with pressure, all gas permeation experiments were performed at the same feed pressure (p_f) of 206.8 kPa (30 psia). The temperature during all experiments was also the same and equal to 23°C. Consequently, the gas transport properties reported in this paper, refer to the effective P_m, D_m, S_m of N_2 in PPO at p_f = 206.8 kPa and T = 23°C.

To pressurize the feed side of membrane and therefore to begin the gas permeation experiment, tank B was first pressurized to the desired pressure, after which valve V2 was quickly opened. Since the volume of tank B is much greater than the volume enclosed between the membrane and the valve V2, (this volume will be denoted as V_f) opening of V2 did not affect the reading of pressure gauge D. Moreover, the pressure at the feed side of membrane remained constant during entire gas permeation experiments.

Before each experiment the system was continuously evacuated for five days to ensure that the highest achievable vacuum of 5.5 Pa is reached and the feed side of membrane is reasonably degassed. During the evacuation step valves V3, V4, V5, V6, and V7 stayed open, while valves V2 and V8 were closed. Consequently, the space between the membrane and the valve V2 was not directly connected to the vacuum pump. As a result, degassing of V_f occurred through the membrane.

It can be shown that during the evacuation step the pressure in V_f (p_f) changes with time (t) according to the following equation:

$$p_f = p_p + (p_{f0} - p_p)\exp\left(-\frac{P_m RTA}{V_f v_{STP} l} t\right) \quad (1)$$

where, p_{f0} is the initial pressure in V_f, p_p is the pressure at the permeate side of membrane (assumed constant during degassing of the system), P_m is the permeability coefficient of N_2 in PPO, A and l are the membrane area and thickness, respectively, T is the absolute temperature, R is the universal gas constant, and v_{STP} is the volume of one mole of gas at standard temperature and pressure conditions. Taking P_m = 3.43 x 10^{-17} m^3(STP) m/(s m^2 Pa)[1], and other parameters corresponding to the actual experimental conditions, that is, p_{f0} = 206.8 kPa, p_p = 5.5 Pa, V_f = 10 x 10^{-6} m^3, A = 9.08 x 10^{-4} m^2, l = 18.4 x 10^{-6} m, T = 296.16 K, as well as, R = 8.314 J/mol K and v_{STP} = 22,414 x 10^{-6} m^3(STP)/mol, it can be shown that p_f after five days (4.32 x 10^5 s) of evacuation becomes of the same order as p_p.

The minimum pressure of 5.5 Pa that could be achieved after extensive evacuation of the system is greater than 4.1 Pa, that is, the minimum pressure in system similar to the one depicted in Fig. 1, in which however a low flow mass flow controller is used instead of the membrane cell [15]. A leak test in the system, excluding the auxiliary tank, was performed at the lowest achievable vacuum and found to be 1.3 x 10^{-3} cm^3(STP)/min. For comparison, when the low flow mass flow controller was used instead of the membrane cell, the leak rate was in the range of 10^{-7} cm^3(STP)/min [15]. The much larger leak rate and the lower vacuum in the system used in this project are therefore are due to the presence of the membrane cell.

The initial pressures at the permeate side of membrane at which gas permeation experiments were performed were varied from 5.5 Pa to 267 Pa (2 mmHg). The permeate side pressure was adjusted by taking the advantage from the existing leak. The leak test

[1] It will be shown later that this is the effective P_m of N_2 in the utilized PPO membrane.

could be carried out until the permeate side pressure of membrane reached the desired value after which the feed side could pressurized to start the permeation experiment. Figure 2 presents the plot of the diffusion coefficient of N_2 (D) at the experimental temperature of 23°C as a function of pressure for the two utilized sizes of the standard stainless steel tube. The pressure range in Fig. 2 corresponds to the range of the experimental initial pressures. For this pressure range and the internal diameters of 0.00386 m and 0.0102 m corresponding to standard 1/4" and 1/2" stainless steel tubes, respectively, the diffusion coefficients determined from the empirical model of Knudsen and slip flow model are similar. The methods of calculation of D in cylindrical tubes have been discussed in the Part I of this series of papers [5].

It is important to emphasize, that because of limitation imposed by the vacuum pump and the existing leak, the membrane was not at absolute vacuum before starting gas permeation experiments. Moreover, the membrane was exposed not only to the experimental N_2, but also to the gases present in air. On the other hand, the absolute pressures at both sides of membrane before every gas permeation experiment were generally low and comparable to each other. Therefore, the application of the Barrer equation to describe the time dependent flux through the membrane, on which the proposed model relies, seems to be justified.

3. Results and Discussion

Part I of this series of papers has identified the conditions, at which the resistance to accumulation of gases is not negligible. The experimental CV system allows simultaneous monitoring of a pressure rise at two different distances from the membrane.

Different pressure responses at different distances from the membrane would confirm the existence of a non-negligible resistance to gas accumulation. For such a proof, the properties of membrane are irrelevant. On the other hand, to validate the model developed in Part I, which allows corrections for the effects of system resistance, the effective gas transport properties of membrane, at given conditions, are required.

3.1 Effective permeability, diffusivity and solubility coefficients of N_2 in PPO

To determine the effective gas transport coefficients of N_2 in the PPO membrane, the resistance of the system should be eliminated or at least minimized. As discussed in Part I, while this can be accomplished either by increasing the diameter of tubing or the initial pressure, the former, because of the requirement of membrane being initially free from permeating species, is preferred [16,17]. The experiments were therefore performed using tube F at the lowest achievable initial pressure of 5.5 Pa. It should be noted that tube F in the experimental configuration is preceded by 0.46 m of the 1/4" connecting tube. Consequently, there are at least three resistances in series during gas permeation experiments involving tube F. In other words, the experimental time lag (θ_{exp}) can be expressed as a summation of at least three terms:

$$\theta_{exp} = \theta_m + \theta_{T1} + \theta_{T2} \tag{2}$$

where, θ_m is the time lag due to membrane resistance, θ_{T1} is the time lag due to resistance in the 1/4" connecting tube, and θ_{T2} is the time lag due to resistance in tube F. It is important to emphasize that Eq. (2) assumes that the resistance due to membrane cell, that is, the resistance imposed by a filter paper and a porous disk on which the membrane sits, is negligible. The time lag due to resistance in tube F can be expressed by [15]:

$$\theta_{T2} = \frac{L_2^2}{6D_2} - \frac{(L_2 - x)^2}{2D_2} \tag{3}$$

where, L_2 is the length (2.04 m) of tube F, D_2 is the diffusion coefficient of N_2 in the 1/2" tube and x is a distance of pressure transducer from valve V4. At p_o = 5.5 Pa and temperature of 23°C, D_2 = 1.97 m^2/s. The two pressure transducers are 0.13 m and 1.92 m from the entrance to tube F. Therefore, according to Eq. (2), θ_{T2} at x = 0.13 m is –0.57 s while θ_{T2} at x = 1.92 m is 0.35 s. This means that θ_{exp} at x = 1.92 m should be approximately 0.9 seconds greater than θ_{exp} at x = 0.13 m.

The determination of the actual θ_m requires also the evaluation of θ_{T1} due to the 1/4" tube. Since both pressure transducers are downstream the 1/4" tube, $x = L_1$ = 0.46 m and therefore:

$$\theta_{T1} = \frac{L_1^2}{6D_1} - \frac{(L_1 - x)^2}{2D_1} = \frac{L_1^2}{6D_1} \tag{4}$$

where, D_1 at 5.5 Pa and 23°C is 0.50 m^2/s. Consequently, according to Eq. (4), θ_{T1} = 0.07 s. Because of its magnitude, θ_{T1} will be neglected in further analysis.

Figure 3 presents the results of one of two identical experiments performed using tube F at the initial pressure of 5.5 Pa. The pressures at both locations were recorded every second. It can be noticed that for a given time, and particularly during the period between 20 s and 50 s, the pressure recorded at x = 0.13 m is slightly greater than the pressure recorded at x = 1.92 m. It is interesting to note that during this period of time, $p(x = 0.13 \text{ m}, t) \approx p(x = 1.92 \text{ m}, t + 1\text{s})$, that is, the pressure response at x = 1.92 m is shifted by approximately one second to the right from the pressure response at x = 0.13 m. This experimentally observed shift corresponds closely to theoretically predicted difference in θ_{exp} at these two locations of 0.9 s. On the other hand, after 150 s the

pressure difference at a given time and the shift in pressure responses disappears. This is because as time progresses the pressure increases, which leads to increase in the diffusion coefficient of gas in tube, and thus a disappearance of system resistance.

The experimental time lag was determined considering the points between 200 s and 300 s (not shown in Fig. 3), when the two pressure responses are indistinguishable, and the pressure rise is a linear function of time. Table 1 summarizes the results of two experiments performed in tube F at p_o = 5.5 Pa. The θ_m of 14.6 s from the first experiment is less than θ_m of 15.3 s from the second experiment. On the other hand, in case of *dp/dt* the situation is opposite. The variation in time lag is most probably due to the accuracy in recording the "zero" time and the existing leak into the system. It is also important to notice that small differences in *dp/dt* might lead to relatively large differences in the experimentally determined of time lags. The properties from the two experiments are averaged out, and these average values are considered to represent the transport properties of N_2 in the PPO membrane at p_f = 206.8 kPa (30 psia) and T = 23°C. The properties of PPO membrane listed in Table 1 are comparable to those reported by Aguilar-Vega and Paul [18] and Alentiev *et al.* [19].

3.2 Experimental time lag in case of significant system resistance

To verify the validity of the model proposed in Part I, the experiment was performed using system configuration and conditions corresponding to the maximum resistance. To minimize the diffusion coefficient of N_2, tube E at the lowest achievable pressure of 5.5 Pa was utilized. At these conditions, the diffusion coefficient of N_2 is 0.50 m^2/s. In addition, valve V7 stayed open during the experiment to maximize the length of

tubing at the permeate side of membrane. It is important to emphasize that unlike the system configuration considered in Section 3.1, all tubes at the permeate side of membrane had the same internal diameter. Therefore, Eq. (2) becomes:

$$\theta_{exp} = \theta_m + \theta_T \tag{4}$$

where θ_T is the time lag due to resistance in the 1/4" tube, which can be evaluated using Eq. (3), in which $D_2 = D = 0.50$ m^2/s and $L_2 = L = 3.90$ m. Therefore, at $x = 0.59$ m, $\theta_T = -5.9$ s and at $x = 2.38$ m, $\theta_T = 2.8$ s. This means as a result of system resistance θ_{exp} at these two locations should differ by 8.7 s.

Figure 4 presents the progress of the first 40 seconds of the actual experiment at $x = 0.59$ m and $x = 2.38$ m, and the theoretically predicted pressure responses at these two locations. In determination of the theoretical pressure responses, the average transport properties of N_2 in the PPO listed in Table 1 were used. There is generally a good match between the experimental and theoretical responses in both positions, which indicates that the proposed model successfully describes the accumulation of N_2, emerging from the membrane, into the experimental CV system. In addition, Fig. 4 indicates that the diffusion coefficient of N_2 in the 1/4" tube and the membrane properties used in simulation were accurate. There are however some small deviations between the experimental data and the model in Fig. 4.

Considering pressure responses depicted in Fig. 4, Fig. 5 compares the experimental and theoretical pressure differences between the two locations as a function of time. The pressure difference at time zero is due to the leak into the system form the membrane cell. It can be noticed that even after correcting for the pressure difference at time zero, the experimental pressure difference is slightly greater than the theoretical one

during the first 25 s of the experiment. On the other hand, for t between 25 s and 30 s, the experimental pressure difference stabilizes and at $t > 30$ s it slightly decreases, whereas the theoretical pressure difference keeps on increasing towards a steady state constant pressure difference. Recalling Fig. 3 from Part I, after 40 s the flux, which is proportional to dp/dt, is still far from its steady state value even for a membrane having the time lag of 9.98 s [2]. This is why the theoretical pressure difference in Fig. 5 at $t = 40$ s keeps on increasing. After approximately 25 – 30 s of the experiment the model starts to overestimate the resistance to gas accumulation. The resistance to gas accumulation, assumed constant in the model, in reality decreases with time because of increase in pressure and thus the diffusion coefficient.

The divergence between the model and the experimental data continues as the time progresses. Figure 6 presents the continuation of the experiment depicted in Fig. 4 showing the pressure responses at both locations from 150 s to 195 s. It can be noticed that the difference between the pressures at the two locations ranges from 1.4 Pa at 150 s to 1.1 Pa at 195 s. At $t > 150$ s, that is, at $t > 10 \times \theta_m$, the flux through the membrane should reach a steady state level and therefore, the pressure responses in Fig. 6 should be suitable for the determination of time lag of membrane. The linear regression on the experimental data shown in Fig. 6 gives the following equations:

$$\text{for } x = 0.59 \text{ m: } p = 0.5144t - 0.2833 \tag{5}$$

$$\text{for } x = 2.38 \text{ m: } p = 0.5210t - 2.6371 \tag{6}$$

Setting $p = p_o$ and solving for t gives the experimental time lag. The initial pressure recorded by the pressure transducer at $x = 0.59$ m was 5.5 Pa; therefore the experimental time lag at this location is 11.28 s. On the other hand, the initial pressure recorded by the

pressure transducer at x = 0.59 m was 5.3 Pa; therefore the experimental time lag at this location is 15.22 s.

In reality, despite perfect linear fits the pressure responses in Fig. 6 are not truly linear. As already noted, the difference between the pressure responses in Fig. 6 decreases with time. Similarly to the pressure responses in Fig. 3, those in Fig. 6 would eventually become indistinguishable. This means that the slopes given by Eqs. (5) and (6) do not correspond to the actual steady state flux of N_2 through the membrane. The difference between the two slopes results from the resistance to accumulation of N_2 at the permeate side of membrane.

One could argue, that errors in the experimentally measured time lag and the steady state flux, discussed above, could be eliminated by considering the pressure response after a time much longer than 200 s when the pressure at the permeate side of membrane is sufficiently large for the resistance to disappear. While in principle such approach appears to be logical, the experimentally determined time lag and the steady state flux might then be influenced by the permeate side pressure. The effect of the initial pressure is discussed in Section 3.4.

3.3 Combined effect of location of pressure transducer and tube length

To study the effect of tube length, two experiments with tube E at the initial pressure of 7.3 Pa were performed. In the first experiment valve V7 stayed closed while in the second one valve V7 was open. The total length of the 1/4" tube at the permeate side of membrane was 2.50 m in the first experiment and 3.90 m in the second experiment. The locations of pressure transducers in tube E are fixed; therefore adding

extra length of tube also affects the relative positions of pressure transducers with respect to the membrane cell. For the experiment in the shorter tube, the dimensionless positions (x/L) of the transducers were 0.236 and 0.952, while for the experiments in the longer tube they were 0.151 and 0.610.

Figures 7a and 7b present the progress of the first 40 s of the experiments in the 2.5 m and 3.9 m long tubes, respectively. Any differences between the experimental pressure responses observed in Fig. 7a and 7b, represent the combined effect of the tube length and the dimensionless position of pressure transducer at the permeate side of membrane. Considering the two figures it can be noticed that there is a better match between the experimental and theoretical data in the shorter tube. The experimental data at both locations in Fig. 7a is shifted to the left compared to the respective theoretical pressure responses. It is important to emphasize that despite this shift the experimental and theoretical pressure differences for a given time in Fig. 7a are comparable. These differences are also comparable in Fig. 7b. This means that for the time frame presented in Figs. 7a and 7b, the system resistance is reasonably well predicted by the theoretical model. The shift between the experimental and theoretical data observed in Fig. 7a, could indicate that the time lag of membrane used in simulation was greater than the actual time lag of membrane. However, if this were the case, a similar shift would also be observed in Fig. 7b, because both experiments were performed at the same initial pressure. Recording of the time zero might be the major cause of discrepancy in this case.

3.4 Effect of initial pressure

To study the effect of initial pressure three experiments utilizing tube E with valve V7 opened were performed at the initial pressures of 26.7 Pa, 133 Pa and 267 Pa. The experimentally observed and theoretically predicted progress of these experiments is presented in Figs. 8a, 8b, and 8c, respectively. The corresponding diffusion coefficients of N_2 in the 1/4" tube at these initial pressures and 23°C are, 1.06 m^2/s, 3.88 m^2/s, and 7.41 m^2/s, respectively.

It can be noticed that in case of all initial pressures, the experimental data at a given position is shifted to the left from the theoretical data. This phenomenon has already been observed in Fig. 7a for the experiment performed in the same tubing configuration. As stated in the previous section, a shift of the experimental data, at a given position, to the left with respect to the theoretical data could indicate that the actual time lag of membrane is less than the value used in generation of the theoretical pressure response. As the initial pressure increases, the concentration of N_2 dissolved in the membrane prior to initiation of the actual gas permeation experiment increases. As a result, the resistance to gas transport through the membrane, which is not entirely degassed before the test, might be less than the resistance to gas transport through the membrane which is completely degassed. A lower resistance to gas transport through the membrane would manifest itself by a lower time lag.

Table 2 summarizes experimentally determined time lags for the experiments depicted in Fig. 8. The time lags were determined based on the average values of dp/dt recorded within a range of permeate side pressures stretching from 400 to 665 Pa. The numerical values of dp/dt are also included in Table 2. The anticipated effect of the initial pressure on the experimentally determined time lag of membrane, that is a decrease in θ_m

with increase in p_o, is not observed in Table 2. On the other hand, all θ_ms listed in Table 2 are less than θ_m = 15 s used in the theoretical model. It is important to emphasize that while the *dp/dt* values in Table 2 are similar, they are not the same. Since time lag is determined by the extrapolation of a linear part of the pressure response curve, even small variations in *dp/dt* might result in significant errors in the measured time lag. In addition, the existing leak into the system could result in error in the experimentally determined *dp/dt*. This is probably why the anticipated trend between p_o and θ_m is not evident in Table 2.

Considering the difference between pressures recorded by the two transducers at a given time one can notice that the experimental difference is greater than theoretical one. This effect is clearly seen in Fig. 8c, because the theoretical pressure difference is close to zero. However, this difference exists in case of experiments performed at all initial pressures. To illustrate this, Fig. 9 presents the comparison of the experimental and theoretical pressure differences for the tests depicted in Fig. 8.

It can be noticed that regardless of the initial pressure, the maximum deviation between the experimental and theoretical pressure differences occurs at around 20-25 s, after which it either remains constant or decreases. The experiments depicted in and Fig. 9 were performed using the same volumes at the permeate side of membrane. Therefore, the corresponding pressure increases at the permeate side of membrane are comparable. However, the relative changes in the diffusion coefficient associated with these pressure increases strongly depend on the initial pressure. For example, considering a 10 Pa increase, at p_o = 26.7 Pa, D = 1.06 m^2/s while at p_o = 36.7 Pa, D = 1.33 m^2/s, which is 25 % greater than D at 26.7 Pa. On the other hand, at p_o = 267 Pa, D = 7.42 m^2/s while at p_o

= 277 Pa, D = 7.68 m^2/s, which is just 3.5 % greater than D at 267 Pa. This is why once the maximum deviation between the experimental and theoretical pressure differences is reached it remains relatively constant in case of tests performed at the initial pressures of 133 Pa and 267 Pa, while it decreases in case of the test performed at the initial pressure of 26.7 Pa. A trend similar to the latter test has also been observed in Fig. 5 for the test performed at the initial pressure of 5.5 Pa.

The magnitude of the maximum deviation between the experimental and theoretical pressure differences is comparable for all tests. They are, 0.5 Pa, 0.3 Pa and 0.3 Pa for the tests at the initial pressures of 26.7 Pa, 133 Pa, and 267 Pa, respectively. Interestingly, in case of two other tests performed in the same system configuration, however at the initial pressures of 5.5 Pa and 7.3 Pa, the deviations between the experimental and theoretical pressure differences of similar magnitude (0.5 Pa and 0.4 Pa, respectively) and at similar times occurred.

A greater difference between the experimental pressures than between the theoretical pressures indicates that the actual resistance between the two pressure transducers in tube E is greater than the theoretically predicted value, based on its length, diameter and the initial pressure. Since this extra resistance seems to be independent of the initial pressure, it most likely originates from valves and fittings as well as dead volumes in the system. Consequently, it might be very difficult to predict its numerical value theoretically. On the other hand, its contribution to the overall system resistance in case of membranes with a short time lag might not be negligible.

4. Conclusions

The existence of the non-negligible resistance to accumulation of gases, at the conditions identified by the theoretical model proposed in Part I of this series of papers, has been verified experimentally. Because of relatively small volume of the permeate side of membrane in the experimental CV system, the proposed model was capable to describe accurately only the first 20 – 30 seconds of the actual gas permeation experiments. After this initial time, a pressure increase at the permeate side of membrane is sufficiently large making the assumption of constant diffusion coefficient invalid. According to slip flow model, which was used to evaluate the diffusion coefficient at the permeate side of membrane, for the range of experimental pressures D increases with pressure and thus with time. The observed discrepancy between the theoretical and experimental pressure responses after the first 20-30 seconds of the experiments have further confirmed the validity of the slip flow model with Maxwell's deduction of the coefficient of slip.

After a period corresponding to 10 times of the actual time lag of membrane, at which according to the Barrer equation, the pressure rise is a linear function of time, the effects of resistance to accumulation of gases might still present. Because of decreasing resistance to accumulation with time, and hence a decrease in the pressure difference between different locations, the slope of the pressure response curve depends on the location of pressure transducer as long as the difference in pressure responses exits. As shown in the experiment with the maximum system resistance, even a small difference in these slopes in combination with a small difference in pressures responses, resulted in a 4 s difference in time lag of the PPO membrane at different locations. If the volume of the permeate side of membrane were larger, the difference in the experimentally measured

time lags would approach the value of 8.7 s predicted theoretically. Despite the limitation of the proposed model due to variation of the diffusion coefficient with time, the theoretically predicted phenomenon of overestimation or underestimation of the measured time lag depending on the position of pressure transducer, has been confirmed in this study.

5. Acknowledgement

The authors gratefully acknowledge the financial support for this project provided by the Natural Science and Engineering Research Council of Canada.

6. References

1. R. Zolandz and G.K. Fleming, Gas permeation, in H. Sirkar (Ed.), Membrane Handbook, Van Nostrand Reinhold, New York, 1992.
2. H.A. Daynes, The process of diffusion through a rubber membrane, Roy. Soc. Proc., 97 (1920) 286.
3. R.M. Barrer, Permeation, diffusion and solution of gases in organic polymers, Trans. Farad. Soc., 35 (1939) 628.
4. D.R. Paul and T. DiBenedetto, Diffusion in amorphous polymers, J. Polym. Sci. Part C, 10 (1965) 17.
5. R. Chapanian and B. Kruczek, Effect of Resistance of Vacuum Tubes on Time Lag of Membrane in Constant Volume Systems. Part I. Theoretical Considerations, submitted to J. Membr. Sci., December 2003.

6. W.J. Koros, D.R. Paul and A.A. Rocha, Carbon dioxide sorption and transport in polycarbonate, J. Polym. Sci., Polym. Phys. Ed., 14 (1976) 687.
7. D.R. Paul and D.R. Kemp, The diffusion time lag in polymer membrane containing adsorptive fillers, J. Polym. Sci., Part C, 41 (1973) 79.
8. A. Tabe Mohammadi, T. Matsuura and S. Sourirajan, Design and construction of gas permeation system for the measurement of low permeation rated and permeate compositions, J. Membr. Sci., 98 (1995) 281.
9. V. Compan, A, Ribes, R. Diaz-Calleja, E, Riande, Mechanical relaxation and diffusional characteristics of coextruded films prepared from copolymers of ethylene-1-octene, Polymer, 36 (1995) 323.
10. A.M. Shishatskii, Yu.P, Yampol'skii, K.-V Peinemann, Effects of film thickness and density on gas permeation parameters of glassy polymers, J. Membr. Sci., 112 (1996) 275.
11. Y.M. Lee, S.Y. Ha, Y.K. Lee, D.H. Suh, S.Y. Hong, Gas separation through conductive polymer membrane. 2. Polyaniline membranes with O_2 selectivity, Ind. Eng. Chem. Res. 38 (1999) 1917.
12. W.-H. Lin, R.H. Vora, T.-S. Chung, Gas transport properties of 6FDA-Durene/1,4-phenylenediamine (pPDA) copolyimides, J. Polym. Sci., Part B: Polym. Phys., 38 (2000), 2703.
13. J. Sanchez, C.L. Gijiu, V. Hynek, O. Muntean, A. Julbe, The application of transient time-lag method for the diffusion coefficient estimation on zeolites composite membranes, Sep. Purification Tech., 25 (2001) 467.

14. E. Favre, N. Morlier, D. Roizard, Experimental evidence and implications of an imperfect upstream pressure step for the time lag technique, J. Membr. Sci., 207 (2002) 59.

15. R. Chapanian, B. Kruczek, Resistance to accumulation of gases in high vacuum systems, submitted to J. Vac. Sci. Technol. A, Sept. 8, 2003.

16. R. M. Barrer, G. Skirrow, Transport and equilibrium phenomena in gas-elastomer systems. I Kinetic phenomena, J. Polym. Sci., 3 (1948) 549.

17. S. W. Rutherford and D.D. Do, Review of Time Lag Permeation Technique as a Method for Characterization of Porous Media and Membranes, Adsorption, 3 (1997) 283.

18. M. Aguilar-Vega, D.R. Paul, Gas transport properties of polyphenylene ethers, J. Polym. Sci., 31 (1993) 1577.

19. A. Alentiev, E. Drioli, M. Gokzhaev, G. Golemme, O. Ilinich, A. Lapkin, V. Volkov, Yu. Yampolskii, Gas permeation properties of phenylene oxide polymers, J. Membr. Sci., 138 (1998) 99.

Table 1 Effective transport properties of N_2 in PPO membrane determined at 23°C and feed pressure of 206.8 kPa (30 psia).[a]

Run #	dp/dt [Pa s^{-1}]	P_m x 10^{17} [m^3(STP)$s^{-1}m^{-1}$ Pa^{-1}]	θ_m [s]	D_m x 10^{12} [m^2 s^{-1}]	S_m x 10^6 [m^3(STP) m^{-3} Pa^{-1}]
1	0.197	3.45	14.6	3.86	8.94
2	0.195	3.41	15.3	3.69	9.24
Avg.	0.196	3.43	15.0	3.78	9.07

[a] Experiments performed in the 1/2" tube at the initial pressure of 5.5 Pa.

Table 2. Influence of the initial pressure on the experimentally measured time lag of PPO membrane. All experiments performed in the 1/4" tube of total length 3.9 m.

p_o [Pa]	dp/dt[a] [Pa s^{-1}]	θ_m [s]	D_m x 10^{12} [m^2 s^{-1}]
26.7	0.556	12.8	4.41
133	0.577	12.9	4.37
267	0.553	14.2	3.97

[a] Based on the pressure response between 400 Pa and 665 Pa

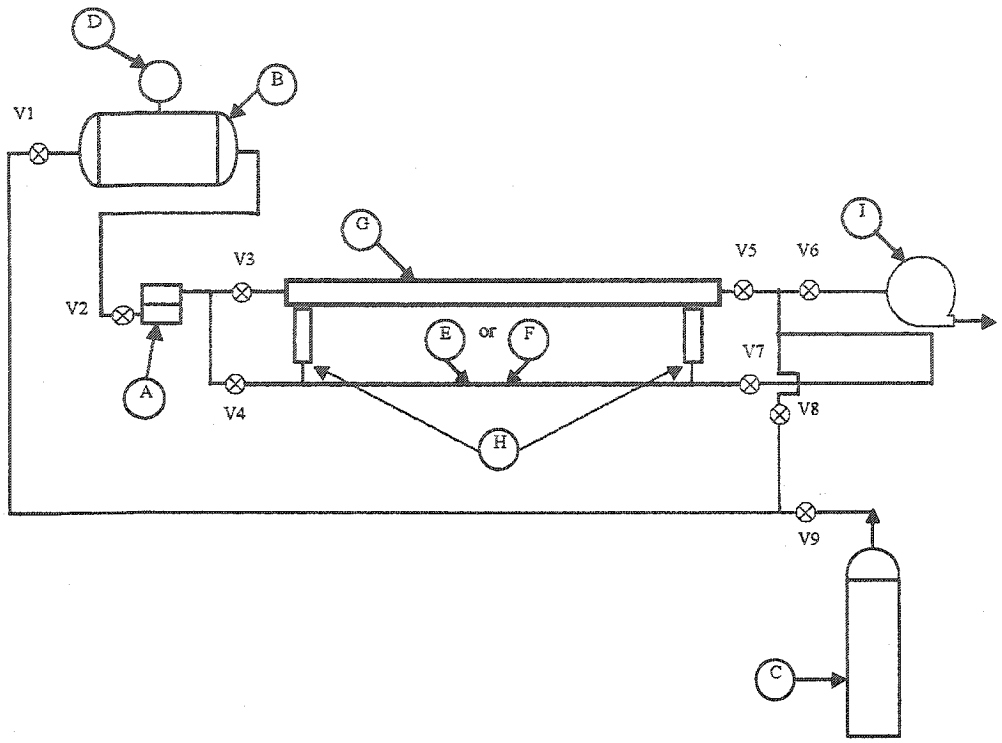

Figure 1. Schematic diagram of the experimental constant volume system. Important components of system: membrane cell (A), feed tank (B), compressed gas cylinder (C), feed pressure gauge (D), tube for accumulating gas (E) or (F), auxiliary tank (G), permeate side pressure transducers (H), rotary vacuum pump (I).

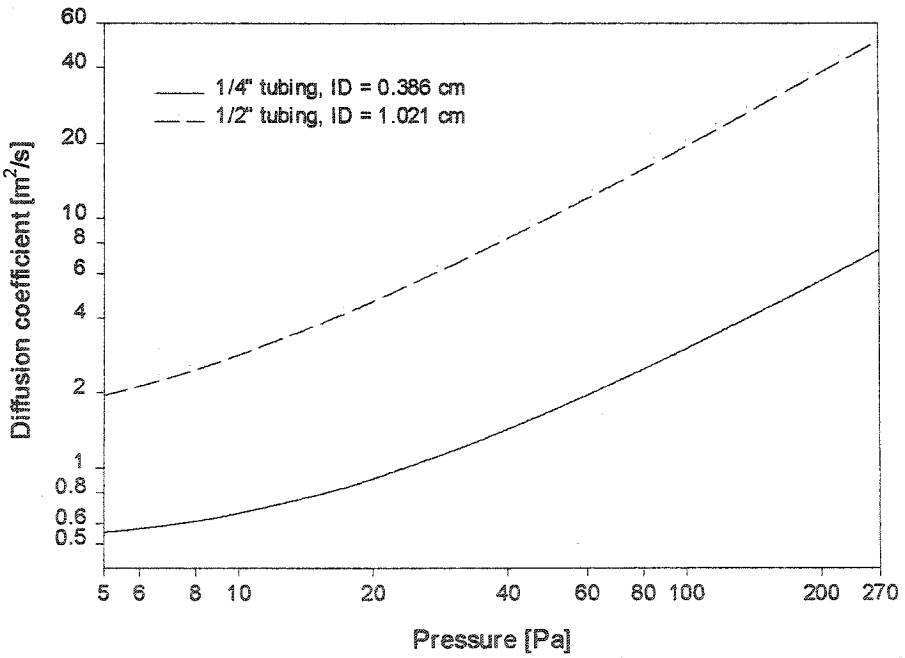

Figure 2. Effect of pressure on the diffusion coefficient of N_2 at 23°C in the experimental tubes (E) and (F).

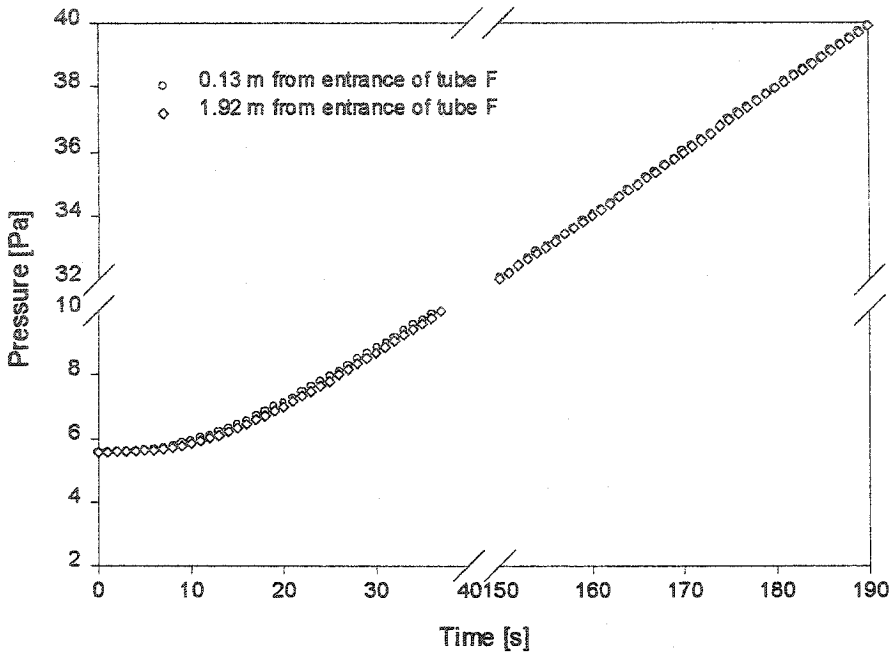

Figure 3. Progress of gas permeation experiment used for determination of the effective transport properties of N_2 in PPO membrane at 23°C and the feed pressure of 207×10^3 Pa. Permeate side consists of tube (F) at the initial pressure of 5.5 Pa.

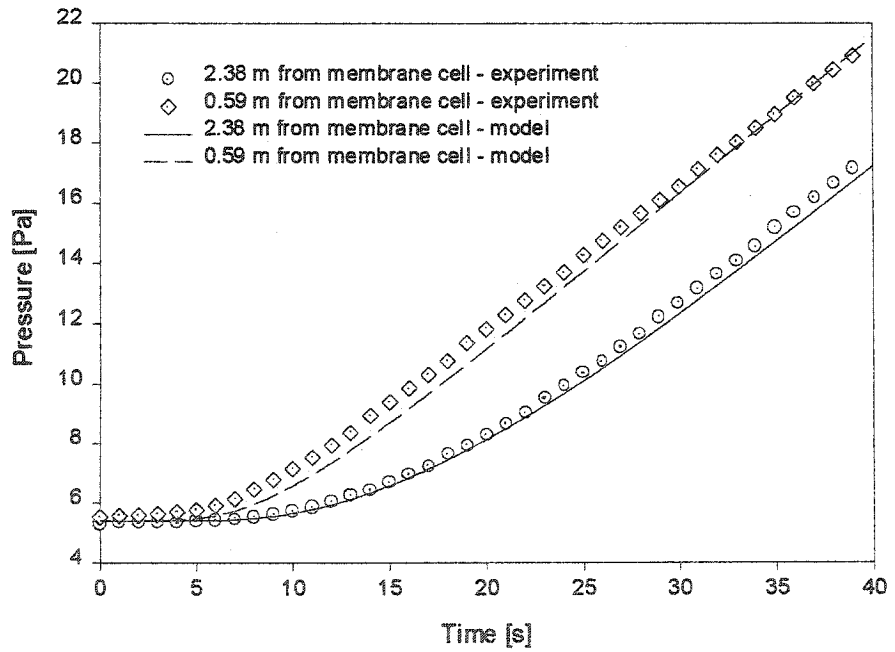

Figure 4. Progress of first 40 s of gas permeation experiment in the 1/4"tube of total length of 3.9 m, initially at 5.5 Pa. Experiment performed at 23°C and the feed pressure of 207×10^3 Pa.

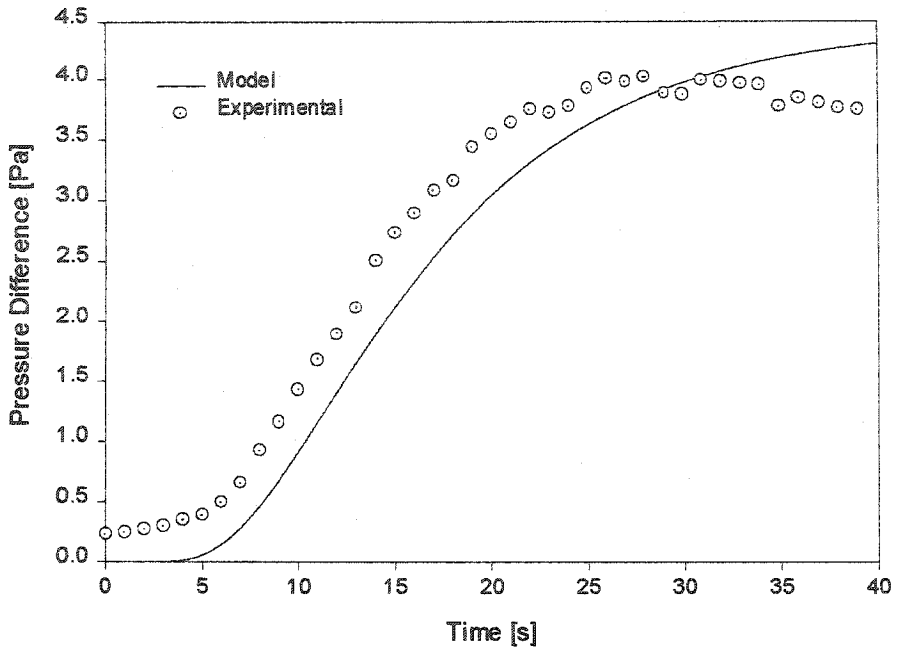

Figure 5. Comparison of theoretically predicted and experimentally observed differences between pressures at x = 0.59 m and x = 2.38 m during gas permeation experiment performed in the 1/4"tube of total length of 3.9 m, initially at 5.5 Pa. Other experimental conditions, T = 23°C, p_f = 207 × 10^3 Pa.

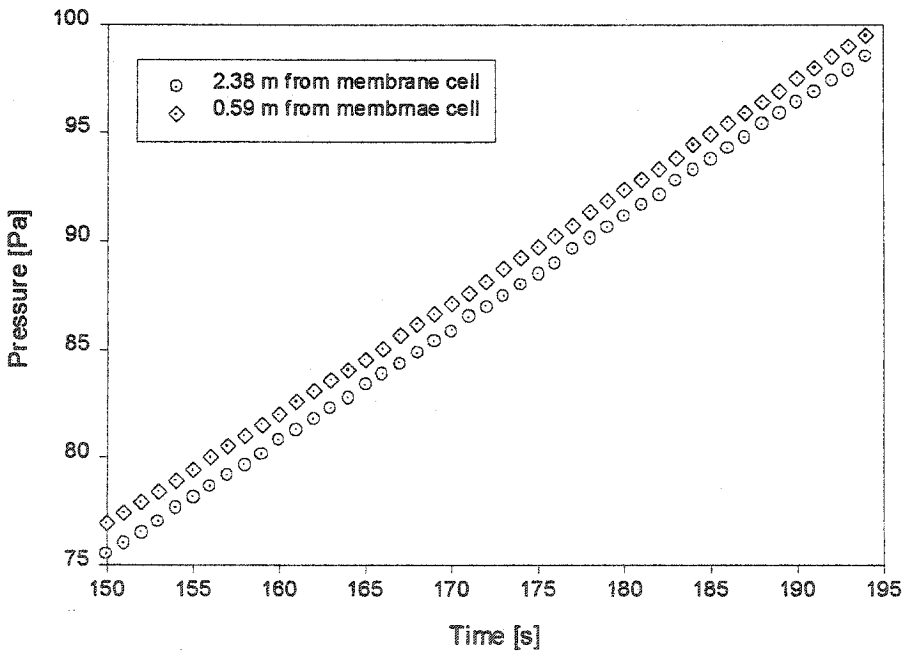

Figure 6. Pressure response between 150 s and 195 s from the initiation of gas permeation experiment in the 1/4"tube of total length of 3.9 m, initially at 5.5 Pa. Experiment performed at 23°C and the feed pressure of 207 × 10^3 Pa.

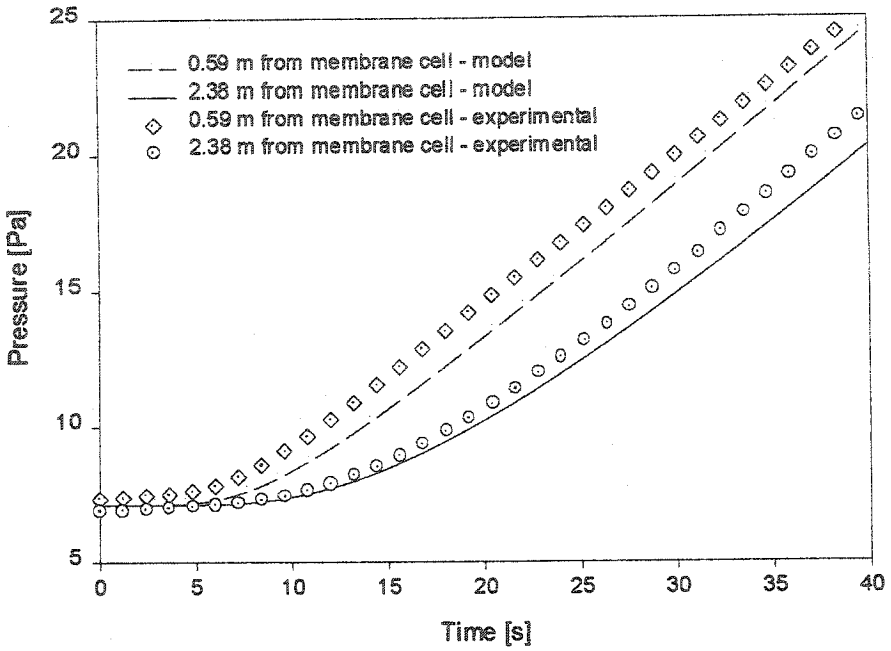

Figure 7-a. Effect of tube length. Figure shows the progress of first 40 s of gas permeation experiments in a tube of 1/4"diameter and 3.9 m length, initially at 7.33 Pa, for an experiment performed at 23°C and the feed pressure of 207×10^3 Pa.

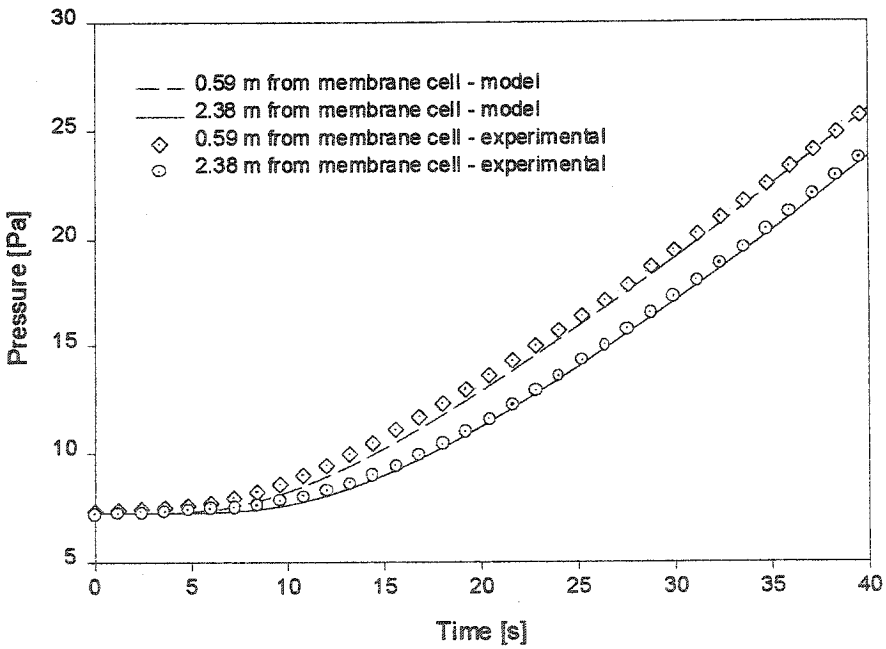

Figure 7-b. Effect of tube length. Figure shows the progress of first 40 s of gas permeation experiments in a tube of 1/4"diameter and 2.5 m length, initially at 7.33 Pa, for an experiment performed at 23°C and the feed pressure of 207×10^3 Pa.

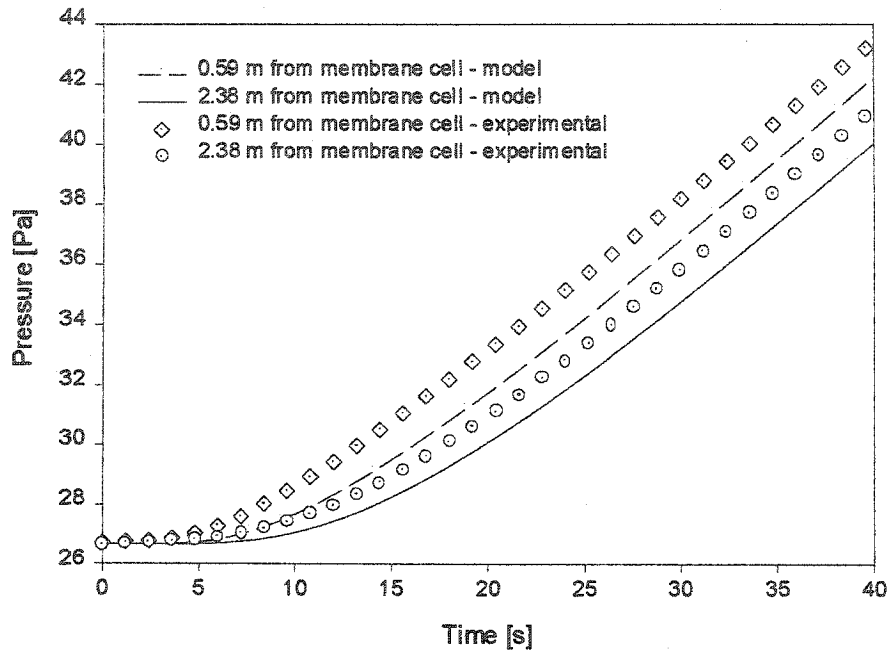

Figure 8-a. Effect of initial pressure. Figure shows the progress of first 40 s of gas permeation experiments in the 1/4"tube of total length of 3.9 m, initially at 26.7 Pa for an experiment performed at 23°C and the feed pressure of 207 $\times 10^3$ Pa.

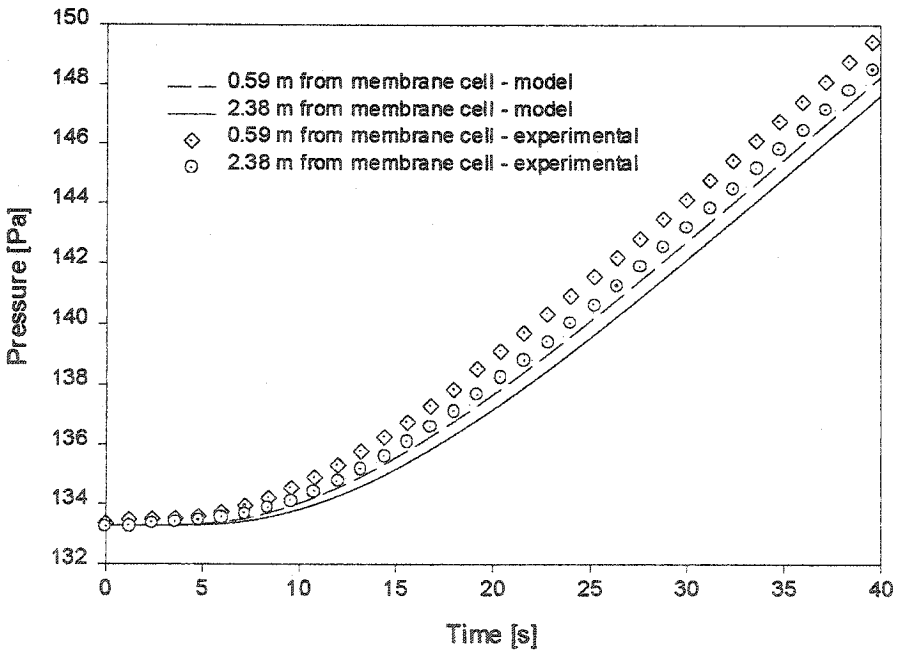

Figure 8-b. Effect of initial pressure. Figure shows the progress of first 40 s of gas permeation experiments in the 1/4"tube of total length of 3.9 m, initially at 133 Pa for an experiments performed at 23°C and the feed pressure of 207 $\times 10^3$ Pa..

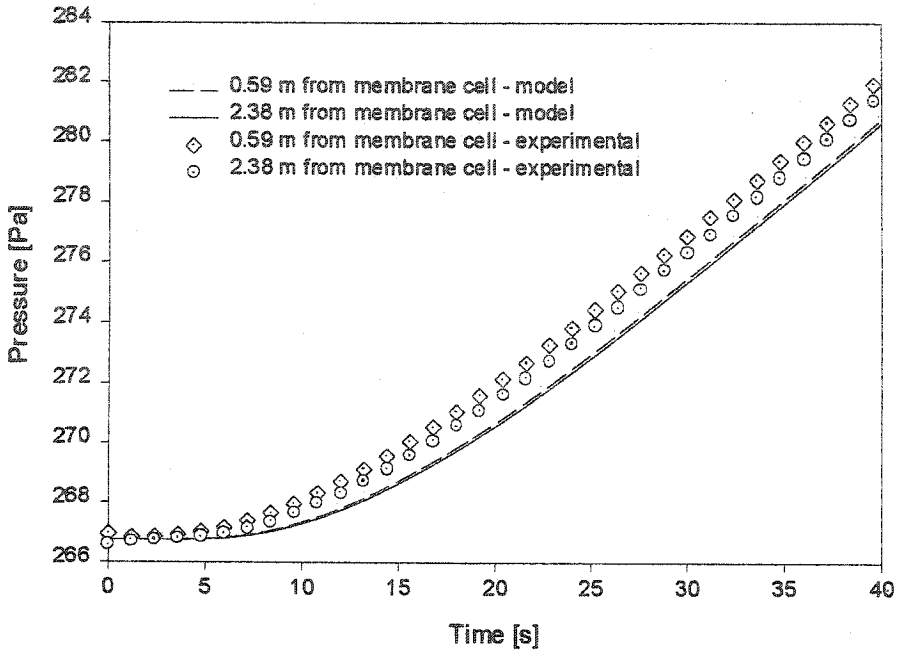

Figure 8-c. Effect of initial pressure. Figure shows the progress of first 40 s of gas permeation experiments in the 1/4"tube of total length of 3.9 m, initially at 267 Pa for an experiment performed at 23°C and the feed pressure of 207 $\times 10^3$ Pa.

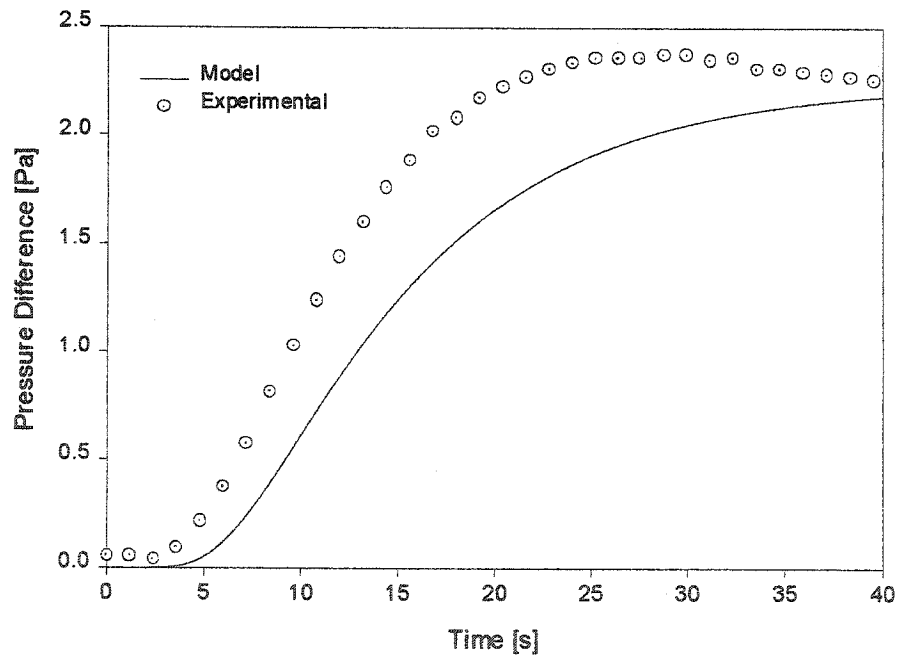

Figure 9-a. Effect of initial pressure on theoretically predicted and experimentally observed differences between pressures at x = 0.59 m and x = 2.38 m during gas permeation experiments performed in the 1/4"tube of total length of 3.9 m, initially at 26.7 Pa for an experiment performed at 23°C and the feed pressure of 207 $\times 10^3$ Pa.

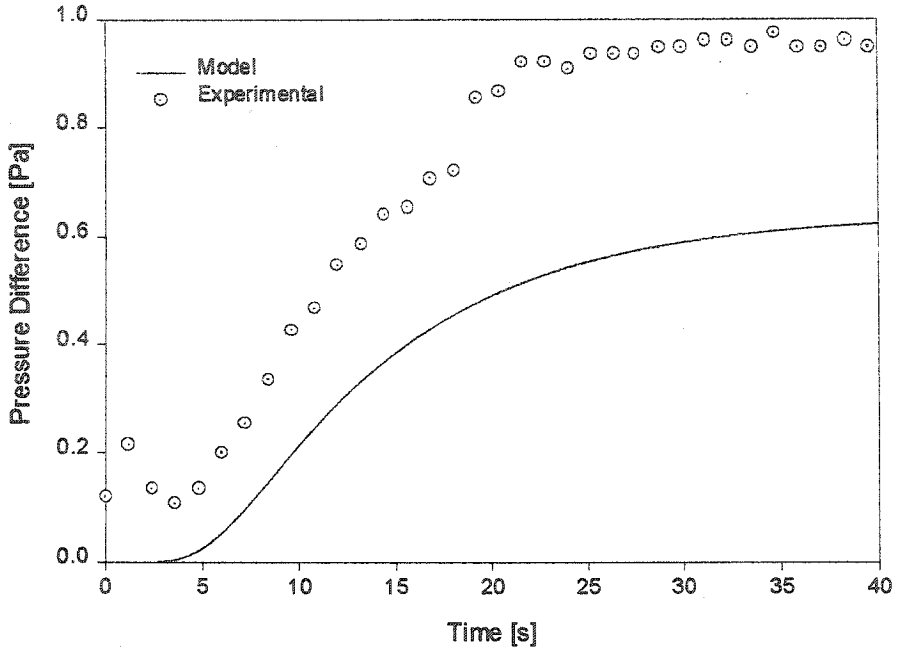

Figure 9-b. Effect of initial pressure on theoretically predicted and experimentally observed differences between pressures at $x = 0.59$ m and $x = 2.38$ m during gas permeation experiments performed in the 1/4"tube of total length of 3.9 m, initially at 133 Pa for an experiment performed at 23°C and the feed pressure of 207×10^3 Pa.

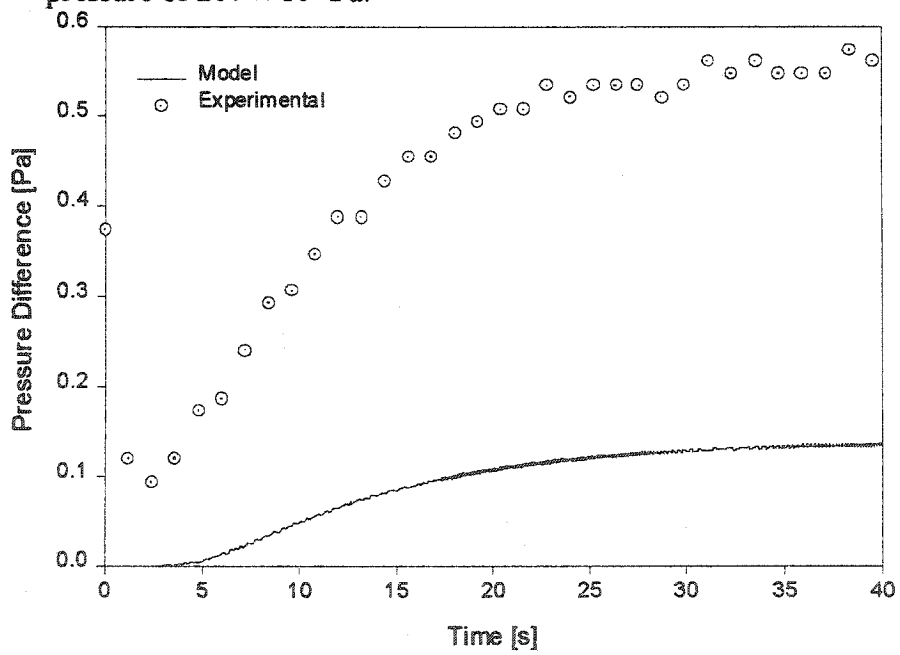

Figure 9-c. Effect of initial pressure on theoretically predicted and experimentally observed differences between pressures at $x = 0.59$ m and $x = 2.38$ m during gas permeation experiments performed in the 1/4"tube of total length of 3.9 m, initially at 267 Pa for an experiment performed at 23°C and the feed pressure of 207×10^3 Pa.

Conclusions and Recommendations

The mechanism of gas accumulation in constant volume systems has been described utilizing the Fick's second law of diffusion as a governing partial differential equation.

For the experimental conditions, the diffusion coefficient in tube evaluated from the slip flow and viscous flow models proved to be applicable. Due to technical limitations, it was impossible to perform experiments at absolute pressures less than 4 Pa, where pure Knudsen flow, or a combination of Knudsen and slip flows would be applicable.

The resistance to gas accumulation in cylindrical vacuum tubes has been characterized by the concepts of time lag and time delay. While the concept of time lag is widely used to describe transient flows through polymeric membranes and porous media, it has never been used for closed cylindrical tubes. It has been shown that time lag in a cylindrical tube of length L in which the diffusion coefficient of gas D is constant depends on the distance x from the open end at which the gas flows into the tube, according to the following equation:

$$\theta_v = \frac{L^2}{6D} - \frac{(L-x)^2}{2D}$$

This equation allows to determine the optimum location of the pressure transducer at which the resistance to gas accumulation in tube would not contribute to the experimentally measured time lag of membrane. The proposed equation is valid for both constant and time-dependent flows at the open end of tube.

The concept of time delay, which has also been introduced in this thesis, refers to the location of pressure transducer at which the error in measurement of flow due to resistance to accumulation of gases will first disappear. Interestingly, the optimum location for minimization of the error in time lag does not correspond to the optimum position for minimization of the time delay.

For the analysis of more complex systems consisting of several tubes of different diameters the concept of resistance and the relevant algebra of resistances has been proposed.

For the experimental verification of theoretically proposed models it was impossible to construct an ideal system, that is, the system without bends, dead volumes, contractions, and expansions. The main reason behind this was a time required for the mass flow controller to stabilize and give a constant flow. This problem was solved utilizing a large auxiliary tank to absorb the initially irregular flow. However, "the price" of this solution was additional number of valves and fittings. Another inherent reason behind non-ideality of the experimental system is dead volume associated with pressure transducers.

Despite non-ideality of the experimental CV system, the theoretically predicted phenomenon of the resistance to accumulation of gases in cylindrical tubes has been successfully demonstrated in the actual experiments. The proposed models along with the evaluated diffusion coefficient accurately describe the pressure response in cylindrical tubes for both constant and time-dependent flows in relatively short experiments.

A qualitatively predicted effect of resistance on gas flow determined from the pressure rise in long-term gas permeation experiments has been verified experimentally.

It is recommended to develop a quantitative model, similar to the one proposed in this thesis, in which however the variation of the diffusion coefficient with time and position is allowed. Such model would be capable to accurately describe the pressure response and thus the flow rate from the pressure rise in long gas permeation experiments.

In experiments in which gas transport properties in membrane are to be determined, it is recommended to redesign the system. First of all, the system should be equipped with appropriate solenoid valves for a more accurate determination of time zero. Also, the design of membrane cell could be modified to minimize possibility of any extra resistances, as well as, only short, straight tubes, not smaller than 1/2", should be used as a connection of the membrane cell with the accumulation tank.

The effect of the initial pressure on gas transport properties in membranes, which has been touched upon in this thesis, should be systematically studied in a resistance-free CV system described above.

Appendix A

Prediction of Diffusion Coefficient from Kinetic Theory of Gases

A1. Slip Law of Flow

Poiseuille law of flow can be applied to describe the laminar flow of gases in long and narrow pipes, where the average mean free path of gas molecules is small compared to the diameter of the tube [1].

The force acting on a differential cylinder of fluid of thickness δr in a tube of inside diameter of r_b is:

$$F_1 = (p_1 - p_2)2\pi r\delta r \tag{A1}$$

In the case of steady state flow, the acceleration is equal to zero. Therefore, the force F_1 is equal to the force of viscous drag acting on the boundaries of the specified differential cylinder.

$$F_1 = F_2 = F_{2o} - F_{2i} = -2\pi\eta(r+\delta r)L\frac{d}{dr}(V + \frac{dV}{dr}\delta r) + 2\pi\eta rL\frac{dV}{dr} \tag{A2}$$

Substituting equation (A1) into equation (A2) and ignoring the term, which contains δr^2, the following differential equation is obtained:

$$\eta rL\frac{d^2V}{dr^2} + \eta L\frac{dV}{dr} + (p_1 - p_2)r = 0 \tag{A3}$$

A particular solution is given by the following equation [1]:

$$V = A - \frac{(p_1 - p_2)}{4\eta L}r^2 \tag{A4}$$

Where, A is a constant. Assuming the velocity to be equal to zero at the wall, equation (A4) becomes:

$$V = \frac{(p_1 - p_2)}{4\eta L}[r_b^2 - r^2] \tag{A5}$$

Integrating the above equation over the cross sectional area gives the expression for the volumetric flow rate:

$$Q = \int_0^{r_b} V dA = \int_0^{r_b} V 2\pi r dr = \frac{\pi(p_1 - p_2) r_b^4}{8\eta L} \tag{A6}$$

The molar flux is then given by the following equation:

$$J = \frac{pQ}{\pi r_b^2 RT} = \frac{p(p_1 - p_2) r_b^2}{8\eta LRT} \tag{A7}$$

Comparing Eq. (A7) with the Fick's first law of diffusion, the expression for the diffusion coefficient, known as a viscous or molecular diffusion coefficient, is given by:

$$D = \frac{p r_b^2}{8\eta} \tag{A8}$$

When the average mean free path of molecules is not negligible compared to the diameter of tube or when the pressure gradient is large across the pipe, Poiseuille law of flow fails because gas molecules no longer form a constant layer at the wall. In order to account for the effect of non-constant layer at the wall, the concept of the external friction and slip coefficient is introduced. The equilibrium condition on a differential cylinder of fluid, whose one face is in contact with the wall, is given by:

$$2\pi r(p_1 - p_2)\delta r = F + 2\pi r L \eta \frac{dV}{dr} \tag{A9}$$

where, F is the frictional force on the surface of the wall given by [1]:

$$F = 2\pi r_b L \varepsilon V \tag{A10}$$

where ε is the coefficient of external friction against the wall. If the layer δr is sufficiently small, the left term in equation (A9) drops and the velocity of gas layer adjacent to the wall is given by the following equation:

$$V_0 = \frac{-\eta}{\varepsilon}\frac{dV}{dr} \tag{A11}$$

Differentiating equation (A4), the following equation is obtained:

$$\frac{dV}{dr} = \frac{-(p_1 - p_2)r}{2\eta L} \tag{A12}$$

Substituting dV/dr from equation (A11) into Eq. (A12), a new boundary condition is obtained:

$$V_{r\to r_b} = V_0 = \frac{r(p_1 - p_2)}{2\varepsilon L} \tag{A13}$$

Substituting Eq. (A13) into the left hand side of Eq. (A6), the volumetric flow rate in the case of existence of slip phenomenon is obtained:

$$Q = \frac{\pi(p_1 - p_2)r^4}{8\eta L}\left(1 + \frac{4\eta}{\varepsilon r}\right) \tag{A14}$$

As a result, the diffusion coefficient in the slip flow region is given by:

$$D = \frac{pr^2}{8\eta}(1 + \frac{4\xi}{r}) \tag{A15}$$

where, $\xi = \eta/\varepsilon$ is known as the coefficient of slip, which gives the ratio of the coefficient of internal friction (coefficient of viscosity) to the coefficient of external friction against the wall and has the dimension of the length.

A2. Knudsen Flow:

According to the Maxwell distribution law, if there are N molecules in 1 cm^3, the number of molecules dN with velocity components between c and $c+dc$ is given by:

$$dN = \frac{4N}{\alpha^3\sqrt{\pi}} c^2 \exp(\frac{-c^2}{\alpha^2})dc \qquad \text{(A16)}$$

where α is the most probable speed or the speed for which dN takes a maximum value. The number of these molecules, which strike 1 cm^2 of surface per second, is equal to: $cdN/4$. Therefore, the momentum given to the unit surface of a wall in 1 second by dN molecules is:

$$B = \frac{1}{4} cdNmw = \frac{1}{4} \kappa c^2 mdN \qquad \text{(A17)}$$

where, w is the component of the velocity of gas molecules parallel to the wall and m is the mass of one molecule. Momentum given to the wall by molecules of all velocities is:

$$B = \frac{1}{4} N\kappa \frac{4}{\sqrt{\pi}} m \int_{c=0}^{c=\infty} \frac{c^4}{\alpha^3} e^{\frac{-c^2}{\alpha^2}} dc = \frac{1}{4} N\kappa m \frac{3}{2}\alpha^2 = \frac{3\pi}{32} Nm\kappa\dot{c}^2 = \frac{3\pi}{32} Nm\dot{c}v \qquad \text{(A18)}$$

where, v, which is the geometric mean of the velocity of all molecules, is given by the following equation:

$$\dot{c} = \frac{\sum c}{N}, \kappa\dot{c} = \frac{\sum \kappa c}{N} = \frac{\sum w}{N} = v \qquad \text{(A19)}$$

The momentum, which a cylindrical tube with length dl and perimeter O obtains in dt seconds, is:

$$B' = \frac{3\pi}{32} Nm\dot{c}vOdldt = \frac{3\pi}{32} \rho \sqrt{\frac{8p}{\pi\rho}} vOdldt = \frac{3}{8}\sqrt{\frac{\pi}{2}} \rho \sqrt{\frac{p}{\rho}} vOdld \qquad \text{(A20)}$$

where,
$$\rho = Nm \text{ and } \dot{c} = \sqrt{\frac{8p}{\pi\rho}} \qquad \text{(A21)}$$

Neglecting the end effects of the wall, or in other words, assuming that the wall *Odl* gets the whole momentum transfer in time *dt*, the momentum transfer in time *dt* due to pressure difference across the area *A* is equal to:

$$-A(\frac{dp}{dl})dldt = \frac{3}{8}\sqrt{\frac{\pi}{2}}\rho\sqrt{\frac{p}{\rho}}vOdldt \tag{A22}$$

As a result:

$$v = -A\frac{dp}{dl}\frac{8}{3\rho O}\sqrt{\frac{2}{\pi}}\sqrt{\frac{\rho}{p}} \tag{A23}$$

The differential volumetric flow rate is then given by:

$$Q_{dl} = Av = -A^2\frac{dp}{dl}\frac{8}{3\rho O}\sqrt{\frac{2}{\pi}}\sqrt{\frac{M}{RT}} \tag{A24}$$

Integrating Q_{dl} over the length of tube gives the flow out of the tube:

$$Q = \frac{4r^3}{3\rho}\sqrt{2\pi}\sqrt{\frac{M}{RT}}\frac{(p_1 - p_2)}{L} \tag{A25}$$

Comparing equation (A25) with the Fick's first law of diffusion, the Knudson diffusion coefficient is found:

$$D = \frac{2}{3}r\sqrt{\frac{8RT}{\pi M}} \tag{A26}$$

A3. Maxwell's Deduction of Coefficient of Slip

Maxwell assumes that as a result of collision with the outer ends of the molecular wall the fraction, *f*, of gas molecules will be absorbed by the wall and lose their

momentum, and the fraction, *1-f*, will be reflected specularly without losing any momentum.

Writing a mass balance for molecules, which arrive to the wall and leave it, the following equation is obtained:

$$\rho_2\phi_2 = f\rho_2'\phi_2' + (1-f)\rho_2\phi_2 = f\rho_2'\phi_2' + (f-1)\rho_1\phi \tag{A27}$$

where, ρ is the density of gas, $\phi, \eta,$ and φ are the velocity vectors at x, y, and z directions. Subscript (1) refers to the molecules approaching to the wall, subscript (2) refers to the molecules rebounding from the wall, and superscript $(')$ refers to the molecules rebounded by evaporation. In addition,

$-\rho_1\phi_1$: represents the quantity of gas molecules incident on a unit surface in unit of time.

$\rho_2\phi_2$: represents the rebounded amount of molecules from a unit surface in unit of time.

$f\rho_2'\phi_2'$: represents the evaporated portion from the rebounded molecules.

$(1-f)\rho_2\phi_2$: represents the reflected amount from the rebounded molecules.

The overall momentum leaving the surface is given by the following equation:

$$\rho_2\phi_2\eta_2 = (1-f)\rho_2\phi_2\eta_2 - f\rho_2'\phi_2'v \tag{A28}$$

$$\rho_2\phi_2\eta_2 = (f-1)\rho_1\phi_1\eta_1 - f\rho_2'\phi_2'v \tag{A29}$$

where, v is the mean value of η or the velocity of gas relative to the surface in contact with. The $-f\rho_2'\phi_2'v$ represents the momentum of evaporated portion of molecules in y direction and also represents the momentum of the reflected portion, which is equal to the momentum of the portion of the incident molecules, which will be reflected without suffering any adsorption. Elimination of $f\rho_2'\phi_2'$ between equations (A27) and (A29) results in the following equation:

$$(1-f)\rho_1\phi_1\eta_1+\rho_2\phi_2\eta_2+v[\rho_2\phi_2+(1-f)\rho_1\phi_1]=0 \tag{A30}$$

In order to find v, Maxwell substitutes the appropriate values for $\rho_1, \rho_2, \eta_1, \eta_2, \phi_1$, and ϕ_2 and integrates them for ϕ from $-\infty$ to 0, and for η and φ from $-\infty$ to $+\infty$. Assuming that there is no difference in the temperature between the gas and the wall, Maxwell finds the following expression for v [1]:

$$v=\frac{\eta}{p}\sqrt{\frac{\pi RT}{2M}}\left(\frac{2-f}{f}\right)\frac{dv}{dx} \tag{A31}$$

Comparing with Eq (A11) and assuming the existence of cylindrical coordinate, the following equation is obtained:

$$\zeta=\frac{\eta}{\varepsilon}=\frac{\eta}{p}\sqrt{\frac{\pi RT}{2M}}\left(\frac{2-f}{f}\right) \tag{A32}$$

References:

1. L. B. Loeb, The Kinetic Theory of Gase, 3rd ed., Dover Publications, New York, 1961.
2. J. C. Maxwell, in The Scientific Papers of James Clerk Maxwell, edited by W. D. Niven, M. A., F. R. S., Dover Publications, New York, 1965.

APPENDIX B

Analytical Solution by Separation of Variables for Constant Flow

Using the method of separation of variables, the solution of specified partial differential equation, subject to given initial and boundary conditions, is obtained as follows. Introducing the following new variables:

$$\theta = p - p_o \tag{B1}$$

$$z = L - x \tag{B2}$$

the governing equation, the initial and the boundary conditions become:

$$\frac{\partial \theta(z,t)}{\partial t} = D\frac{\partial^2 \theta(z,t)}{\partial z^2} \tag{B3}$$

$$\theta(z,0) = 0 \tag{B4}$$

$$qRT = D\frac{\partial \theta(z,t)}{\partial z} \tag{B5}$$

$$\frac{\partial \theta(z,t)}{\partial z} = 0 \tag{B6}$$

Replacing θ by the summation three new functions:

$$\theta(z,t) = \psi(z,t) + Z(z) + S(t) \tag{B7}$$

equations (B3), (B4), (B5), (B6) become:

$$\frac{\partial \psi(z,t)}{\partial t} + \frac{dS(t)}{dt} = D\frac{\partial^2 \psi(z,t)}{\partial z^2} + D\frac{d^2 Z(z)}{dz^2} \tag{B8}$$

$$\psi(z,0) + Z(z) + S(0) = 0 \tag{B9}$$

$$\frac{qRT}{D} = \frac{\partial \psi(L,t)}{\partial z} + \frac{dZ(0)}{dz} \tag{B10}$$

$$\frac{\partial \psi(0,t)}{\partial z} + \frac{dZ(0)}{dz} = 0 \tag{B11}$$

According to the superposition principle, equations (B7), (B8), (B9), and (B10) can be split into:

$$\frac{\partial \psi(z,t)}{\partial t} = D\frac{\partial^2 \psi(z,t)}{\partial z^2} \tag{B12}$$

$$\frac{dS(t)}{dt} = D\frac{d^2 Z(z)}{dz^2} \tag{B13}$$

$$\psi(z,0) = -Z(z) \tag{B14}$$

$$S(0) = 0 \tag{B15}$$

$$\frac{\partial \psi(L,t)}{\partial z} = 0 \tag{B16}$$

$$\frac{dZ(L)}{dz} = \frac{qRT}{D} \tag{B17}$$

$$\frac{d\psi(0,t)}{dz} = 0 \tag{B18}$$

$$\frac{dZ(0)}{dz} = 0 \tag{B19}$$

Solving equation (B13), utilizing equations (B15), (B17) and (B19), the following equations are obtained:

$$Z(z) = \frac{z^2}{2}\frac{qRT}{DL} + C \tag{B20}$$

$$S(t) = \frac{qt}{L} \tag{B21}$$

Solving equation (B12), utilizing equations: (B14), (B16) and (B18), the following equation is obtained:

$$\psi(z,t) = e^{-\lambda^2 Dt}(A\cos\lambda z + B\sin\lambda z) \tag{B22}$$

where, $\lambda_n = \frac{n\pi}{L}$ and $n = 0,1,2, \ldots$.

Using the Fourier series expansion the following equation is obtained:

$$\psi(z,t) = \frac{-qL}{6D} - C - \frac{2q}{LD}\sum_{n=1}^{n=\infty}\frac{(-1)^n}{\lambda_n^2} e^{-\lambda_n^2 Dt}\cos\lambda_n z \qquad \text{(B23)}$$

Substituting equations (B20), (B21) and (B23) into equation (B7) and then going back into the original variables, the final solution is obtained:

$$p(x,t) = p_o + \frac{qRT}{DL}\left(Dt + \frac{(L-x)^2}{2} - \frac{L^2}{6}\right) - \frac{2qRT}{DL}\sum_{n=1}^{\infty}\frac{(-1)^n}{\lambda_n^2} e^{-\lambda_n^2 Dt}\cos[\lambda_n (L-x)] \qquad \text{(B24)}$$

APPENDIX C

Reliability of Low Flow Mass Flow Controller

The low flow mass flow controller (MFC) represents the heart of the experimental system discussed in Chapter II. It operates utilizing thermal principle, in which a probe installed in a gas streamline is maintained at a constant temperature and the energy required to do so is measured and correlated with gas flow rate.

The set flow rates of N_2 have been evaluated experimentally from the respective pressure responses in different system configurations and starting at different initial pressures. Table C1 summarizes the experimentally obtained data. The first column presents the initial static pressure before initiation of the experiment. The second column is the set flow rate of N_2, the third column presents the slope of the dynamic pressure rise determined between 333.3 Pa (2.5 mmHg) and 666.6 Pa (5 mmHg), the fourth column presents the flow rates calculated using Eq. (1) from Chapter II with the *dp/dt* values from the previous column. The last two columns present the slope and the calculated flow rate utilizing the pressure rise between 533.3 Pa (4 mmHg) and 666.6 Pa (5 cmHg).

The accuracy of flow rates calculated from the *dp/dt* values depends on the accuracy of pressure transducers. According to the manufacturer of the MFC, the maximum error is not greater than 0.12% of the read value. Considering the calculated flow rates in Table C1 using the slopes of the pressure responses between 333.3 Pa and 666.6 Pa and between 533.3 Pa and 666.6 Pa, it can be concluded that the MFC indeed provides a constant flow.

Figure C1 presents the coefficient of variation as a function of set flow. The coefficient of variation, which is the sample standard deviation divided by the mean

value, was calculated for each set flow utilizing the actual flows from eight independent experiments. The coefficient of variation or the variation of flow around the mean value is larger for smaller flows compared to higher flows, which means that the MFC functions more effectively for higher set flow rates, in particular for the flow rates greater than 0.05 cm^3(STP)/min. The behavior of the coefficient of variation leads to a conclusion that heat transfer coefficient between gas molecules and the thermal probe, as expected, increases with increase in flow rate.

In our mathematical simulation, the actual flow rate was calculated from the linear portion of pressure rise. Statistically, we should have used the mean value of actual flow rates at the same conditions. However, the 5 % variation for the lowest flow rate values and an insignificant variation of the slope between the two pressure regions justify the use of single experiment for the determination of the actual flow rate of gas.

Table C1: Experimental data for the case of constant flow

Case1- L = 7.67 m

P_o (torr)	Q_{set} (cm^3STP/min)	dp/dt Pa/s(2.5-5torr	Q_{actual} (cm^3STP/min)	dp/dt Pa/s(4-5torr)	Q_{actual} (cm^3STP/min)
0.031	0.005	0.04793	0.01684	0.04810	0.01690
0.050	0.005	0.04965	0.01744	0.04946	0.01737
0.075	0.005	0.04961	0.01743	0.04962	0.01743
0.100	0.005	0.05049	0.01774	0.05016	0.01762
0.250	0.005	0.04863	0.01708	0.04805	0.01688
0.500	0.005	0.05103	0.01792	0.05107	0.01794
0.750	0.005	0.05116	0.01797	0.05123	0.01800
1.000	0.005	0.04831	0.01697	0.04821	0.01694
0.031	0.020	0.09129	0.03207	0.09145	0.03212
0.050	0.020	0.09127	0.03206	0.09217	0.03238
0.075	0.020	0.09265	0.03255	0.09297	0.03266
0.100	0.020	0.09217	0.03238	0.09204	0.03233
0.250	0.020	0.09081	0.03190	0.09091	0.03194
0.500	0.020	0.09288	0.03263	0.09305	0.03269
0.750	0.020	0.09388	0.03298	0.09365	0.03290
1.000	0.020	0.09033	0.03173	0.09042	0.03176

P_o (torr)	Q_{set} (cm^3STP/min)	dp/dt Pa/s(2.5-5torr)	Q_{actual} (cm^3STP/min)	dp/dt Pa/s(4-5torr)	Q_{actual} (cm^3STP/min)
0.031	0.042	0.15479	0.05438	0.15443	0.05425
0.050	0.042	0.15363	0.05397	0.15469	0.05434
0.075	0.042	0.15601	0.05480	0.15595	0.05478
0.100	0.042	0.15354	0.05394	0.15364	0.05397
0.250	0.042	0.15393	0.05407	0.15416	0.05415
0.500	0.042	0.15650	0.05498	0.15652	0.05498
0.750	0.042	0.15462	0.05432	0.15463	0.05432
1.000	0.042	0.15313	0.05379	0.15309	0.05378
0.031	0.075	0.25105	0.08819	0.25138	0.08831
0.050	0.075	0.24971	0.08772	0.24962	0.08769
0.075	0.075	0.25388	0.08918	0.25369	0.08912
0.100	0.075	0.25156	0.08837	0.25146	0.08833
0.250	0.075	0.25226	0.08862	0.25218	0.08859
0.500	0.075	0.25380	0.08916	0.25362	0.08909
0.750	0.075	0.25183	0.08846	0.25197	0.08851
1.000	0.075	0.25099	0.08817	0.25070	0.08807
0.031	0.100	0.32829	0.11532	0.32824	0.11531
0.050	0.100	0.32508	0.11420	0.32507	0.11419
0.075	0.100	0.32923	0.11565	0.32905	0.11559
0.100	0.100	0.32577	0.11444	0.32552	0.11435
0.250	0.100	0.32814	0.11527	0.32801	0.11523
0.500	0.100	0.32816	0.11528	0.32816	0.11528
0.750	0.100	0.32570	0.11441	0.32560	0.11438
1.000	0.100	0.32505	0.11419	0.32487	0.11412
0.031	0.150	0.47673	0.16747	0.47677	0.16748
0.050	0.150	0.47693	0.16754	0.47678	0.16749
0.075	0.150	0.48019	0.16868	0.48039	0.16875
0.100	0.150	0.47719	0.16763	0.47715	0.16762
0.250	0.150	0.47891	0.16823	0.47881	0.16820
0.500	0.150	0.47806	0.16794	0.47801	0.16792
0.750	0.150	0.47593	0.16719	0.47602	0.16722
1.000	0.150	0.47586	0.16716	0.47562	0.16708
0.031	0.200	0.62958	0.22116	0.62920	0.22103
0.050	0.200	0.63275	0.22228	0.63269	0.22226
0.075	0.200	0.63572	0.22332	0.63507	0.22309
0.100	0.200	0.63366	0.22260	0.63353	0.22255
0.250	0.200	0.63560	0.22328	0.63563	0.22329
0.500	0.200	0.63270	0.22226	0.63260	0.22222
0.750	0.200	0.63027	0.22141	0.63032	0.22142
1.000	0.200	0.62955	0.22115	0.62926	0.22105

Case2- L = 3.83 m

P_o (torr)	Q_{set} (cm^3STP/min)	dp/dt Pa/s(2.5-5torr	Q_{actual} (cm^3STP/min)	dp/dt Pa/s(4-5torr)	Q_{actual} (cm^3STP/min)
0.031	0.005	0.43710	0.01939	0.43650	0.01923
0.050	0.005	0.43900	0.01947	0.43890	0.01934
0.075	0.005	0.42700	0.01894	0.42290	0.01863
0.100	0.005	0.40800	0.01810	0.40890	0.01801
0.250	0.005	0.39910	0.01770	0.39560	0.01743
0.500	0.005	0.38260	0.01697	0.38350	0.01690
0.750	0.005	0.39060	0.01733	0.39210	0.01727
1.000	0.005	0.39200	0.01739	0.39180	0.01726
0.031	0.020	0.76340	0.03386	0.76360	0.03364
0.050	0.020	0.79140	0.03510	0.79060	0.03483
0.075	0.020	0.77580	0.03441	0.77540	0.03416
0.100	0.020	0.75530	0.03350	0.75300	0.03317
0.250	0.020	0.74150	0.03289	0.74220	0.03270
0.500	0.020	0.73940	0.03280	0.73790	0.03251
0.750	0.020	0.73830	0.03275	0.73900	0.03256
1.000	0.020	0.70430	0.03124	0.70390	0.03101
0.031	0.042	1.25020	0.05545	1.25060	0.05510
0.050	0.042	1.28260	0.05689	1.28210	0.05648
0.075	0.042	1.27690	0.05664	1.27810	0.05631
0.100	0.042	1.25040	0.05546	1.24980	0.05506
0.250	0.042	1.21570	0.05392	1.21600	0.05357
0.500	0.042	1.24080	0.05504	1.24150	0.05470
0.750	0.042	1.23490	0.05478	1.23540	0.05443
1.000	0.042	1.23990	0.05500	1.24040	0.05465
0.031	0.075	2.02350	0.08976	2.02600	0.08926
0.050	0.075	2.07200	0.09191	2.07450	0.09139
0.075	0.075	2.05560	0.09118	2.05700	0.09062
0.100	0.075	2.03230	0.09015	2.03580	0.08969
0.250	0.075	2.02440	0.08980	2.02880	0.08938
0.500	0.075	2.02240	0.08971	2.02500	0.08921
0.750	0.075	2.01830	0.08952	2.02040	0.08901
1.000	0.075	2.01670	0.08945	2.01990	0.08899
0.031	0.100	2.61560	0.11602	2.62190	0.11551
0.050	0.100	2.66730	0.11831	2.67290	0.11776
0.075	0.100	2.65710	0.11786	2.66010	0.11719
0.100	0.100	2.63460	0.11686	2.63990	0.11630
0.250	0.100	2.62320	0.11636	2.62890	0.11582
0.500	0.100	2.61580	0.11603	2.62120	0.11548
0.750	0.100	2.61300	0.11590	2.61750	0.11532
1.000	0.100	2.61190	0.11585	2.61500	0.11521
0.031	0.150	3.81340	0.16915	3.82740	0.16862
0.050	0.150	3.86480	0.17143	3.87630	0.17077
0.075	0.150	3.84660	0.17062	3.85820	0.16998
0.100	0.150	3.83500	0.17011	3.84580	0.16943
0.250	0.150	3.79280	0.16824	3.80200	0.16750
0.500	0.150	3.81980	0.16943	3.82740	0.16862
0.750	0.150	3.82880	0.16983	3.83780	0.16908
1.000	0.150	3.80100	0.16860	3.81120	0.16791

P_o (torr)	Q_{set} (cm^3STP/min)	dp/dt Pa/s(2.5-5torr)	Q_{actual} (cm^3STP/min)	dp/dt Pa/s(4-5torr)	Q_{actual} (cm^3STP/min)
0.031	0.200	5.04460	0.22376	5.06210	0.22302
0.050	0.200	5.11460	0.22687	5.13980	0.22644
0.075	0.200	5.07350	0.22504	5.10540	0.22492
0.100	0.200	5.06310	0.22458	5.08420	0.22399
0.250	0.200	5.01960	0.22265	5.03710	0.22191
0.500	0.200	5.06430	0.22463	5.07000	0.22336
0.750	0.200	5.07370	0.22505	5.09350	0.22440
1.000	0.200	5.04660	0.22385	5.05820	0.22284

Case3- L = 2.42 m

P_o (torr)	Q_{set} (cm^3STP/min)	dp/dt Pa/s(2.5-5torr)	Q_{actual} (cm^3STP/min)	dp/dt Pa/s(4-5torr)	Q_{actual} (cm^3STP/min)
0.031	0.005	0.62050	0.01898	0.61870	0.01892
0.050	0.005	0.64030	0.01958	0.63960	0.01956
0.075	0.005	0.65680	0.02009	0.65700	0.02009
0.100	0.005	0.64230	0.01964	0.64160	0.01962
0.250	0.005	0.64380	0.01969	0.64340	0.01968
0.500	0.005	0.67930	0.02078	0.68010	0.02080
0.750	0.005	0.67750	0.02072	0.67710	0.02071
1.000	0.005	0.69480	0.02125	0.69370	0.02122
0.031	0.020	1.14850	0.03513	1.14640	0.03506
0.050	0.020	1.16580	0.03566	1.16600	0.03566
0.075	0.020	1.13270	0.03464	1.13190	0.03462
0.100	0.020	1.13550	0.03473	1.13510	0.03472
0.250	0.020	1.17210	0.03585	1.17100	0.03581
0.500	0.020	1.17960	0.03608	1.18150	0.03614
0.750	0.020	1.17350	0.03589	1.17210	0.03585
1.000	0.020	1.19250	0.03647	1.19280	0.03648
0.031	0.042	1.90280	0.05820	1.90310	0.05821
0.050	0.042	1.86110	0.05692	1.86030	0.05690
0.075	0.042	1.84090	0.05630	1.84120	0.05631
0.100	0.042	1.85810	0.05683	1.85800	0.05683
0.250	0.042	1.89550	0.05797	1.89600	0.05799
0.500	0.042	1.90470	0.05825	1.90530	0.05827
0.750	0.042	1.89400	0.05793	1.89490	0.05795
1.000	0.042	1.90390	0.05823	1.90550	0.05828
0.031	0.075	3.04870	0.09324	3.05350	0.09339
0.050	0.075	2.98110	0.09118	2.98470	0.09129
0.075	0.075	2.97700	0.09105	2.97840	0.09109
0.100	0.075	2.97190	0.09089	2.97440	0.09097
0.250	0.075	3.02120	0.09240	3.02470	0.09251
0.500	0.075	3.03610	0.09286	3.03700	0.09288
0.750	0.075	3.02860	0.09263	3.02900	0.09264
1.000	0.075	3.02930	0.09265	3.03480	0.09282

P_o (torr)	Q_{set} (cm^3STP/min)	dp/dt Pa/s(2.5-5torr	Q_{actual} (cm^3STP/min)	dp/dt Pa/s(4-5torr)	Q_{actual} (cm^3STP/min)
0.031	0.100	3.88330	0.11877	3.88400	0.11879
0.050	0.100	3.83410	0.11726	3.83920	0.11742
0.075	0.100	3.86330	0.11816	3.86990	0.11836
0.100	0.100	3.84130	0.11748	3.84960	0.11774
0.250	0.100	3.88460	0.11881	3.89160	0.11902
0.500	0.100	3.90000	0.11928	3.90440	0.11941
0.750	0.100	3.88910	0.11895	3.89190	0.11903
1.000	0.100	3.89910	0.11925	3.90100	0.11931
0.031	0.150	5.63510	0.17235	5.64830	0.17275
0.050	0.150	5.58400	0.17078	5.59910	0.17125
0.075	0.150	5.58690	0.17087	5.59610	0.17115
0.100	0.150	5.60890	0.17155	5.62250	0.17196
0.250	0.150	5.62260	0.17196	5.63120	0.17223
0.500	0.150	5.64080	0.17252	5.65110	0.17284
0.750	0.150	5.63200	0.17225	5.64580	0.17267
1.000	0.150	5.63120	0.17223	5.63700	0.17240
0.031	0.200	7.43770	0.22748	7.44830	0.22780
0.050	0.200	7.41090	0.22666	7.42640	0.22713
0.075	0.200	7.39720	0.22624	7.42180	0.22699
0.100	0.200	7.39790	0.22626	7.41290	0.22672
0.250	0.200	7.40940	0.22661	7.43920	0.22752
0.500	0.200	7.43800	0.22749	7.44900	0.22782
0.750	0.200	7.42540	0.22710	7.43240	0.22732
1.000	0.200	7.42500	0.22709	7.44180	0.22760

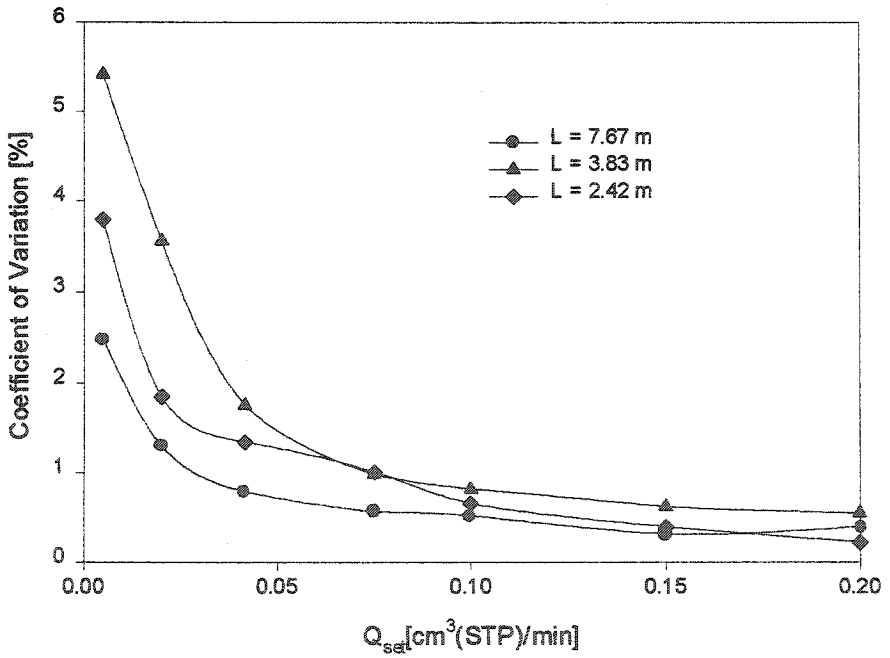

Figure C-1. Reliability of low flow mass flow controller.

APPENDIX D

Appendix D presents figures for mathematically predicted and experimentally observed pressure rise for different magnitudes of constant flow rate of gas performed in tubing F having valve V_5 opened or closed and in tubing I at two initial pressures of 4.13 and 13.3 Pa. The proposed mathematical model with constant D becomes valid for shorter period of times when the magnitude of flow rate of gas increases, which emphasizes the importance of development of a mathematical model, where diffusion coefficient is a function of pressure.

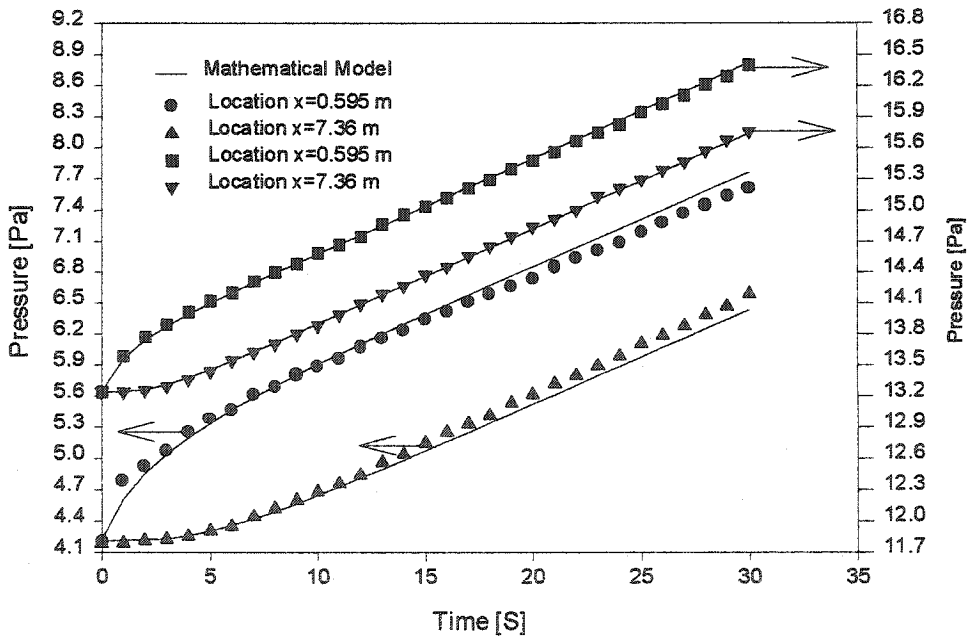

Figure D-1 Effect of the initial pressure on the theoretical and experimental pressure responses to a constant flow rate of 0.032 cm^3(STP)/min of N_2 at the positions x = 0.595 m and x = 7.36 m in a 7.67 m long, 0.0102 m internal diameter tube, and initial pressures of 4.13 and 13.3 Pa.

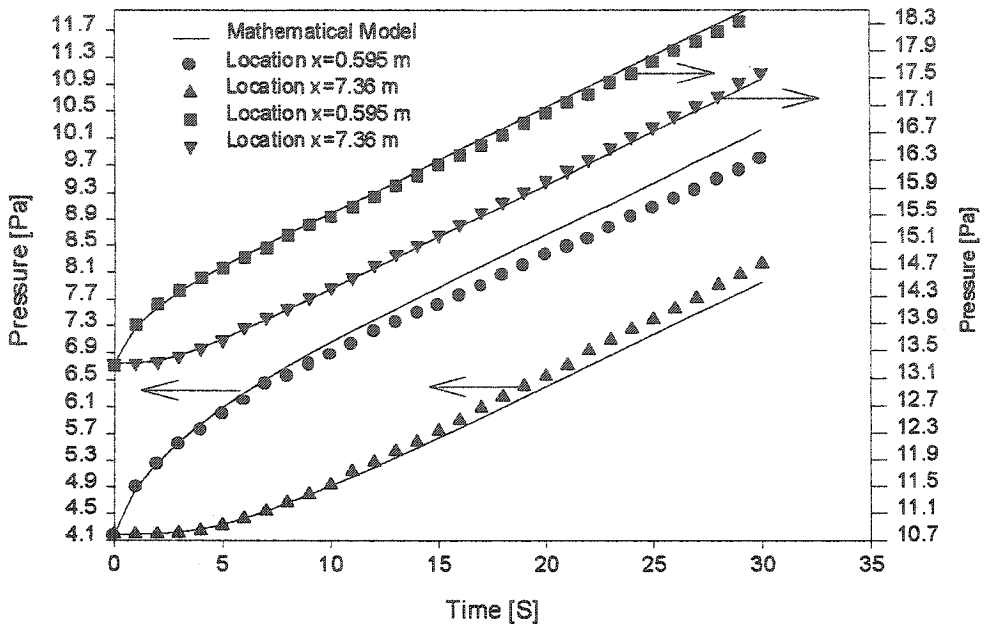

Figure D-2 Effect of the initial pressure on the theoretical and experimental pressure responses to a constant flow rate of 0.054 cm^3(STP)/min of N_2 at the positions x = 0.595 m and x = 7.36 m in a 7.67 m long, 0.0102 m internal diameter tube, and initial pressures of 4.13 and 13.3 Pa.

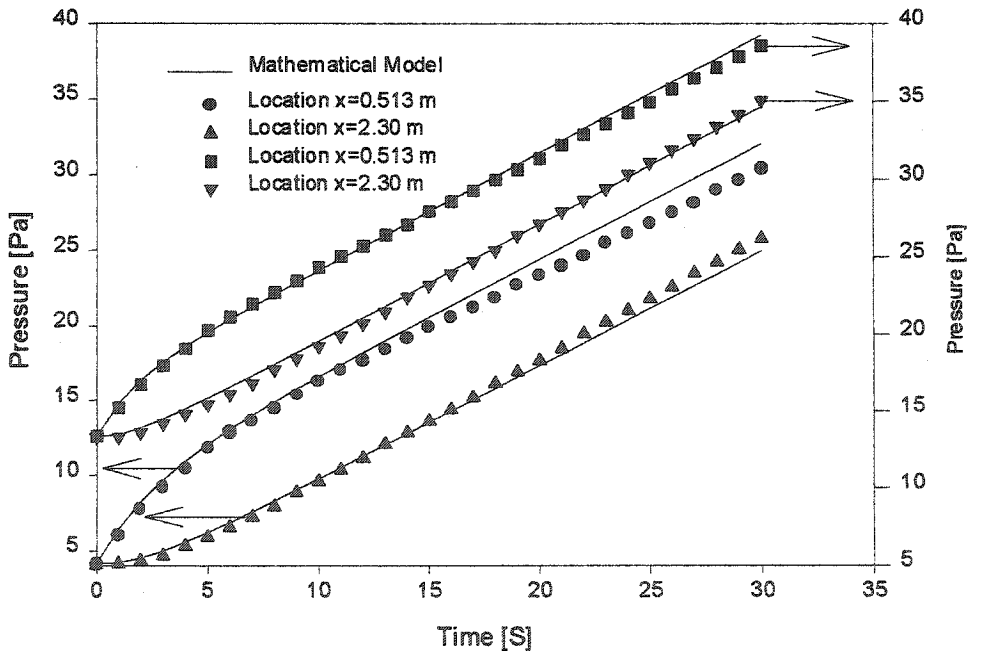

Figure D-3 Effect of the initial pressure on the theoretical and experimental pressure responses to a constant flow rate of 0.034 cm^3(STP)/min of N_2 at the positions x = 0.513 m and x = 2.30 m in a 3.83 m long, 0.00386 m internal diameter tube, and initial pressures of 4.13 and 13.3 Pa.

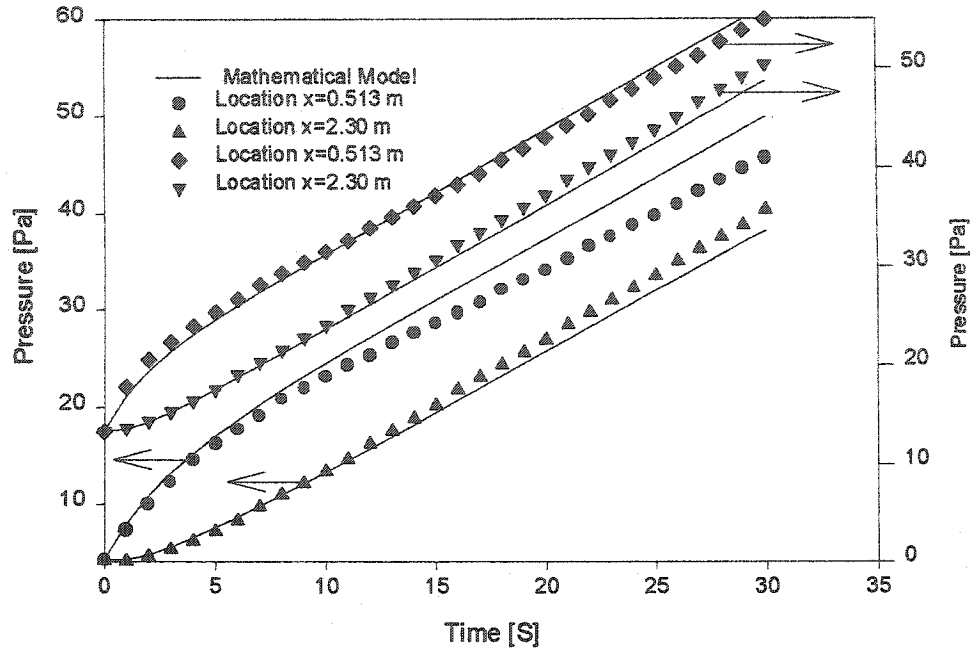

Figure D-4 Effect of the initial pressure on the theoretical and experimental pressure responses to a constant flow rate of 0.055 cm^3(STP)/min of N_2 at the positions x = 0.513 m and x = 2.30 m in a 3.83 m long, 0.00386 m internal diameter tube, and initial pressures of 4.13 and 13.3 Pa.

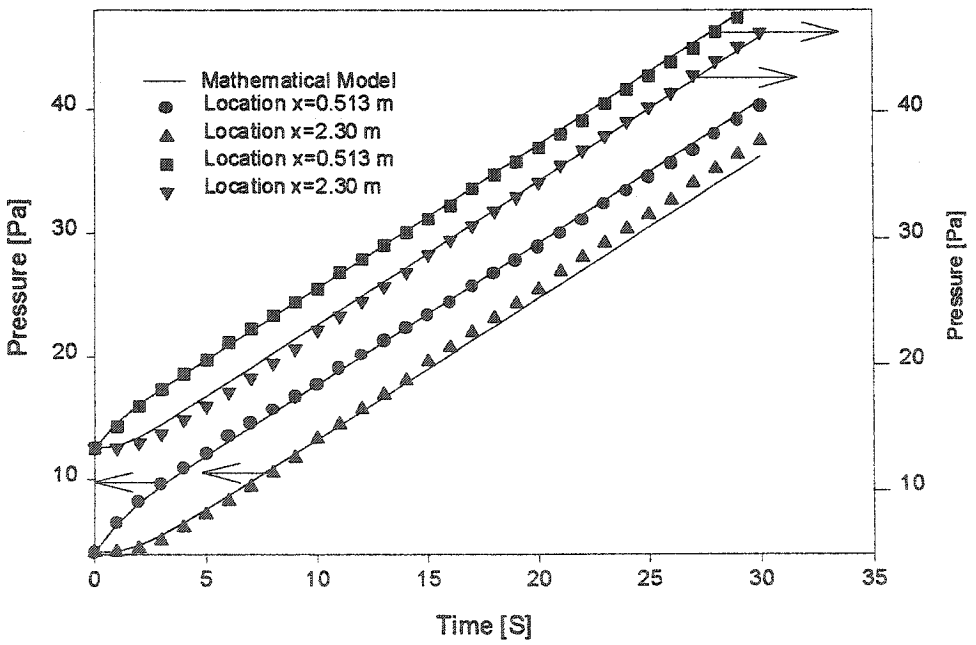

Figure D-5 Effect of the initial pressure on the theoretical and experimental pressure responses to a constant flow rate of 0.035 cm^3(STP)/min of N_2 at the positions x = 0.513 m and x = 2.30 m in a 2.42 m long, 0.00386 m internal diameter tube, and initial pressures of 4.13 and 13.3 Pa.

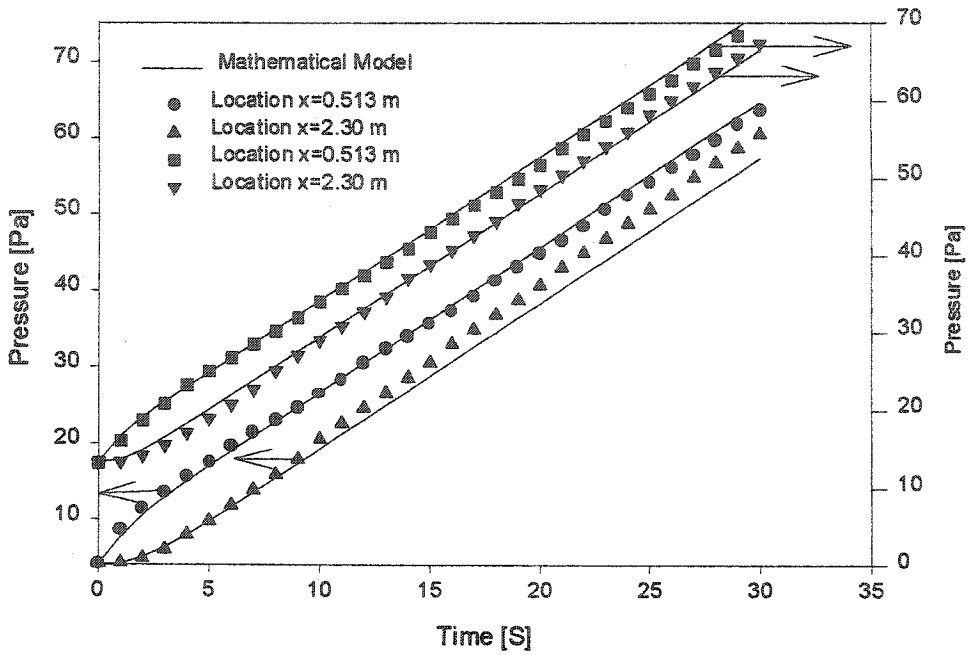

Figure D-6 Effect of the initial pressure on the theoretical and experimental pressure responses to a constant flow rate of 0.058 cm^3(STP)/min of N_2 at the positions x = 0.513 m and x = 2.30 m in a 2.42 m long, 0.00386 m internal diameter tube, and initial pressures of 4.13 and 13.3 Pa.

APPENDIX E

Numerical solution by finite difference method for time dependent flow

Governing equation, initial and boundary condition equations are:

$$\frac{\partial p(x,t)}{\partial t} = D\frac{\partial^2 p(x,t)}{\partial x^2} \tag{E1}$$

$$t = 0, \qquad p(x,0) = p_0 \tag{E2}$$

$$x = 0, \qquad -\frac{D}{RT}\frac{\partial p(0,t)}{\partial x} = \frac{A_m D_m p_f SL}{Vl}[1 + 2\sum_{n=1}^{n=\infty}(-1)^n \exp(\frac{-D_m n^2\pi^2 t}{l^2})] \tag{E3}$$

$$x = L, \qquad \frac{\partial p(L,t)}{\partial x} = 0 \tag{E4}$$

In order to have dimensionless equations, the following variables are introduced:

$$X = \frac{x}{L}, \qquad P = \frac{p}{p_0}, \qquad T = \frac{tD}{L^2} \tag{E5}$$

Substituting variables given in Eq. (E5) into equations (E1), (E2), (E3) and (E4), the following dimensionless equations are obtained:

$$\frac{\partial P}{\partial T} = \frac{\partial^2 P}{\partial X^2} \tag{E6}$$

$$T = 0, \qquad P = 1 \tag{E7}$$

$$X = 0, \qquad -\frac{p_0}{RTL}\frac{\partial P}{\partial X} = \frac{A_m D_m p_f SL}{Vl}[1 + 2\sum_{n=1}^{n=\infty}(-1)^n \exp(\frac{-D_m n^2\pi^2 TL^2}{l^2 D})] \tag{E8}$$

$$X = 1, \qquad \frac{\partial P}{\partial X} = 0 \tag{E9}$$

Applying the explicit method of finite-difference approximation, equations (E6), (E7), (E8), and (E9) are transferred into:

$$P_{i,j+1} = P_{i,j} + \frac{\Delta j}{\Delta i^2}[P_{i+1,j} - 2P_{i,j} + P_{i-1,j}] \tag{E10}$$

$$P_{i,0} = 1 \qquad \text{(E11)}$$

$$P_{0,j+1} = P_{0,j} + \frac{2\Delta j}{\Delta i^2}[P_{1,j} - P_{0,j} + \frac{\Delta i D_m A_m SRTp_f L^2}{p_0 DlV}\sum_{n=1}^{n=\infty} 1 + 2\sum_{n=1}^{n=\infty}(-1)^n \exp(\frac{-D_m n^2 \pi^2 j\Delta j L^2}{l^2 D})](\text{E12})$$

$$P_{m,j+1} = P_{m,j} + \frac{2\Delta j}{\Delta i^2}[P_{m-1,j} - P_{m,j}] \qquad \text{(E13)}$$

Where, $i = 0,1,2,3$---m and $j = 0,1,2,3$-----k, Δi represents the grid size of x-axis (location axis) and Δj represents the grid size of y-axis (time axis).

APPENDIX F

C++ program used for numerical simulation

```
# include <iostream.h>
# include "math.h"
# include <fstream.h>
int main()
{
ofstream fout;
double dt,dx,Dm,Pf,l,D,Po,L,A1,B,C,E,F,Am,V,T,S;
double a=2.0;
double b=-1.0;
double Pi=3.141592654;
double R=8.314;
int i,j,n;
int col=21;
int row=6000;
double rafi[6000][21];
double sum_E=0;
cout<<"enter the value of dt"<<endl; //dt represents dj.
cin>>dt;
cout<<"enter the value of dx"<<endl; //dx represents di.
cin>>dx;
cout<<"enter the value of cylinder length L in m"<<endl;
cin>>L;
cout<<"enter the value of diffusion coefficient in the membrane Dm in m2/sec:"<<endl;
cin>>Dm;
cout<<"enter the value of the feed pressure on membrane side Pf in pascal:"<<endl;
cin>>Pf;
cout<<"enter the value of the initial pressure in the cylinder in pascal:"<<endl;
cin>>Po;
cout<<"enter the value of diffusion coeifficient in vacuum tube D in m2/sec:"<<endl;
cin>>D;
cout<<"enter the thickness of the membrane l in m:"<<endl;
cin>>l;
cout<<"enter the area of the membrane Am in m2:"<<endl;
cin>>Am;
cout<<"enter the volume of the vacuum cylinder in m3:"<<endl;
cin>>V;
cout<<"Enter the value of room temperature in K:"<<endl;
cin>>T;
cout<<"Enter the value of solubility in mol/m3.Pa:"<<endl;
cin>>S;
```

```
for (i=0;i<col;i++)
{
rafi[0][i]=1;
}
for (j=1;j<row;j++)
{
A1=(dx*Dm*Am*S*R*T*Pf*L*L)/(Po*D*l*V);
for (n=1;n<=1000;n++)
{
B=pow(b,n);
C=exp((b*n*n*Pi*Pi*Dm*L*L*dt*j)/(l*l*D));
E=B*C;
sum_E+=E;
}
F=A1+(a*A1*sum_E);
rafi[j][0]=rafi[j-1][0]+((a*dt*(rafi[j-1][1]-rafi[j-1][0]+F))/pow(dx,2));
rafi[j][col-1]=rafi[j-1][col-1]+((a*dt*(rafi[j-1][col-2]-rafi[j-1][col-1]))/pow(dx,2));
for (i=1;i<col-1;i++)
{
rafi[j][i]=rafi[j-1][i]+((dt*(rafi[j-1][i+1]-(a*rafi[j-1][i])+rafi[j-1][i-1]))/pow(dx,2));
}
sum_E=0;
}
fout.open("hovig.txt");
for (j=0;j<row;j++){
for(i=0;i<col;i++){
fout<<rafi[j][i]<<"\t";
}
fout<<"\n";
}
fout.close();
return 0;
}
```

APPENDIX G

Figure G-1 Description of Membrane Cell

The information on the design of membrane cell, could dilute Paper III presented in Chapter IV, and therefore has not been provided. On the other hand, for a complete picture of the work performed in this thesis, the details pertinent to the membrane cell are important.

Figure G1 presents a schematic diagram of the membrane cell, which has been referred to as item (A) on Fig. 1 in Paper III. The cell consist of a feed (top) part and a permeate (bottom) part. A 0.1 cm thick and 3.3 cm diameter porous plate sits over approximately 2 cm^3 of dead volume enclosed in the bottom part of the cell. The gas that permeates through the membrane is transported across the porous plate into the dead volume from which it converges into a 1/4" tube. A flat 0.1 cm thick stainless steel ring having the width and the inner diameter of 0.2 cm and 3.5 cm, respectively, is machined at the top part of the cell to provide the primary seal in the cell. In addition, a 5.7 cm rubber o-ring, sitting in a 0.2 cm x 0.2 cm groove machined in the top part of the cell, provides a secondary seal, and prevents the membrane from being damaged by the primary seal when the top and bottom parts of the cell are pressed together by a screw thread. The membrane is never in a direct contact with a porous plate during gas permeation tests, because it sits on a filter paper allocated between the membrane and the porous media. In addition, two identical paraffin film rings of inner diameter slightly smaller than the inner diameter of stainless steal ring are installed at the top and bottom

surfaces of the membrane as a protection from possible damages at the edges of the primary seal.

Figure G-1 Membrane cell configuration

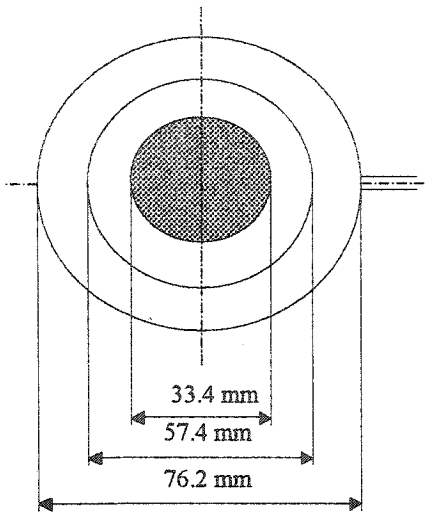

Upper view of permeate part

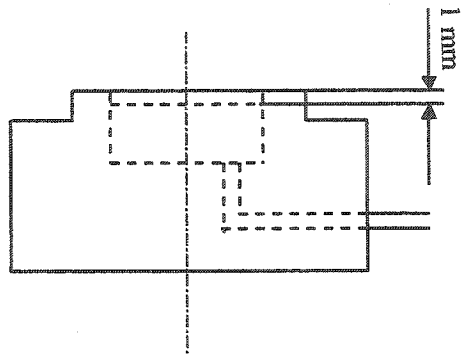

Side view of permeate part

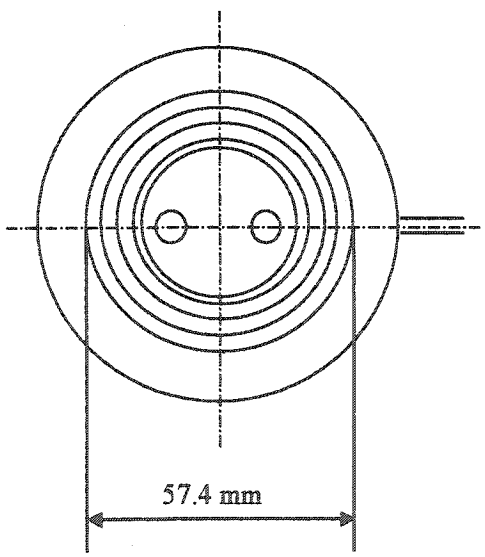

Upper view of feed part

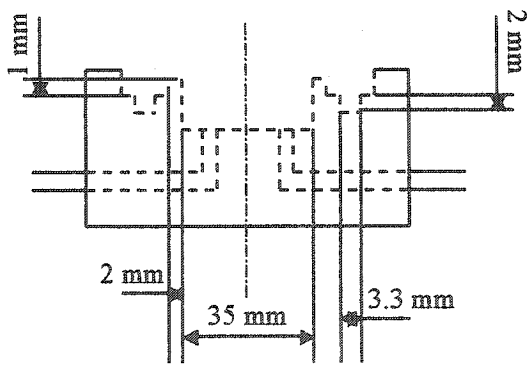

Side view of feed part